NTNU – Trondheim
Norwegian University of
Science and Technology

Combined Dynamic Positioning and Optimal Wave Frequency Motion Damping of Surface Effect Ship

Per Sondre Sodeland

Marine Technology
Submission date: June 2015
Supervisor: Asgeir Johan Sørensen, IMT
Co-supervisor: Øyvind Fidje Auestad, Umoe Mandal

Norwegian University of Science and Technology
Department of Marine Technology

NTNU Trondheim
Norwegian University of Science and Technology
Department of Marine Technology

MASTER THESIS IN MARINE CYBERNETICS

Spring 2015

for

Per Sondre Sodeland

Combined Dynamic Positioning and Optimal Wave Frequency Motion Damping of Surface Effect Ship

Work description

The shipyard Umoe Mandal is currently (as of February 2015) testing their newest SES design, the Wave Craft. Featuring a large Ride Control Capacity, i.e. large fan capacity and large variable leakage areas, combined with narrow side hulls, to minimize the hydrodynamic forces. The yard is now thinking about developing a concept meant for offshore purposes, where a SES could be used for large-scale transportation of crew and equipment to offshore oilrigs. For operations near oil-related installations this vessel would have to feature some sort of dynamical positioning system. The large fan capacity already installed in the vessel can hypothetically be used to provide lateral thrust, inducing translations and/or rotations on the vessel. The aim for this thesis is to investigate the possibilities of using the already existing 'hardware' to implement horizontal control in the vessel, and combine it with the vertical control showed in my project thesis.

Scope of work

- Describe the concept of Surface Effect Ships and the background for this project
- Do a literature review of relevant literature and previous work on the subject of horizontal and vertical SES control.
- Formulate a mathematic model for the system, including:
    - An accurate representation of the cushion pressure dynamics.
    - Fludmechanical analysis of the thrust provided by the airflow, and optimization.
    - 6 DOF dynamics including kinematics in surge, sway, heave and yaw
    - Low Frequency Dynamics for the horizontal problem
    - Qualitative model of environmental loads
- Derive a control scheme based on pressure and directional leakage area where you combine the individual desires for vertical and horizontal actuator displacements. This should include
    - Control objective
    - Maneuvering and station keeping control
    - Wave Frequency motion damping using air-cushion actuators

- Thrust allocation using combined air thrust and water jets
- Actuator capacites/saturations
- Thrust Control of air-thrust and water jets.

- Do simulations where Dynamic Positioning and wave frequency motion damping capacities are demonstrated.

The report shall be written in English and edited as a research report including literature survey, description of mathematical models, description of control algorithms, simulation results, model test results, discussion and a conclusion including a proposal for further work. Source code should be provided on a CD with code listing enclosed in appendix. It is supposed that Department of Marine Technology, NTNU, can use the results freely in its research work, unless otherwise agreed upon, by referring to the student's work. The thesis should be submitted in two copies within June 10th.

Co-supervisor: Øyvind Auestad

Professor Asgeir J. Sørensen
Supervisor

Acknowledgements

This thesis was written with Professor Asgeir Johan Sørensen at the Norwegian University of Science- and Technology as supervisor. I would like to thank him for his enthusiasm, always having an answer and, most importantly, sharing some healthy perspectives on the industry, career and, I'll say, life in general.

My co-supervisor was Phd. Øyvind Fidje Auestad, at Umoe Mandal. He deserves a lot of gratitude, for answering emails in the middle of the night, phone calls Sunday morning, providing insight and helpful feedback for the numerous discussions about problems I've encountered and my thesis in general.

I would also like to thank Umoe Mandal for sharing information and being helpful.

Per Sondre Sodeland

Trondheim, June 12, 2015

Abstract

The offshore wind industry is requesting high annual accessibility to wind-turbines. The turbines are located increasingly further from the shore. Simultaneously, operations & maintenance costs are to be minimized, therefore innovation is needed for the turbine service vessels which transfer crew and equipment. Surface Effect Ships (SESs) are fast and fuel-efficient when sailing long distances. Active damping of vertical motions means that low motion levels can be achieved even for small vessels in high seas. However, safe interaction with fixed offshore installations necessitates automatic control of the horizontal vessel motions. Such control has never been implemented on a SES before, and was therefore investigated for the work of this thesis. We derived the necessary dynamics, describing both the horizontal- and vertical states of the plant. Since conventional bow thrusters are hard to fit in SESs we derived a model for the lateral thrust capabilities obtainable by controlling the direction of the out flow from the SES air cushion. To successfully simulate the derived plant for somewhat realistic conditions, the model was augmented to include the effects of environmental disturbances. The control problem was dual: While the main objective was to investigate the possibilities for dynamic positioning of the plant. Due to the fast dynamics of the air cushion actuators, we also wanted to check the potential for damping of horizontal and vertical, 1st order wave induced motions. The latter controller was derived by an augmentation and slight alteration of an already existing control scheme based on optimal control, while the former was a simple PID controller solely intended to prove the potential of dynamic positioning of the derived plant. Due to large levels of saturation and mutually inflicting control desires, much care was given in ensuring that the phases of the wave frequency motion damping control signals where tuned to minimize the degree of infliction. The simulations show strong performance of the controllers, while the derived model seems to provide accurate indications regarding the behaviour of the real plant. For moderate sea states, we obtained almost 80% damping of the heave motions while we reduced the wave frequency motions in sway by as much as 50%. The two wave frequency controllers was also run simultaneously, where the controller achieved a damping in sway and heave of 32- and 60%, respectively, for 0.5m high waves. The DP controller also performed well, and the vessel seemed to maintain position, by the means of water jets and airflow thrust, in 15m/s wind, 1m/s current and regular waves of 2m. We also performed simultaneous station keeping and vertical motion damping, which revealed a strong dependency between the airflow thrust demand and heave compensation capacity of the vessel, but still indicated that such simultaneous operation was indeed possible.

Abstract - Norwegian Version

For å gjøre offshore produksjon av elektrisitet lønnsomt er man avhengig av lite nedetid og lave operasjons- og vedlikeholdskostnader. Siden slike vindmøllefelt blir plassert stadig lengre fra land, kreves det nytenkning rundt fartøyene som frakter service-personell og utstyr ut til feltene. Surface Effect Ships (SESs) er raske, og bruker relativt lite drivstoff på lange distanser. Ved hjelp av aktiv dempning av vertikal-bevegelsene kan man også oppnå gode sjøegenskaper i relativt små fartøyer også i høye sjøtilstander. Skal man gjennomføre sikre operasjoner nær faste offshore installasjoner er man avhengig av automatisk posisjonsregulering, noe som aldri før har blitt implementert på et SESs fartøy. Motivasjonen bak arbeidet med denne hovedoppgaven var å undersøke mulighetene for slik regulering, og utvikle et reguleringssystem til oppgaven gjennom matematisk modellering av fartøyet og dynamikken i luftpute-trykket. I tillegg til automatisk regulering av de horisontale frihetsgradene ønsket vi å undersøke mulighetene for å dempe så mye som mulig av førsteordens-bølgeeffekt-induserte bevegelser. På grunn av den smale baugkonstruksjonen i SES fartøyer med stor kapasitet for demping av vertikalbevegelser, er det vanskelig å installere konvensjonelle baugpropellere. I stedet undersøkte vi muligheten for å benytte den kraftige luftstrømmen fra løfteviftene som erstatning. På grunn av den raske dynamikken i aktuatorene relatert til regulering av luftputen kan denne luftstrømmen, hypotetisk sett, også benyttes til å kompensere for førsteordens bølgeeffekt-induserte bevegelser i fartøyet, både horisontalt og vertikalt. Dette ble kalt bølgefrekvensproblemet, og ble, sammen med systemet for dynamisk posisjonering, en del av det todelte reguleringsobjektivet i oppgaven. Vi utledet en matematisk modell for systemets dynamikk, inkludert sidekreftene fra luftstrømningen ut av luftputen og effekten av eksterne forstyrrelser fra bølger og vind. Bølgefrekvens-regulatoren ble utviklet ved å utvide eksisterende teknologi til å inkludere optimal tilbakekobling av lufttrykk og sidebevegelser, mens DP-regulatoren var en enkel PID regulator. Aktuatorene til luftputen når metning relativt fort, derfor brukte vi mye tid på å tune parametrene i LQR-algoritmen for å oppnå korrekt fase mellom signalene. Resultatene viser, ved simulering, at vi kan oppnå så mye som 80% dempning av vertikal bevegelsene og 50% dempning av førsteordens horisontalbevegelser. Ved kombinert regulering i bølgefrekvens-problemet oppnådde vi, henholdsvis, 32- og 60% dempning av horisontal og vertikal bevegelsene ombord i fartøyet, i en halv meter høye bølger. DP systemet viste seg å fungere bra, og fartøyet holdt seg stødig på referanseposisjonen selv i 15 sekundmeter vind, 1 sekundmeters strøm og 2 meter høye bølger. Vi undersøkte også mulighetene for å kombinere demping av vertikalbevegelsene med dynamisk posisjonering, noe simuleringene indikerte et stort potensiale for.

Contents

List of Figures

Nomenclature

Constant	unit	Definition
b	m	Width of air cushion
A_c	m^2	Area of air cushion
L	m	Length of air cushion
V_{c0}	m^3	Equilibrium volume of air cushion
c	m/s	Speed of sound at 20° C
g	m/s^2	Acceleration of gravity
p_0	[Pa]	Equilibrium pressure inside air cushion
p_a	[Pa]	Atmoshpheric pressure
ρ_{c0}	$[Kg/m^3]$	Density of air in cushion at cushion equilibrium pressure p_0
ρ_w	$[Kg/m^3]$	Density of sea water
γ	[-]	Heat capacity ratio
K	[-]	Wave number
λ	$[m]$	Wave length
x_{cp}	$[m]$	Longitudinal distance between COG and Centre of Pressure
A_0	$[m^2]$	Total equilibrium bias opening of vent valve louvers
u_y^{vv}	$[N]$	Net lateral thrust from vent valves
$u_{y,wj}^{p}$	$[N]$	Lateral thrust from port water jet
$u_{x,wj}^{p}$	$[N]$	Longitudinal thrust from port water jet
$u_{y,wj}^{sb}$	$[N]$	Lateral thrust from starboard water jet
$u_{x,wj}^{sb}$	$[N]$	Longitudinal thrust from starboard water jet
l_x^{vv}	$[m]$	Longitudinal distance between Vent Valves and COG
$l_x^{wj,p}$	$[m]$	Longitudinal distance between port water jet and COG
$l_y^{wj,p}$	$[m]$	Lateral distance between port water jet and COG
$l_x^{wj,sb}$	$[m]$	Longitudinal distance between starboard water jet and COG
$l_y^{wj,sb}$	$[m]$	Lateral distance between starboard water jet and COG

Table 1: Table of important constants used in the thesis

Variable	Unit	Definition
ω_w	[rad/s]	Frequency of incoming waves at a fixed observation point
ω_e		Frequency of wave encountering
$p_u(t)$	[Pa]	Uniform cushion gauge pressure
$\rho_c(t)$	[Kg/m^3]	Density of air at pressure $p_u(t)$
$V_c(t)$	[m^3]	Volume of air cushion
$\mu(t)$	[-]	Normalized uniform pressure
$\dot{V}_w(t)$	[m^3/s]	Wave volume pumping
$\xi(x,t)$	[m]	Surface elevation
$Q_{i,in}(\mu)$	[m^3]	Inflow from lift fan i
$A^{fp}(\eta)$	[m^2]	State dependent bow seal (passive) leakage area
$A^{ap}(\eta)$	[m^2]	State dependent aft seal (passive) leakage area
$\tau(t)$	[N] ([Nm])	Body fixed forces and moments
$V_w(t)$	[m/s]	Wind speed
$V_c(t)$	[m/s]	Current speed
$\tau_{pid}(t)$	[N] ([NM])	Output from DP-controller
$u_c^l(t)$		WF control output
$\eta_s(t)$		Seakeeping state vector
$\eta_{lin}(t)$		Control plant state vector
$e(t)$		Set point error in {n}
u_c		Vector of decomposed thrust components from each individual thruster
$A^l(t)$	[m^2]	Total leakage area
$A^l_{sb}(t)$	[m^2]	Starboard vent valve leakage area
$A^l_p(t)$	[m^2]	Port vent valve leakage area
$\Delta A^l_{vert}(t)$	[m^2]	Vertical motion damping control output
$u_c^{vv}(t)$	[N]	Lateral motion damping control output
$\Delta A^l_{lat}(t)$	[m^2]	Corresponding lateral leakage area
$\alpha_{a,i}(u_c)$	[rad]	Azimut angle of water jet i
$d_{rev,i}(u_c)$	[-]	State of deflector shield of water jet i

Table 2: Table of important variables used in the thesis

Acronym/abreviation	Definition
SES	Surface Effect Ship
BCS	Boarding Control System
RCS	Ride Control System
DP	Dynamic Positioning
WF	Wave Frequency
LF	Low Frequency
MCMV	Mine countermeasures vessel
OSV	Offshore Supply Vessel
PSV	Platform Supply Vessel
LQR	Linear Quadratic Regulator
GPS	Global Positioning System
NED	Nort-East-Down
DOF	Degree of Freedom
LTI	Linear Time Invariant

Table 3: Table of Acronyms and abbreviations used in the thesis

Chapter 1

Introduction and Motivation for Work

1.1 Motivation for Work

The shipyard Umoe Mandal, located in the most southern part of Norway, has played a leading role within construction and development of Surface Effect Ships (SESs) since the early 90s. The adventure began when the yard, then named Kværner Mandal, got awarded the contract of building a series of 9 Mine Countermeasure Vessels (MCMVs), the Oksøy- and Alta-class, respectively, for the Royal Norwegian Navy. Following the successful delivery of the MCMV-series, the yard started development of the new series of Norwegian Coastal Corvettes, the Skjold-class, figure 1.1.

Figure 1.1: The Skjold-class

The prototype vessel, *Skjold*, was commissioned April 1999, and a series of 5 additional vessels was ordered in 2002, where the last one, *Gnist*, was delivered in December 2007. These vessels

features stealth-properties, 4 Pratt & Whitney gas turbines, with a total power output of 12,170 Kilowatts and 2×MTU 735Kw diesel engines powering the lift fans. They are the worlds fastest military vessels in active service, with a top speed of more than 60 knots, and a 800nm range at 46 knots. After the two successful military programs, Umoe Mandal turned to the civilian marked. A report given by the European Environment Agency (EEA, 2008) indicates that there, in 2020, will be 30-40 times the installed wind turbine capacity there was in 2008, as illustrated by the histogram in figure 1.2.

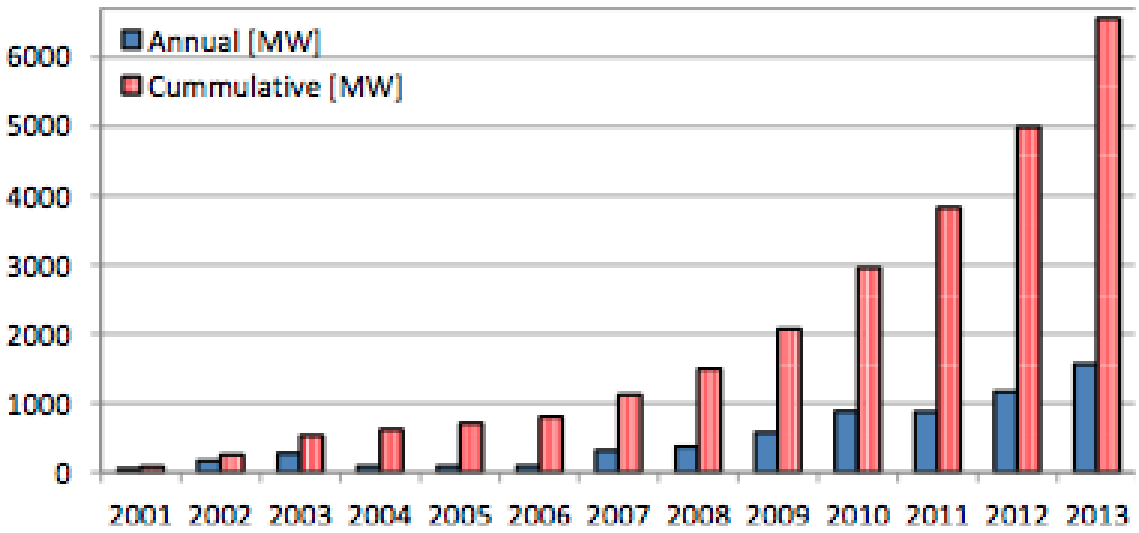

Figure 1.2: Annual and cumulative offshore wind installations

Due to this expected growth in the offshore wind-industry, in 2012, Umoe Mandal started development of a 25m, narrow-side-hull SES with high lift fan capacity, intended to serve as a crew transport- and service vessel for offshore wind turbines. One of the most important cost driving terms for offshore wind farms is downtime due to sea states preventing technicians and maintenance personnel from boarding the turbine. The new vessel features a new *Boarding Control System* (BCS), developed by (Auestad et al., 2014) and (Auestad et al., 2015), which damps the vertical motions significantly at zero forward velocities, thus improving accessibility to the turbines and widening the operational window. The vessel is called the $Wave\ Craft$, and the simulation results presented in this thesis is based on a generic SES ship with the same size as the Wave Craft. However, let it be clear, the results presented do not represent the design or performance of the Wave Craft series. The Wave Craft is a 25m long SES, with a top speed of 40+ knots and supplied

with airflow capacity higher than a traditional SES. A one-sider, intended for advertising purposes, containing the main dimensions and properties of the Wave Craft is included in Appendix E. While conventional service vessels in the offshore wind industry are unable to perform safe crew transfers for significant wave heights any higher than 1.5m, the Wave Craft increases this limit to close to 2.5m, which, according to (OWA, 2010), corresponds to an annual increase in "safe sea state days" from 54- to 79%.

The trend in the wind industry is also that the fields are located further and further from the shore, making them challenging, or even impossible, for conventional small service vessels to reach in a work day. This necessitates the use of larger platforms with accommodation capacities to perform the crew transfers. These vessels are called Offshore Service Vessels (OSVs), and are much similar to conventional Platform Supply Vessels (PSVs), often equipped with motion compensated gangways to enable safe transfers. These are expensive, slow vessels with small operational windows and relatively large levels of motions causing discomfort for the crew members. There are indications that a large SES would be a strong alternative to such traditional OSVs. Due to their large width, SESs exhibit good stability properties and they are also able to travel nearly twice as fast, with the same propulsive power as conventional OSVs. Further, the strong results from the zero speed vertical motion damping done in (Auestad et al., 2015) suggests that a SES could be made significantly smaller than a conventional OSV, while still maintaining strong seakeeping properties. There are, however, a couple of un-investigated obstacles. Interaction of large vessels with fixed offshore structures requires some sort of automated control over the horizontal motions. A SES is, in theory, fully actuated in the horizontal plane, thus it should be possible to implement a Dynamic Positioning system to perform station keeping. This has never been done, and there are a few features of the plant that complicates this process. If we want to utilize the airflow through the vent valves for thrust, there will be strong limitations in capacity compared to conventional bow thrusters. The latter is, unfortunately, impossible, or at least; highly *impractical*, to fit in the Wave Craft due to the extremely narrow bow construction. The fast dynamics of the actuators related to the cushion control of a SES does, on the other hand, imply entirely new possibilities for 1st order motion damping, and this thesis will investigate the possibilities of, in fact, using the vent valves as bow thrusters, in combination with the water jets, for implementation of a dynamic positioning system. We will also investigate an augmentation of the excisting BCS, (Auestad et al., 2015), to include cushion pressure feedback and, as far as possible, damping of the 1st order motions in sway.

1.2 Surface Effect Ships

Surface Effect Ships (SESs), also known as sidewall hovercrafts, are vessels with a twin hull configuration and an air cushion which is enclosed laterally by rigid side hulls and longitudinally by the flexible rubber *bow-* and *stern seals*. The rigid side hulls differ these vessels from conventional hovercrafts and allow for water jet propulsion, but also ensures sufficient directional stability, as opposed to the hovercrafts where the latter is a major problem. A set of one or more *lifting fans* provides an inflow of air to the air cushion, which increases the *uniform cushion pressure* to provide lift. The main channel for out flow of air is through the *vent valves*, which is controlled by the *vent valve louvers*, illustrated in figure 1.3.

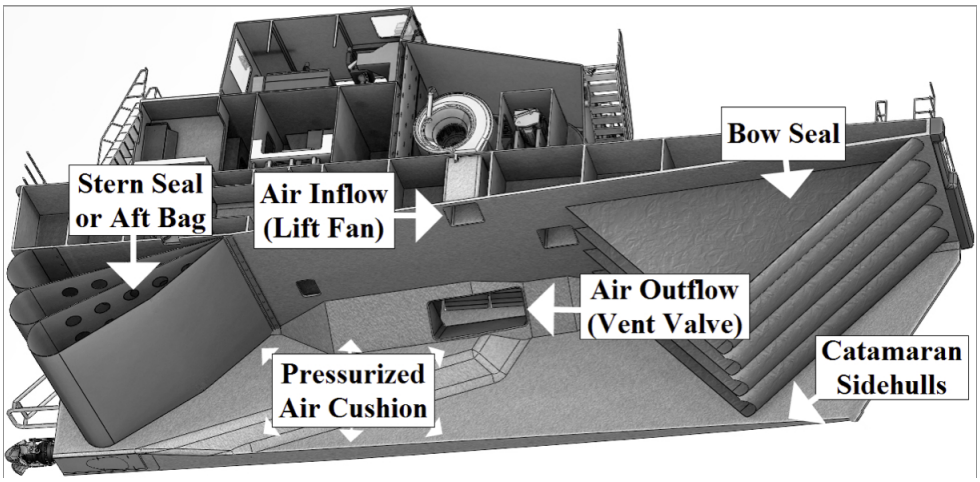

Figure 1.3: Key SES structure

The excess pressure inside the air cushion can account for the lift of as much as 80% of the total displacement, and, because of this, only a minor part of the side hull surface will be submerged and subject to hydrodynamic- and hydrostatic loads. This means that the SESs exhibit extremely low water resistance, which enables them to achieve high velocities with relatively low propulsive power. The stern seal *bag*, illustrated in figure 1.4 for a *three lobe*-configuration, is pressurized by an individual fan, to ensure sufficient sealing from the atmosphere. These fans are called *booster fans* and supplies the bag with a higher (delta) pressure than the pressure found in the cushion. The desired delta pressure is typically 5-15%.

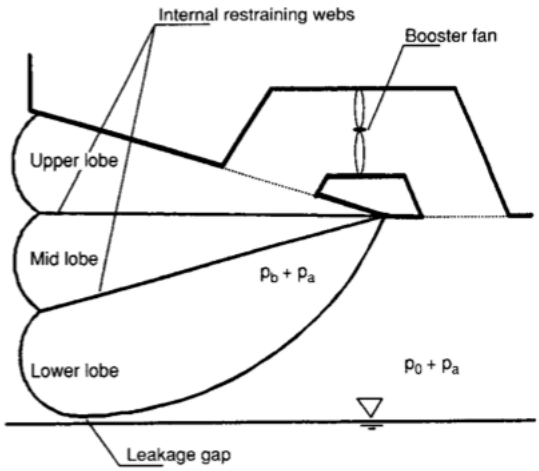

Figure 1.4: Stern seal of SES, from (Faltinsen, 2005)

The bow seal *fingers*, in figure 1.5, are of a "self sealing nature", thus the excess pressure inside the cushion should ensure sufficient ambient sealing by "blowing themselves up" or expanding themselves toward the neighbour finger. There will be leakages through these seals, however, around equilibrium and in calm sea- conditions these leakages are negligible compared to the flow through the vent valves. The leakages beneath the stern- and bow seals, and underneath the side hulls in severe conditions is denoted *passive leakages*, while the airflow through the louvers is called *louver leakage*. The latter will, in most conditions, be significantly larger than the former.

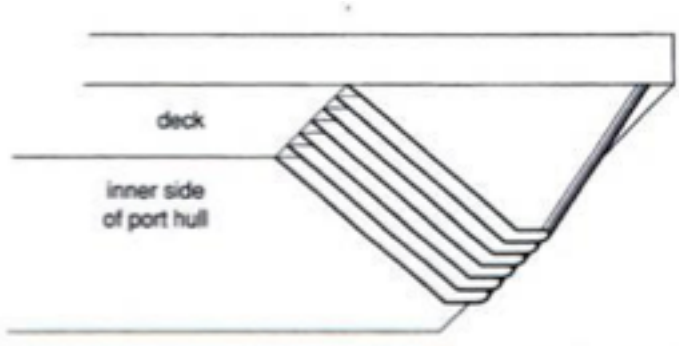

Figure 1.5: Bow seal comprised of individual fingers, from (Faltinsen, 2005)

This thesis will concern a SES with extremely narrow side hulls, and an installed lift fan capacity around twice of what you normally find on SESs of comparable size. By changing the angle of the Vent Valve Louvers, the leakage area A^l can be adjusted, in turn controlling outflow of air and, thus, the pressure inside the cushion. The possible pressure variation is a function of lift fan capacity, total vent valve leakage area, vertical hull height and seal design. Typically, the bag geometry should allow the propulsion system to stay submerged while the bottom point of the fingers should

be close to the baseline. In higher seas, the relative motion between the vessel and the free surface can induce rather large pressure variations.

The United States Navy launched a 10-ton test craft called the XR-1 in 1963, and, by that, introduced the modern SES concept. The US navy introduced more experimental crafts, among these the SES-100b which could achieve a speed of 91.9 knots (Butler, 1985). The SES vessel type has later been used in several applications, spanning from military use to high-speed passenger vessels. In Norway, production of the first commercial SESs began in the 1980s, by the shipyard Brødrene Aa (Yun and Bliault, 2012). They produced a series of 17 passenger SESs, which mostly ended up serving in the Mediterranean- and the Caribbean ocean. With top speeds close to 50 knots, these SESs proved themselves serious competitors to the conventional high speed passenger ferries.

Unless controlled, all SESs suffers from vertical accelerations in the heave-cushion pressure resonance frequencies. When the encountered wave frequencies approaches the resonance domain, the "Cobblestone effect" occurs, and active control of the cushion becomes necessary. The *Cobblestone effect* is more thoroughly described in section 2.2.1 and found negligible for the scope of this thesis due to the low vessel velocities. This effect is, in short, uniform and spatially varying pressure fluctuations, acoustic modes, occurring at resonant frequency, thus able to induce rather large vertical motions.

Figure 1.6: Illustration of the Wave Craft when docked, courtesy of Umoe Mandal

The first Ride Control Systems (RCS), designed to compensate for these effects allowed small amounts of air to escape the cushion, and some of the first literature work on the field was done by (Kaplan and Davis, 1974). Sørensen and Egeland (1995) described and solved the problem using partial differential equations and a dissipative control approach. A Boarding Control System (BCS) for vertical, zero forward speed, motion damping was introduced by (Auestad et al., 2015) for the Wave Craft, figure 1.6, and the theory and assumptions behind his work makes the basis for some of the vertical motion damping presented in this thesis, which is developed to concern horizontal motion damping as well and cushion pressure feedback as well. Both Auestads and the work of this thesis is done in cooperation with the shipyard Umoe Mandal and The Norwegian University

of Science- and Technology (NTNU).

1.3 Dynamic Positioning

According to *Det Norske Veritas* (, DNV), a Dynamically Positioned vessel is a vessel which automatically maintains its position and heading exclusively my means of active thrusters. Modern DP systems are normally comprised of the blocks illustrated in figure 1.7

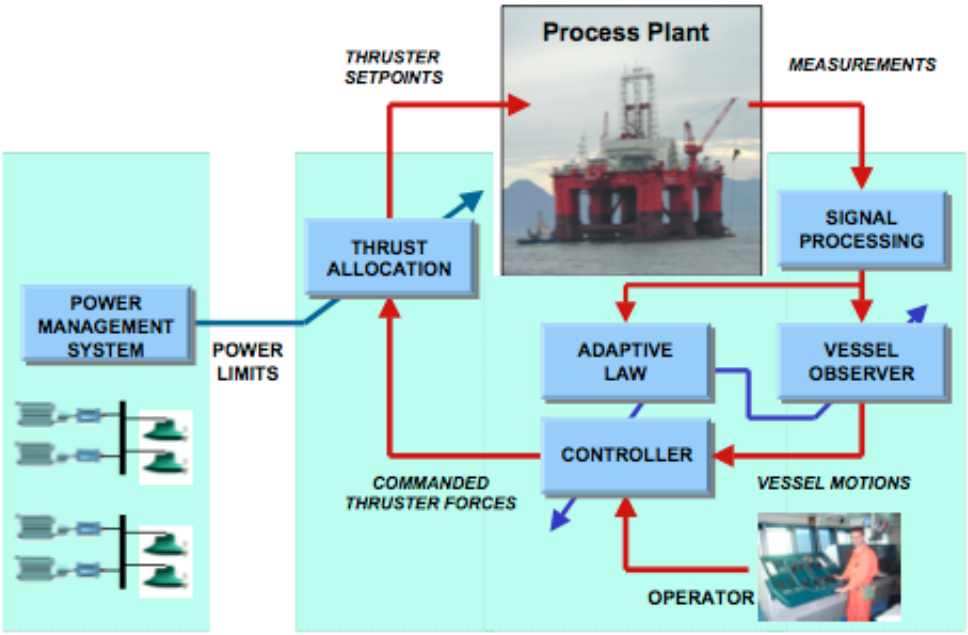

Figure 1.7: Main DP-components, from (Sørensen, 2013), exemplified for a Semi-Submersible drilling rig

The respective blocks will be thoroughly explained in chapter 3, and a mere short introduction to the functionality will be given here. Modern DP systems are based on the use of vessel observers in separating the low frequency- and the wave frequency motions from each other as well as estimating unmeasured states. E.g., a source of position measurements could be through the means of a GPS sensor, a *taut-wire* or a *hydro-acoustic*-system. The heading angle of the vessel can be easily measured by a gyrocompass. The respective velocities, however, are hard to measure accurately and should be estimated by the use of an observer in combination with the available sensor data. Due to the nature and slow dynamics of common DP actuators, i.e. azimuth thrusters, tunnel thrusters, diesel engines etc, the system is only able to compensate for the slowly varying forces

affecting the system. The total motion of the vessel is comprised of both a high frequency- and a low frequency component, where it is highly unfavourable to send information regarding the former in to the controller, as this will only harm the performance. Therefore, by using a mathematical model of the vessel dynamics, an appropriately tuned observer should separate these components so that only the slowly varying signals are sent to the controller.

The controller compares the actual earth-fixed position of the vessel with a reference position and generates an output based on the difference between thefse two. This output is a vector containing the desired forces and moments necessary to move the vessel towards the reference position or keep it stationary at it. This output is sent to the thrust allocation block, which distributes the desired thrust among the available thrusters in a manner such that the resulting forces made by the individual thruster forces equals the desired output from the controller. Several methods and algorithms have been investigated for this process, and one based on optimization is presented and derived for the SES in chapter 3. The output from the controller can also be overridden by the DP-operator, and the result of the above is that the vessel moves as desired by the DP system or the operator, or performs station keeping, i.e. it does not move, at all. This enables several operations in sea states that would have made them impossible without automatic thruster control.

1.4 Previous Work

1.4.1 SES Dynamics and Motion Control

The unique coupling between thermodynamics and hydrodynamics in SESs generates some special phenomenons that has been studied ever since the very first vessels where launched in the early 1960s. The following section will present a short, somewhat chronological presentation of the different work done within the field. Kaplan and Davis (1974) provided the first mathematic model of the vertical plane dynamics of SESs, which set the foundation for most of the following work within the field together with the work done in (Kaplan et al., 1981). Thorough investigations of these dynamics were necessitated by the Cobblestone oscillations, which, hypothetically, are able to induce rather large vertical motions causing uncomfortable conditions on board the vessel. In order to achieve comfort and crew workability, these motions must be damped. Kaplan et al. (1981) based their work on the assumption that the majority of the induced motions are due to the forces from the dynamic, uniform cushion pressure, and used the coupled equations of motion to derive a ride controller which did reduce the vertical vibrations on board the

vessel. Sørensen and Egeland (1995) and (Steen, 1993) extended this work to include the effect of both the uniform- and spatially resonant pressure components, the Cobblestone oscillations. They derived the dynamics of the spatially varying pressure components as acoustic resonances and developed a control system that provided active damping of both the uniform pressure and the acoustic modes. Full-scale tests were performed on a 35m long test craft, with highly satisfying results. Ulstein and Faltinsen (1995) extended the work to include an analysis containing the dynamics of the flexible stern seal bag, and its effect on the cobblestone oscillations. The Oksøy- and Alta class MCMV-vessels features the first examples we could find of utilizing the potential energy in the cushion to provide lateral thrust, however we can not seem to find any published articles concerning this subject. The system featured by the MCMVs is quite simple, and based on fully opening or closing either of the two vent valves, shown as the small dark rectangle in the bow in figure 1.8. This directs the entire airflow in one direction, thus producing a net thrust as will be explained in chapter 2.2.5. The system was developed by Maritime Dynamics (MDI) and Kongsberg Maritime. There is no gain control of this system, and the lateral thrust is thus either 0% or 100%. Despite its simplicity, experiences shared by the crew on board the vessels reveals that this is a highly valued feature and an important tool, which, in special, simplifies the process of docking the vessel. Until late 2000s, most of the work done on SESs concerned damping of motions at medium/high forward velocities, by feedback of the dynamic pressure components. Basturk and Krstic (2013) proposes a method for adaptive wave cancellation by acceleration feedback, for ramp-connected SESs at low- to zero speed. The motivation was to reduce the relative motions between the SES and an LMSR (Large, medium-speed, roll-on/roll-off-vessel) to simplify cargo transfer between the two. Auestad et al. (2015) developed the *Boarding Control System* (BCS) which, based on state-feedback control, performed significant damping of the vertical motions of a free-floating- and wind-turbine column

Figure 1.8: Vent Valves of the Oksøy-class, courtesy of Umoe Mandal

docked SES, figure 1.6. The work was done in cooperation with Umoe Mandal, and full-scale testing of the Wave Craft vessel during sea trials in March 2015 proved the effect of the controller.

1.4.2 Dynamic Positioning

Faÿ et al. (1990) provides a thorough description of the early history of automatic position control of marine vessels. As for so many other technological revolutions, this invention came as a result of a desire to extract more oil. The first underwater oil wells were drilled in quite close proximity to the shore. These wells were drilled from fixed installations, connected to land by wood- or steel constructions. As the oil exploration moved further offshore, the need for stationary, floating structures, in order to be able to perform drilling, was revealed. Until the 1950s, this was done from moored platforms. However, as the water became deeper and the conditions got worse, as the distance from land increased, the limitations behind mooring lines became apparent. Not only did the moored vessels exhibit oscillatory motions of rather large amplitudes in hostile conditions, due to low hydrodynamic damping and the respective construction, but the nature of the system also implied that even the slightest change in position necessitated quite large operations in rising the mooring lines etc. Thus, in 1961, as a result of the *Mohole*-project, the drilling vessel *Cuss* 1, figure 1.9, performed station keeping by the means of 4 manually controlled thrusters and a hydro acoustic positioning system, within a 180m radius circle. Compared to todays standards, this barely classifies as station keeping, however compared to the state of the art in the 1950s, this was a technological leap. Later the same year, the vessel *Eureka*, from the *Shell Oil Company*, performed station keeping by utilizing an automatic control system and three years later the *Caldrill*1 maintained position with four 300hp thrusters and a double taut-wire positioning system. These three vessels marks the start of the era of modern station keeping. Simultaneously with the American adventure, *Gaz de France* con-

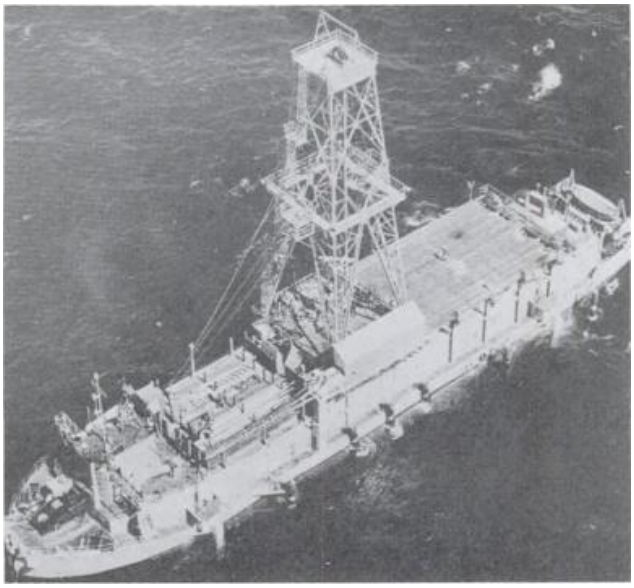

Figure 1.9: Cuss 1, (Faÿ et al., 1990)

ducted experiments with the vessel *Terebel*, which by 1971 was able to perform station keeping, install subsea wellheads, laying hoses and equipment on the seabed, etc, enabled by an analog, automatic station keeping controller. The first DP systems used simple PID-controllers and notch filters, or even a mere low-pass filter, in order to filter out noise and some high frequency motion components from the position sensor signals. However, such filtering is not able to reconstruct unmeasured states, perform dead-reckoning nor do any effective wave filtering, as opposed to modern observer theory. In the early 1960s, (Kalman, 1960) and (Kalman and Bucy, 1961) introduced the *Kalman* filter, which in 1976 enabled (Balchen et al., 1976) to develop the *modern* DP system, based on optimal filtering and control theory. This was further developed by (Balchen et al., 1980). This was regarded a large breakthrough, and a significant contribution to other aspects of marine control systems. Fossen (1994) provides a significant simplification of the notation related to the mathematic modelling of such plants, with the vectorial form exemplified by equation (2.65), chapter 2.3.1, later in this thesis. Strand and Fossen (1999) introduces a passive, nonlinear observer with adaptive wave filtering, which reduces the complexity found in many traditional observers. In the later years, much of the work on the field has been motivated by a desire to make operation in new and harsher conditions possible. Lindegaard (2003) proposes the use of acceleration feedback in order to enhance the performance of DP systems in severe seas, while (Nguyen et al., 2009) proposes a model for dynamic positioning in ice conditions. There is not much work found regarding DP operations of high-speed vessels, specifically, however (Hamilton, 2007) argues for the use of water jet drives as a mean of main propulsion for DP operated vessels. The first example found of utilizing the vent valve airflow for lateral thrust is by the MCMV Oksøy class, however we can not seem to find any published work regarding this project.

1.5 Contributions

1.5.1 Nonlinear Cushion Pressure Model

Common practice within the field of vertical SES dynamics is to use a linear model describing the pressure dynamics around the equilibrium working point of the system. This leads to several simplifications, and yields a linear vessel model, which is useful in e.g. a control design setting. This thesis, however, introduces a nonlinear model of the pressure dynamics, which should lead to higher accuracy for larger pressure variations, and is to be used as a process plant model. We will also present an in-depth study of the equations behind the cushion dynamics, by using Reynolds

Transport Theorem and Eulers equations as a foundation, which we have not found presented in any other published work.

The nonlinear model introduces a state dependency of the cushion air leakage (section 2.2.3). This should account for the fact that the leakage beneath the bow- and stern seals of the cushion increases at a very high rate as the vessel pitches and heaves above a given set point. Implementation of these effects by saturating the pressure state was considered, but found to remove too much of the real-life dynamics of the plant, where the pressure trajectory strongly depends on the vessel trajectory. The effect of this state-dependent leakage area was implemented by a higher-degree polynomial, so that the passive leakage became significant as the heave excitation exceeded -0.6m (according to the sign convention defined in chapter 2) from the equilibrium state, 'on-cushion'. The *tuning* of this polynomial was done by comparing the step responses of the system with experiences from the model tests done by (Auestad et al., 2015).

1.5.2 Mathematical Modeling- and Control of Lateral Forces on a SES

For DP-applications, we are primarily concerned about counteracting the slowly varying 2nd order loads. Due to relatively slow actuator dynamics and high inertial forces, these loads are the only one traditional setups are able to handle. This thesis, however, concerns damping of 1st order heave motions, and will also investigate the possibilities for utilizing the vent valve thrust to compensate for 1st order motions in sway as well. This should be feasible due to the quick dynamics of the hydraulic vent valve louver actuators, which means that the maximum thrust can be transferred from fully port to fully starboard in about one tenth of a second. We present a model for these forces, and a control scheme for computing the lateral leakage (ref chapter 3.6) corresponding to a given lateral thrust.

1.5.3 Control of Total- and Lateral leakage of Vent Valves, With Saturation Handling

Chapter 3.6 also derives a scheme for saturation handling of the above mentioned controller, which can prioritize either of the two desires, total leakage area or lateral leakage area. This controller also distributes the commanded leakage areas between the two vent valves, the port and starboard, in a manner so that the different control desires are fulfilled as far as possible.

1.5.4 Linear Thrust Region Representation of SES

Certain thrust-allocation methods, specially those based on quadratic programming, as used in this thesis, necessitates a linear representation of the thruster capacities, the $thrust - region$. We could not find any literature describing such a representation for a twin-hulled water jet propelled vessel, nor for a SES where the vent valve ducts can be used as a source of lateral thrust. We will present a linearized thrust envelope for each of the SES thrusters, including the vent valves, which are described in section 3.5.2.

1.5.5 Thrust and Azimuth Control of Water Jets

Since there are DP systems in commercial use today that features water jets as main propulsors, it is highly likely that there exists some algorithms for zero speed, 360° thrust- and azimuth control of these. However, we could not seem to find any published articles or papers regarding the subject, and we will therefore propose a method of obtaining the desired thrust- magnitude and direction from a water jet drive, in section 3.7.

1.5.6 Dynamic Positioning and Horizontal WF Motion Damping of SES

The result of the derivations and findings in this thesis means that we have developed a control system which, verified by simulations, should enable a SES to perform station keeping when subject to rather severe environmental loads and also reduce the amplitudes of the lateral wave frequency motions.

1.6 Thesis

This thesis will investigate the potential for utilizing the potential energy in the pressurised cushion to provide lateral thrust, and how to apply this in combination with the water jets to obtain control of the vessels in both the horizontal- and vertical plane. To do this, we need to derive an accurate model for the cushion pressure dynamics, and an expression for the potential thrust it can provide. To perform simulations, and investigate the validity of the model, it is also necessary with a set of equations describing the dynamics of the vessel, both when subject to rapidly oscillating forces, but also for a low frequency situation, such as the station keeping problem. We will also define the necessary kinematics in order to simulate the vessel dynamics in an inertial, *global* reference frame. We will develop and propose a control system, where the control outputs will be based on state- and

state-derivative feedback. A method for thrust allocation is also necessary in order to distribute the desires for body fixed forces among the different actuators, which in turn yields a demand for local thrust/actuator control in order for the respective actuators to perform their assigned tasks. The validity of the derived model, and the efficiency of the controller is illustrated by simulations using MATLAB and Simulink.

1.6.1 Organization of Thesis

Chapter 2 - Mathematic Modelling derives a mathematic model for the system being investigated. We first define the regular kinematic equations necessary for analysis and control of the maneuvering- and station keeping problem as well as the different reference frames and sign conventions used in the thesis. We propose a nonlinear model for the cushion pressure dynamics and a generic expression for the thrust provided by the airflow through the vent valves which will be utilized later in the station keeping controller as well as the Wave Frequency motion damping. The different mechanisms of a water jet propulsor, as well as a qualitative expression for the provided thrust is presented, before we define the regular expressions for the vessel dynamics, for both the low- and wave frequency problem. The chapter ends with a model for the environmental loads on the system, which will be used to simulate the external disturbances in chapter 4.

Chapter 3 - Control System Design regards all the different aspects of the SES control system. In the beginning of the chapter, the control objective is defined, and we differ between the Low- and Wave Frequency problem. We will then derive the control plant model. Since the feedback gains for the wave frequency motion compensation is model based, we need a linearized, simplified model describing the dynamics of the system. The feedback gains are, in turn, computed using an LQR-like synthesis, and the proper state trajectory weighting is calculated by a proposed method based on a desired phase shift between two control signals. The simple PID-controller used for the DP problem is then defined, before we propose a method for thrust allocation, based on quadratic programming. This necessitates a linear representation of the thruster-capacities, which is then, in turn, derived and implemented in the optimization problem in order to provide the necessary thrust from each individual thruster so that the desire for body fixed linear forces and momentums from the respective controllers are obtained. The chapter ends with two sections about thrust control, for the vent valves and water jets respectively. The first of these two regards the problem of combining the desires for lateral- and total leakage area in order to satisfy both the heave compensation problem

and the desire for lateral force. The water jet section describes a method of obtaining a given azimuth angle and thrust magnitude from a single water jet drive, by the means of engine speed, the angle of the steering nozzle and the state of the deflector shield.

Chapter 4 - Results and Discussion This chapter is meant to show the effect and validity of the previous chapters. The models derived in chapter 2 are tested for different inputs and disturbances, and the controllers derived in chapter 3 are tested for various conditions in order to prove that they are effective. In addition, the WF process plant is tested in an uncontrolled environment, subject to different disturbances in order to obtain a qualitative understanding of its uncontrolled behaviour. The respective controllers are also tested simultaneously, which, among other things, indicates that the system is able to perform strong vertical motion damping and station keeping simultaneously. The chapter is summed up in a discussion section, where we evaluate the results and comment on any special findings.

Chapter 5 - Concluding Remarks provides a conclusion of the work done in the thesis, and the findings from the simulations. We will evaluate the potential of this concept and also, in a further work section, what needs to be done in order to present a working system.

Appendix, contains all relevant information about the parameters used in the simulations. We have also included a one-pager with some key-facts about the Wave Craft.

Chapter 2

Mathematic Modelling

2.1 Kinematics and Points of Reference

This thesis will investigate a 6 Degrees of Freedom (DOF) problem. The hydrodynamic equations, the lift- and thrust from the uniform pressure inside the cushion and the thrust from the water jets will be derived in a body fixed coordinate system $\{b\}=(x_b,\ y_b,\ z_b)$ with origin o_b, while the "global" orientation and position of the vessel will be described in an inertial reference frame, i.e. the North-East-Down (NED) frame, $\{\text{n}\}=(x_n,\ y_n,\ z_n)$ with origin o_n. The oscillatory motions around equilibrium, i.e. the wave frequency motions of the vessel will be described in a sea keeping reference frame {s}, with origin o_s. The sign conventions and notations will be in compliance with the proceedings of the Society of Naval Architects and Marine Engineers from 1950, (SNAME, 1952), and are summarized in table 2.1, as given in (Fossen, 2011) but altered to include the displacements in {s}.

DOF	Forces and moments	Linear and angular velocities	Positions and Euler angles	Position in {s}
1 motions in the x direction (surge)	X	u	x	η_1
2 motions in the y direction (sway)	Y	v	y	η_2
3 motions in the z direction (heave)	Z	w	z	η_3
4 rotation about the x axis (roll)	K	p	ϕ	η_4
5 rotation about the y axis (pitch)	M	q	θ	η_5
6 rotation about the z axis (yaw)	N	r	ψ	η_6

Table 2.1: Summary of the SNAME convention

The x_b-axis is the longitudinal axis directed from aft to fore, positive y-axis is directed to the starboard side of the vessel while the positive z-axis is the normal axis to the horizontal plane pointing downwards. Thus, in compliance with the right-hand-screw rule, i.e. a right hand screw advancing in the positive direction of the axis of rotation, positive pitch is defined as bow up while positive yaw-motion is defined clockwise. The roll-motions of the vessel will not be given any significant attention in this thesis, as they are uncontrollable with the actuators assumed available. The body-relative orientation of {b} is illustrated in figure 2.1

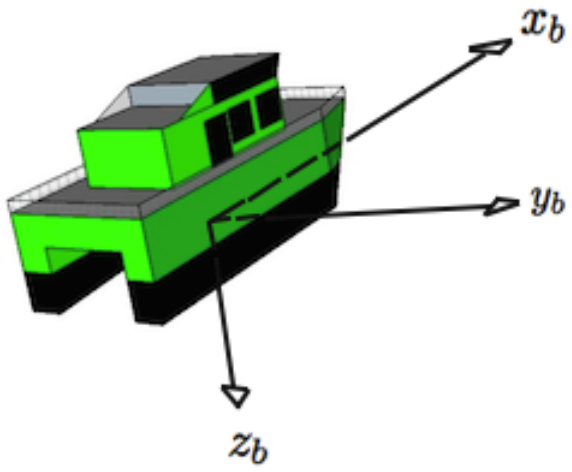

Figure 2.1: Body-fixed coordinate system {b}

The Body-fixed linear-, and angular velocities given by table 2.1 are unified in the vectors $V^b_{b/n}$ and $\omega^b_{b/n}$, as given by equations (2.1) and (2.2).

$$\mathbf{v}^b_{b/n} = \begin{bmatrix} u & v & w \end{bmatrix}^T \in \mathbb{R}^3, \tag{2.1}$$

$$\omega^b_{b/n} = \begin{bmatrix} p & q & r \end{bmatrix}^T \in \mathbb{R}^3. \tag{2.2}$$

The notation used above, e.g. for $V^b_{b/n}$ indicates that we are investigating the velocity of $\{b\}$ with respect to $\{n\}$, expressed in $\{b\}$. The positions and Euler angles defined in table 2.1, are relative to some fixed, inertial reference frame, in our case {n}, i.e., for the euler angle ψ, which represents

the vessels yaw-motion, it is defined as the angle from the vertical plane $z_n x_n$ to the vertical plane $z_n x_b$, positive in the positive sense of rotation about the z_n-axis according to the right-hand screw rule. The NED frame is thoroughly described in (Fossen, 2011), and is the coordinate system we refer to in our everyday life, thus, the reference frame $\{n\}$ is defined as the tangent plane on the surface of the earth. The x-axis of {n}, x_n, points towards true north, y_n points towards east while z_n points downwards normal to the earth's surface. For a vessel at low speeds operating in a local area, such as for the dynamic positioning problem, this frame can be regarded inertial. The NED positions are unified by the vector $p^n_{b/n}$.

$$p^n_{b/n} = \begin{bmatrix} N & E & D \end{bmatrix}^T \in \mathbb{R}^3 \tag{2.3}$$

The attitude, i.e. the orientation of the vessel, is in a similar manner given by the vector Θ_{nb}, where the subscript notation denotes the *euler*-angles between {n} and {b}.

$$\Theta_{nb} = \begin{bmatrix} \phi & \theta & \psi \end{bmatrix}^T \in \mathbb{S}^3, \tag{2.4}$$

where the set $\mathbb{S}^3$ is a sphere. The angle ψ, illustrated in figure 2.2, is called the *heading* angle and it denotes the orientation of the vessel in the horizontal plane, thus it is of great importance in dynamical positioning. The variable θ denotes the pitch-angle and ϕ denotes the roll motions of the vessel.

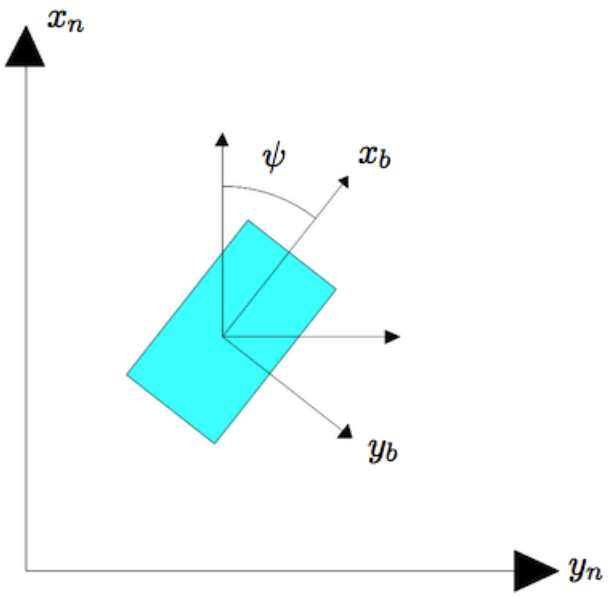

Figure 2.2: Definition of the quantity ψ

We combine the displacements in {n} and velocities in {b} into two vectors, and define:

$$\eta_n = \begin{bmatrix} p^n_{b/n} \\ \Theta_{nb} \end{bmatrix} \in \mathbb{R}^3 x \mathbb{S}^3 \quad \text{and} \quad \nu = \begin{bmatrix} v^b_{b/n} \\ \omega^b_{b/n} \end{bmatrix} \in \mathbb{R}^6. \tag{2.5}$$

The vector containing the states in {s} is defined as

$$\eta_s = \begin{bmatrix} \eta_1 & \eta_2 & \eta_3 & \eta_4 & \eta_5 & \eta_6 \end{bmatrix}^T, \tag{2.6}$$

which follows the same sign conventions as given above. We will also define a vector f^b_b containing the body fixed forces, running through the point o_b and a moment vector m^b_b, containing moments about the point o_b, in the respective planes, as in equation (2.7a) and (2.7b)

$$f^b_b = \begin{bmatrix} X \\ Y \\ Z \end{bmatrix} \in \mathbb{R}^3, \tag{2.7a}$$

$$m^b_b = \begin{bmatrix} K \\ M \\ N \end{bmatrix} \in \mathbb{R}^3. \tag{2.7b}$$

The two vectors given by equations (2.46a) and (2.46b) can be further unified into the vector τ, defined in equation(2.8).

$$\tau = \begin{bmatrix} f^b_b \\ m^b_b \end{bmatrix}. \tag{2.8}$$

Hence the general motion of the 6 DOF system is described by the vectors η_n, ν and τ. Further, the following definitions are made:

1. The point o_b is defined as the origin in the body fixed reference system {b}, and is placed in the equilibrium water plane, on the line passing through the vessels centre of gravity.

2. o_n is defined as the origin of the inertial reference frame {n}. The translational exceptions, i.e. in surge, sway and heave, are defined as the motions of o_b, relative to o_n. In the equilibrium state, o_n and o_b will coincide.

3. The point o_s is defined as the origin of the seakeeping reference frame. The WF motion study of this thesis will investigate the motions of o_b relative to o_s. This point is placed in the equilibrium waterline, and coincides with o_b in the equilibrium state.

The relationship between {b} and {n} will be described by the means of Euler angles. These represent an intuitive relationship between the two frames, and are easily computed. Euler angles as the mean of orientation representation implies a singularity in $\theta = \pi/2$ (Ang Jr and Tourassis, 1987), however this is not relevant for the scope of this thesis as such pitch angles are (hopefully) avoided and since we only will be looking at the horizontal problem in {n} we can safely neglect these singularities. The transformation is done according to the method explained in (Fossen, 2011). The transformation uses the Euler angles ϕ, θ and ψ to rotate the body-fixed linear velocity vector $v^b_{b/n}$ into {n}. From this, the linear velocities in {n} can be expressed as given by equation (2.9):

$$v^n_{b/n} = R^n_b(\Theta_{nb}) v^b_{b/n}, \tag{2.9}$$

where $R^n_b(\Theta_{nb})$ is a rotation matrix. This is a product of three principal rotation matrices, where each single one rotates the system around one of the inertial reference frames respective axis. Expanded, this rotation matrix is given by:

$$R^n_b(\Theta_{nb}) = \begin{bmatrix} c\psi c\theta & -s\psi c\phi + c\psi s\theta s\phi & s\psi s\phi + c\psi c\phi s\theta \\ s\psi c\theta & c\psi c\phi + s\phi s\theta s\phi & -c\phi s\phi + s\theta s\psi c\phi \\ -s\theta & c\theta s\phi & c\theta c\phi \end{bmatrix}, \tag{2.10}$$

where $s(\cdot)$, $c(\cdot)$ and $t(\cdot)$ denotes the sine, cosine and tangent of the given argument, respectively. The angular transformations are done in a similar manner, through the relation given by equation (2.11)

$$\dot{\Theta}_{nb} = T_\Theta(\Theta_{nb}) \omega^b_{b/n}, \tag{2.11}$$

were the transformation matrix $T_\Theta(\Theta_{nb})$ is defined as

$$T_\Theta(\Theta_{nb}) = \begin{bmatrix} 1 & s\phi t\theta & c\phi t\theta \\ 0 & c\phi & -s\phi \\ 0 & s\phi/c\theta & c\phi/c\theta \end{bmatrix}. \tag{2.12}$$

Notice that

$$p_{b_n}^n = \int_0^t v_{b/n}^n(\tau)d\tau, \tag{2.13}$$

for some dummy-variable τ. We can then summarize equations (2.9) and (2.11) into the 6 DOF kinematic equations expressed in vector form as

$$\dot{\eta_n} = J_\Theta(\eta_n)\nu \tag{2.14a}$$

$$\Updownarrow \tag{2.14b}$$

$$\begin{bmatrix} \dot{p}_{b/n}^n \\ \dot{\Theta}_{nb} \end{bmatrix} = \begin{bmatrix} R_b^n(\Theta_{nb}) & 0_{3x3} \\ 0_{3x3} & T_\Theta(\Theta_{nb}) \end{bmatrix} \begin{bmatrix} v_{b/n}^b \\ \omega_{b/n}^b \end{bmatrix}. \tag{2.14c}$$

This allows us to derive the hydrodynamic equations for the body fixed reference frame {b} in a regular manner. If we only look at a 3 DOF problem in the NED, i.e. the surge-, sway- and yaw motions, the transformation can be simplified to

$$\dot{\eta_{3n}} = R_{3d}(\psi)\nu, \tag{2.15}$$

where $\eta_{3n} = \begin{bmatrix} x & y & \psi \end{bmatrix}^T$ and

$$R_{3d}(\psi) = \begin{bmatrix} c\psi & -s\psi & 0 \\ s\psi & c\psi & 0 \\ 0 & 0 & 1 \end{bmatrix}. \tag{2.16}$$

2.2 Pressure Effects

This plant will exhibit a strong coupling between the state trajectories in heave and pitch, and the excess pressure inside the cushion. By commanding different vent valve leakage areas on both sides, the airflow is also able to induce significant levels of lateral thrust, which can be exploited for control of the vessel in the horizontal plane as well.

For calm seas, the cushion pressure depends mainly on the leakage areas of the vent valve louvers and the speed of the lift fan engine(s). In most real life sea states, however, the cushion pressure will, in addition to the controlled leakage areas, be influenced by the excitations of the vessel in the vertical DOFs and the experienced wave propagation. Experiences also show that there will be leakages of air beneath the bow- and stern seals, which exhibits a strong dependency on the heave- and pitch levels. The excess pressure in the cushion will be comprised of both a spatially varying

component and a uniform component, both will be explained in the following.

2.2.1 Spatially Varying Pressure

In addition to the uniformly varying pressure, the vessel will exhibit spatially varying, resonant pressure components, acoustic modes. These components are closely described in (Sørensen and Egeland, 1995). This phenomena, which is part of the Cobblestone effect can, for the odd modes, induce rapidly oscillating pitch motions due to non symmetries in the pressure relative to the $y_b z_b$ plane. Each acoustic mode corresponds to one of the spatially varying air cushion eigenfrequencies. The eigenfrequency ω_j for mode j is given by equation (2.17)

$$\omega_j = c\frac{j\pi}{L}, j = 1, 2, 3, ..., \tag{2.17}$$

where L denotes the length of the cushion and c is the speed of sound, roughly equal to 340m/s. Excitations by high-energy waves in these frequencies can for the odd modes induce relatively large pitch motions, oscillating at the given frequency, causing large levels of discomfort for the crew. For the Wave Craft, by inserting numerical values, we find that the lowest spatially varying eigenfrequency of the air cushion is $\omega_1 \approx 50[rad/s]$. The sea states relevant for this thesis are mainly with high-energy waves with periods between 5 and 10 seconds. Since we are only investigating a low- to zero speed problem, only small ripples can possible occur at such high frequencies as ω_1. Since these carry far from enough energy to cause any large excitations we notice that the Cobblestone effect will only be of concern for high velocities and/or long air cushions. For nonzero velocities, the experienced frequency, i.e. the frequency experienced by an observer moving along with the vessel, is given by the frequency of encounter, ω_e, in equation (2.18).

$$\omega_e = \omega_w - \frac{\omega_w^2}{g}\cos(\beta_{wa}), \tag{2.18}$$

where ω_w is the frequency of the waves observed by a stationary observer in an inertial reference frame, g is the gravitational acceleration and β_{wa} is the angle of wave encountering relative to x_b. For instance, for the Skjold-class of coastal corvettes, illustrated in figure 1.1, with a cushion length of around 40 meters, and wave periods of 2 seconds, the first acoustic mode will be significant already at 42 knots, whereas the Wave Craft would have to travel at 89 knots for the given waves to reach the eigenfrequency of its first acoustic mode. Thus, for the scope of this work we can safely

neglect the effect of the spatially varying pressure components even at top speed, and luckily for the operators of the Skjold-class, effective RCSs are invented to take care of the acoustic modes. It should still be noted that the uniform pressure is also able to induce pitch motions, due to the fact the centre of pressure (COP) and the centre of gravity (COG) of the vessel does not perfectly coincide.

As a side-note: these spatially varying pressure components are actually of equal nature as regular sound waves, however, they are normally of too low frequencies for humans to hear. Based on equations (2.17) and (2.18) and the fact that humans are normally able to hear frequencies as low as 20Hz; if we look at the third acoustic mode of the Wave Craft and hypothetically were able to propel the vessel up to around 290 knots, you should theoretically be able to hear quite loud humming from the air cushion. At that speed, however, the noise would not be your only concern.

2.2.2 Reynolds Transport Theorem

In the derivation of the uniform cushion pressure dynamics common practice in the field is to start out with a relation commonly described as a global continuity equation. This derives from Reynolds Transport Theorem (White, 1986), which states:

Reynolds Transport Theorem. *By letting B be any property of a fluid being investigated (e.g. energy, momentum, enthalpy, etc.), and $\beta_{re} = \frac{\partial B}{\partial m}$ be the intensive value, or the amount of B per unit mass in any small element of the fluid, we can define the total amount of B in the control volume, $\mathcal{V}$, as:*

$$B_{sys} = \int_{C\mathcal{V}} \beta_{re} dm = \int_{C\mathcal{V}} \beta_{re} \rho d\mathcal{V}, \tag{2.19}$$

where ρ is the density of the fluid under investigation. Any change in the amount of B in the control volume must be due to one of three effects:

1. *A change within the control volume, e.g. a density change in a mass conservation-study $\frac{\partial}{\partial t}\left(\int_{C\mathcal{V}} \beta_{re}\rho d\mathcal{V}\right)$.*
2. *An inflow of β to the control volume: $\int_{CS} \beta_{re}\rho V \cos\theta_{re} dA_{in}$.*
3. *An outflow of β from the control volume: $\int_{CS} \beta_{re}\rho V \cos\theta_{re} dA_{out}$.*

In these short derivations θ_{re} represents the relative angle between the unit normal vector of the control surface and the fluid velocity vector, and must not be confused with θ, used to describe the pitch-angle of the vessel. A_{in} represents the surface area of the control volume where there is

a positive net flux of the fluid property of interest, while A_{out} represents the areas with negative flux. $C\mathcal{V}$ denotes the Control Volume subject to investigation, while CS denotes the corresponding Control Surface.

By summing up the effects listed above, and differentiating the total amount if B in $C\mathcal{V}$, B_{sys}, with respect to time we obtain an expression for the change in B_{sys}, which is known as Reynolds transport theorem.

$$\frac{\partial}{\partial t}(B_{sys}) = \frac{\partial}{\partial t}\left(\int_{C\mathcal{V}} \beta_{re}\rho d\mathcal{V}\right) + \int_{CS} \beta_{re}\rho \mathbf{V}\cos\theta_{re} dA_{out} - \int_{CS} \beta_{re}\rho \mathbf{V}\cos\theta_{re} dA_{in}. \tag{2.20}$$

$\mathbf{V}$ is the fluid velocity vector. By defining $\mathbf{n}$ as the outward normal unit vector everywhere on the control surface, then $\mathbf{V}\cdot\mathbf{n}=V_n$ (normal component of flow) for outflow and $\mathbf{V}\cdot\mathbf{n}=-V_n$ for inflow. The expression can then be simplified to

$$\frac{\partial}{\partial t}(B_{sys}) = \frac{\partial}{\partial t}\left(\int_{C\mathcal{V}} \beta_{re}\rho d\mathcal{V}\right) + \int_{CS} \beta_{re}\rho(\mathbf{V}\cdot\mathbf{n}) dA. \tag{2.21}$$

If leakages through the bow- and stern seals are neglected, some of the *fluid-property* fluxes for C$\mathcal{V}$ can be simplified as one dimensional, and we only assume a flux at simplified inlets and exits (fan inlet and vent valve outlet). This means that we assume that the flow properties are nearly uniform over the cross section of the inlet and outlet ducts. This assumption must be justified for the individual fluid property B being investigated. However, at moderate pressures, where the leakages through the bow- and stern seals are nearly negligible, the simplifications will hold when fluid *mass* is the property being investigated, which is the case in this thesis. By including a slight modification, this simplification will also be valid when investigating the linear momentum of the fluid flow, which will be done during the derivations of an expression for the lateral thrust, induced by the fluid flow. If the uniform-flow property assumption holds, the in- and outflow terms can be rewritten as a sum of product terms for each cross section, and equation (2.21) can be rewritten as

$$\frac{\partial}{\partial t}(B_{sys}) = \frac{\partial}{\partial t}\left(\int_{C\mathcal{V}} \beta_{re}\rho d\mathcal{V}\right) + \sum_i (\beta_{re}\rho A_i V_i)_{out} - \sum_i (\beta_{re}\rho A_i V_i)_{in}, \tag{2.22}$$

where A_i is the leakage area of effector i and V_i is the corresponding flow velocity.

2.2.3 Nonlinear Uniform Pressure Equation

To derive the dynamics of the uniform pressure component in the air cushion we perform a mass-conservation study, thus we replace the somewhat arbitrary B from the generic equation(2.22) with m (mass), and $\beta = \frac{\partial m}{\partial m} = 1$. One of natures fundamental laws is that mass must be conserved for all control volumes. Equation (2.22) can therefore be rewritten:

$$\frac{\partial m}{\partial t}_{sys} = 0 = \frac{\partial}{\partial t}\left(\int_{C\mathcal{V}} \rho d\mathcal{V}\right) + \sum_i (\rho_i A_i V_i)_{in} - \sum_i (\rho_i A_i V_i)_{out}, \tag{2.23}$$

where the control volume $C\nu$ is defined by the red dotted lines in figure 2.3, which shows a cross-sectional view of a SES air cushion seen from the stern. Q_{out} simply denotes that those are the main channels for outflow. When deriving an expression for the lateral thrust, the lateral differences in outflow are important. For the uniform pressure, however, the direction of the flow is irrelevant.

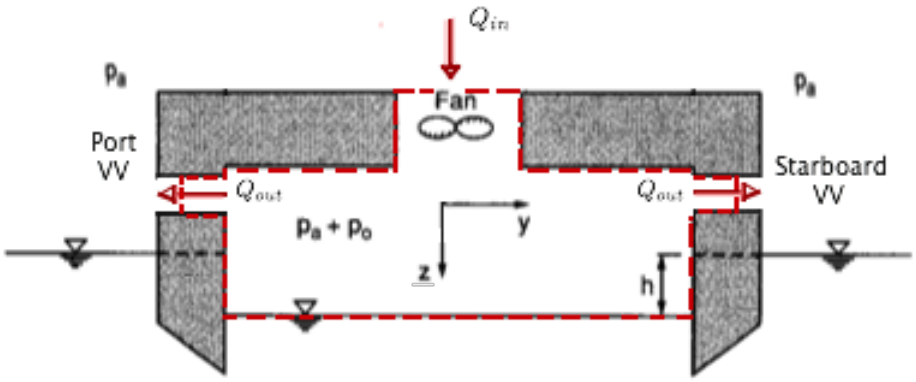

Figure 2.3: Control Volume used in the derivations of the pressure dynamics

As presented in (Sørensen and Egeland, 1995); by moving the last two terms on the right hand side of equation (2.23) to the left side of the equality, we obtain a global continuity equation:

$$w_{in}(t) - w_{out} = \frac{\partial}{\partial t}\left(\int_{-\frac{L}{2}}^{\frac{L}{2}} \rho_c(x,t) V_c(t) dx\right). \tag{2.24}$$

Equation (2.24) states that the difference between the mass flow into- and out from the volume, w_{in} and w_{out}, should equal the variations of the air density, integrated over C$\mathcal{V}$, from figure 2.3. The right hand term is integrated over the cushion length L, $\rho_c(x,t)$ is the density of the air inside the cushion while $V_c(t)$ is the total volume of $C\mathcal{V}$. The space dependency on the right-hand side of equation (2.24) is added to account for spatial variations of the pressure within the confined space

of interest. If we neglect the spatial variations and expand the right hand term of equation (2.24), we obtain

$$w_{in}(t) - w_{out}(t) = \frac{\partial}{\partial t}\rho(t)V_c(t) = \dot{\rho}(t)V_c(t) + \rho(t)\dot{V}_c(t). \tag{2.25}$$

The first term on the right hand side of equation (2.25) can be derived from the adiabatic pressure-density relation, which states that:

$$\rho(t) = \rho_{c0}\left[\frac{p_a + p_u(t)}{p_a + p_0}\right]^{\frac{1}{\gamma}}, \tag{2.26}$$

where ρ_{c0} is the density of the air at the equilibrium pressure p_0, p_a is the atmospheric pressure and p_u is the uniformly varying excess pressure component. γ is the *heat capacity ratio*. By defining:

$$\mu(t) = \frac{p_u(t) - p_0}{p_0} \rightarrow p_u(t) = p_0 + \mu(t)p_0, \tag{2.27}$$

equation (2.26) can be rewritten

$$\rho_c(t) = \rho_{c0}\left[\frac{p_a + p_0 + \mu(t)p_0}{p_a + p_0}\right]^{\frac{1}{\gamma}}. \tag{2.28}$$

It is common, when investigating small pressure fluctuations for similar plants, to linearize around the equilibrium point $\mu = 0$. Instead, to obtain a generic expression valid for larger pressure fluctuations to be used in a process plant model, equation (2.28) is simply differentiated, and the following relation is obtained:

$$\dot{\rho}_c(t) = \frac{\partial \rho_c}{\partial t} = \frac{\partial \rho_c(t)}{\partial U}\frac{\partial U}{\partial t} = \frac{\rho_c(t)}{\gamma(\frac{p_a}{p_0} + 1)}\left[\frac{p_a + p_0 + \mu(t)p_0}{p_a + p_0}\right]^{\frac{1}{\gamma}-1}\dot{\mu}(t). \tag{2.29}$$

In the following derivations ρ_c will be assumed constant, which simplifies the notation. This can be justified by plotting the adiabatic pressure-density relation, given by equation (2.28), as μ runs from -1 to 1, which is a relatively long interval.

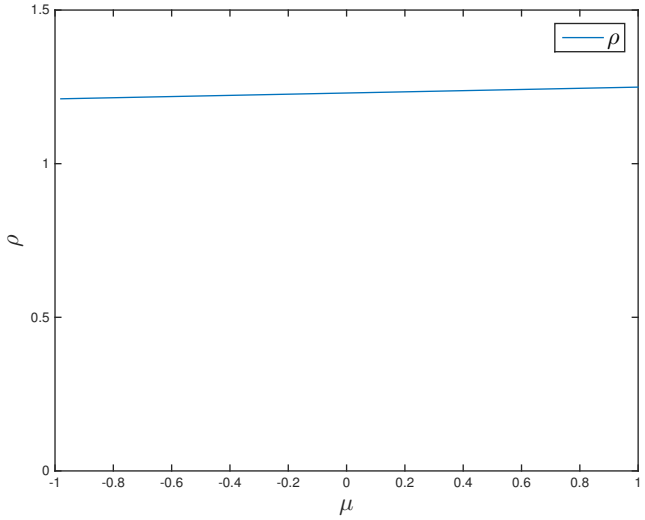

Figure 2.4: Density of air as function of pressure

The plot shows that the variations in density of the air inside the cushion are of a small magnitude and for the uniform pressure equation, ρ_c will cancel out, thus they will be neglected for the derivation of the pressure dynamics. The atmospheric air density ρ_a , however, influences the volumetric outflow of air, as will be shown later. The second right-hand term of equation (2.25), the variations in the volume, are caused by vessel translations and rotations as well as the propagating waves. The latter is given by:

$$\dot{V}_w = b \int_{\frac{-L}{2}}^{\frac{L}{2}} \dot{\xi}(x,t)dx, \tag{2.30}$$

where $\dot{V}_w$ denotes the wave volume pumping due to propagating waves, and b is the width of the air cushion. For regular, head seas, by evaluating the integral and assuming regular waves, i.e. surface elevations on the form $\xi(t) = \xi_a \cos(\omega_w t)$, where ω_w is the wave frequency and ξ_a is the wave amplitude, the wave volume pumping can be rewritten:

$$\dot{V}_w = A_c \xi_a \omega_e \frac{\sin\frac{kL}{2}}{kL} \cos(\omega_e t), \tag{2.31}$$

where k is the wave number $k = \frac{2\pi}{\lambda}$, λ is the wave length and ω_e is the frequency of encounter given by equation (2.18). For zero forward velocity, ω_e equals ω_w. The volume pumping due to vessel excitations are given by the following two relations:

$$\dot{V}_{\eta_5}(t) = A_c x_{cp} \dot{\eta}_5(t), \tag{2.32a}$$

$$\dot{V}_{\eta_3}(t) = -A_c \dot{\eta}_3(t), \tag{2.32b}$$

Where we recall the sign conventions defined in the beginning of the chapter, positive z-axis pointing downwards and positive pitch defined as bow up. By summing up equation (2.31), (2.32a) and (2.32b) the total volume pumping can be expressed as:

$$\dot{V}_c(t) = A_c x_{cp} \dot{\eta}_5(t) - A_c \dot{\eta}_3(t) + b \int_{\frac{-L}{2}}^{\frac{L}{2}} \dot{\xi}(x,t) dx. \tag{2.33}$$

The left-hand side of equation (2.24) considers the mass flow into- and out of the volume. The inflow is provided by the lift fans, and can be found as a function of the pressure by taking the inverse of the *fan characteristics*, which would provide the airflow as a function of the excess pressure. Given the fan characteristics, this function is known, and, for the process plant, there is really no need to linearize it.

$$w_{in}(t) = \rho_c(t) \sum_{i=1}^{r} Q_i(\mu(t)). \tag{2.34}$$

Q_i is the airflow from lift fan number i. An example of a typical fan characteristic, for one lift fan on a SES is shown in figure 2.5.

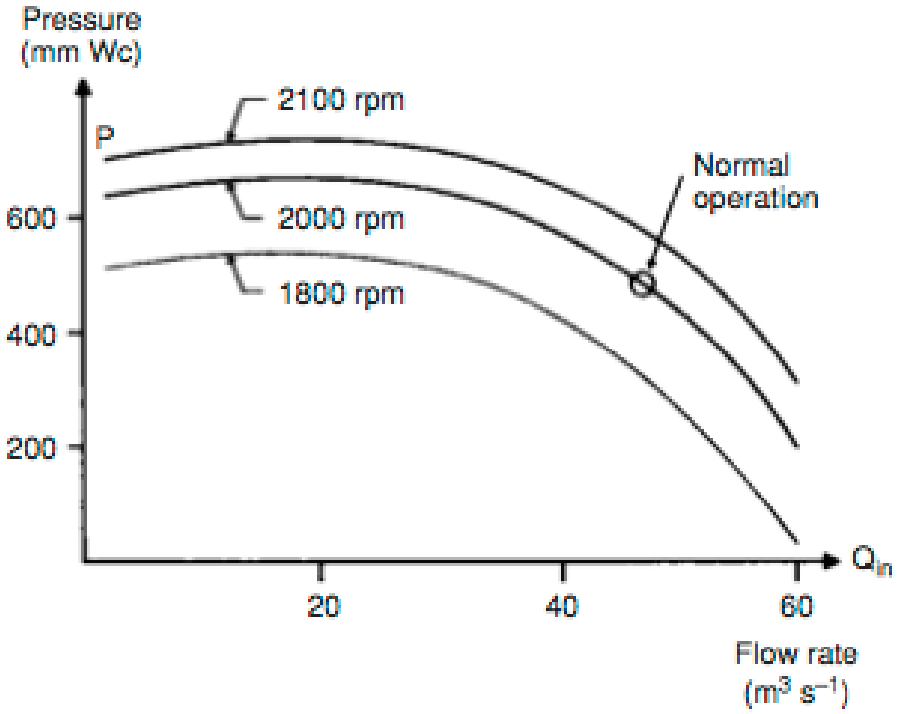

Figure 2.5: Example of fan-characteristics for a Surface Effect Ship, (Faltinsen, 2005)

As the figure above shows, it is important that the operating point of the system is located in a steep declining region of the fan characteristics, which gives the system a strong self stabilizing

effect as, e.g. an increase in the cushion pressure leads to a relative strong reduction in the mass flow, thus the system will be stable around the equilibrium operating point. For an analytic proof of the system stability, the keen reader is referred to (Auestad et al., 2015).

Recall from the introduction that the flow of air out of the cushion can be divided into two contributions, i.e. passive leakage, and vent valve leakage. A common practice is to further divide the vent valve leakage into the flow through a variable leakage area, and a fixed (equilibrium) bias opening (the leakage area, at flat sea and for a stationary vessel, necessary to make the actual cushion pressure equal to the desired equilibrium pressure). We denote this bias opening A_0. The out flow through the different orifices, i.e. leakage areas, can be derived from the simple Euler's equation, given by (2.35), by assuming the flow to be frictionless and the gravitational effects to be negligible. The last assumption holds due to the low density of air, and the relatively small vertical extent of the system being studied.

$$\rho \frac{\partial V}{\partial t} = -\Delta p. \tag{2.35}$$

For the simplest one dimensional pressure-gradient case, equation (2.35) simplifies to

$$\rho V dV = -dp. \tag{2.36}$$

By integrating equation (2.36) between two points along a streamline, the following relation is obtained:

$$(p_1 - p_2) = -(\frac{\rho_2}{2} v_2^2 - \frac{\rho_1}{2} v_1^2), \tag{2.37}$$

where the first of 'the two points' is located inside the air-cushion of the SES, and the other one is located outside at atmospheric pressure. Thus $p_2 = p_{atm}$ and we can rewrite the equation

$$p_c - p_{atm} = p_0 + \mu(t) p_0 = \frac{1}{2}(\rho_a v_2^2 - \rho_c v_1^2), \tag{2.38}$$

where p_c is the absolute cushion pressure. Even though there will be a chaotic flow inside the air cushion, for this study it is convenient to look at the air cushion as a pressure reservoir, we will therefore assume the average lateral velocity of the air inside the cushion, V_1, to be equal to zero,

and obtain the following expression for the outflow escape velocity of the air:

$$v_2 = \sqrt{\frac{2(p_0 + \mu(t)p_0)}{\rho_a}}[m/s]. \tag{2.39}$$

Note that we, by using this equation, are assuming frictionless, i.e. inviscid, flow. In reality there will be factors contributing to losses in this flow, such as duct-entrance effects (albeit small due to low entrance velocity), friction losses etc. There will also be inertial effects, however the dynamics of the airflow is most likely quick enough to be neglected. The volumetric out-flow is found by multiplying the velocity of the escaping air with the leakage area and any loss-coefficients which might apply. The following expressions for the mass flow are then obtained:

$$W_{out,eq} = c_n(A^{ap}(\eta_s) + A^{fp}(\eta_s) + A_0)\rho_c\sqrt{\frac{2(p_0 + \mu(t)p_0)}{\rho_a}}, \tag{2.40a}$$

$$W_{out,RCS} = c_n \sum_{i=1}^{r} \Delta A_i \rho_c \sqrt{\frac{2(p_0 + \mu(t)p_0)}{\rho_a}}, \tag{2.40b}$$

$$w_{out} = W_{out,eq} + w_{out,RCS}, \tag{2.40c}$$

where $A^{ap}(\eta_s)$ and $A^{fp}(\eta_s)$ are the leakage areas related to the aft and bow seals, respectively. η_s denotes the vessel state displacement vector in $\{\mathrm{s}\}$, and the state-dependency is included due to the fact the these leakage areas are strongly increasing as the vessel pitches or heaves. ΔA_i is the variable leakage area of vent valve i around the bias opening. c_n is an orifice coefficient describing the losses in the flow through an orifice. This is a function of several factors, which includes the ratio between size of reservoir and characteristic length of the orifice, imperfect flow, difference from perfect nozzles etc. A conservative result can usually be found by setting this equal to 0.61, however experiences from full scale testing suggests that the losses really are significantly smaller. A more accurate expression could be found by a *Computational Fluid Dynamics* (CFD) analyses, which we recommend to do for the specific problem of investigation if one wishes to develop an accurate process plant model.

The seal-leakage areas at the equilibrium states will be very small, proven by model tests to be almost negligible, however they are, as mentioned, strongly state dependent. For large positive values of heave, and large absolute values for pitch, a strongly increasing leakage area will be revealed, limiting the maximum excitations in these DOFs. The increment of the total leakage areas exhibits nearly discrete properties for the excitation levels were they occur, and should be

included as they lead to strong limitations in the system capacity.

Combining equations (2.26) through (2.40c) into equation (2.25), yields the following relation:

$$\sum_{i=1}^{r} Q_i(\mu(t)) - (K_2 + c_n \sum_{i=1}^{r} \Delta A_i)\sqrt{\frac{2(p_0+\mu(t)p_0)}{p_a}} =$$
$$\left[-A_c x_{cp}\dot{\eta}_5(t) + A_c\dot{\eta}_3(t) + b\int_{\frac{-L}{2}}^{\frac{L}{2}} \dot{\xi}(x,t)dx\right] + K_1(t)(p_a+\mu(t)p_0+p_0)^{\frac{1}{\gamma}-1}\dot{\mu}(t). \tag{2.41a}$$

Where, K_1 and K_2 are, for convenience, defined as:

$$K_1(t) = \frac{V(t)}{\gamma(\frac{p_a}{p_0}+1)(p_a+p_0)^{\frac{1}{\gamma}-1}}, \tag{2.42a}$$

$$K_2(\eta_s) = c_n(A^{ap}(\eta_s) + A^{fp}(\eta_s) + A_0). \tag{2.42b}$$

This relation can be defined on State-Space form as

$$\dot{\mu}(t) = \mathbf{f}(x,t) + \mathbf{B}(u,t) + \mathbf{G}(x,t). \tag{2.43a}$$

Where $\mathbf{B}$(u,t) and $\mathbf{G}$(x,t) are the input and disturbance functions, respectively. $\mathbf{f}$(x,t) describes the undisturbed system dynamics.

$$\mathbf{f}(x,t) = \frac{\sum_{i=1}^{r} Q_i(\mu) - K_2\sqrt{\frac{2(p_0+\mu(t)p_0)}{\rho_a}}}{K_1(p_a+\mu(t)p_0+p_0)^{\frac{1}{\gamma}-1}} \tag{2.44a}$$

$$\mathbf{B}(u,t) = \frac{-c_n\sum_i \Delta A_i\sqrt{\frac{2(p_0+\mu(t)p_0)}{\rho_a}}}{K_1(p_a+\mu(t)p_0+p_0)^{\frac{1}{\gamma}-1}} \tag{2.44b}$$

and

$$\mathbf{G}(x,t) = \frac{-\left[A_c x_{cp}\dot{\eta}_5 - A_c\dot{\eta}_3 + b\int_{\frac{-L}{2}}^{\frac{L}{2}} \dot{\xi}(x,t)dx\right]}{K_1(p_a+\mu(t)p_0+p_0)^{\frac{1}{\gamma}-1}} \tag{2.44c}$$

The system input u corresponds to $\sum \Delta A_i$. Notice that, in the equilibrium state of the undisturbed system, the inflow from the fan and the outflow through the leakage areas will cancel each other out.

2.2.4 Effect of Pressure on System Dynamics

The excess pressure in the cushion will affect the dynamics of the vessel through the simple relation

$$P = \frac{Force}{Area}. \tag{2.45}$$

In addition, the pressure will induce a pitch moment, where the arm x_{cp} is the distance between COP and COG, and the force is the same term as above. Since we're looking for another term for the total excitation forces, we solve for the force and moment and insert the terms from our specific problem. Thus, we have:

$$Z_c = P \cdot Area = -p_0 \mu(t) A_c, \tag{2.46a}$$

$$M_c = P \cdot Area \cdot arm = p_0 \mu(t) A_c x_{cp}, \tag{2.46b}$$

where Z_c and M_c denotes the heave force and pitch moment from the cushion, respectively. Only the effect of the varying uniform pressure component is included in equation (2.46a) and (2.46b). This is because the *equilibrium component* will be cancelled out by the gravity forces together with the difference between the buoancy of the submerged volumes and the lift force from the equilibrium pressure.

2.2.5 Lateral Thrust Forces - Conservation of Linear Momentum

To obtain an expression for the thrust provided by the accelerated airflow out of the cushion, we turn to equation (2.22) and the control volume defined in figure 2.3. In this analysis the fluid property of interest is the linear momentum, thus B=m$\mathbf{V}$, and accordingly $\beta = \frac{\partial(m\mathbf{V})}{\partial t} = m\frac{\partial V}{\partial t} = Force$. We remember that $\mathbf{V}$ is the velocity vector of the fluid flow, thus we obtain the vector sum of all forces acting on the system by evaluating the following equation:

$$\frac{\partial}{\partial t}(m\mathbf{V}) = \sum \mathbf{F} = \frac{\partial}{\partial t}\left(\int_{C\mathcal{V}} \mathbf{V}\rho d\mathcal{V}\right) + \int_{CS} \mathbf{V}\rho(\mathbf{V}_r \cdot \mathbf{n}) dA. \tag{2.47}$$

Since this equation contains vector relations, the equation has three components which corresponds to x_b, y_b and z_b in {b}. For this case we are only interested in the y_b-component of the flow, thus

equation (2.47) can be rewritten:

$$\sum \mathbf{F} = \frac{\partial}{\partial t}\left(\int_{C\mathcal{V}} \mathbf{V}\rho d\mathcal{V}\right) + \int_{CS} v\rho(\mathbf{V}_r \cdot \mathbf{n})dA. \tag{2.48}$$

Before we simplify this equation in a similar manner as was done to obtain equation (2.22), we must remember that even in a relatively narrow duct such as the one featured in the SES, the flow will not be perfectly uniform. Therefore the simple momentum flux calculation $\int_{CS} v\rho(\mathbf{V}\cdot\mathbf{n})dA = \dot{m}V$, where $\dot{m} = \rho VA$, A being the area of the duct of interest, denotes the mass-flow, is somewhat in error. A momentum flux correction factor must be introduced. Common convention, (White, 1986), denotes this with the letter β, however this conflicts with the intensive value of the generic fluid property defined earlier in this chapter. Therefore, this factor will be denoted α in the following short justification of neglection. The factor α is to account for the variations in the velocity field over the cross section of the ducts, and is defined by computing the exact momentum flux, and equating it to a flux based on the average velocity in the duct:

$$\begin{aligned} \rho\int_{A_{duct}} u(x',y')^2 dA_{duct} = \alpha\dot{m}V_{av} = \alpha\rho A_{duct}V_{av}^2, \\ \alpha = \frac{1}{A_{duct}}\int_{A_{duct}}\left(\frac{u(x',y')}{V_{av}}\right)^2 dA_{duct}, \end{aligned} \tag{2.49}$$

for some x' and y' axis defining the area of the duct. However, experiences show that the correction factors for turbulent flow are so close to unity that they can be neglected. The flow through the short vent valves of the SES will accelerate up to velocities higher than $50\frac{m}{s}$. With the definition of Reynolds number

$$Re = \frac{vD_h}{\nu}, \tag{2.50}$$

where D_h is the *hydraulic diameter* of the duct, v the velocity of the flow and ν the kinematic viscosity of the fluid being studied, we find that the Reynolds number for this flow is at the magnitude of 10^6, which is in the turbulent zone. Thus, for this qualitative study, the momentum flux correction factor will be conveniently omitted. This allows us to rewrite equation (2.48) to

$$\sum F = \frac{\partial}{\partial t}\left(\int_{C\mathcal{V}} \mathbf{V}\rho_c d\mathcal{V}\right) + \sum_i (\dot{m}_i V_i)_{out} - \sum_i (\dot{m}_i V_i)_{in}, \tag{2.51}$$

where $\dot{m}_i$ denotes the mass flow going into- or out from orifice i, while V_i denotes its velocity. Since we're only interested in the lateral components of this linear momentum flux, and know that the

flux entering the control volume has zero lateral components, the lateral momentum flux going into the volume equals zero. Further, we also assume that there will be an average of zero variations in the linear momentum within the volume, illustrated in figure 2.6. Thus, the net force from the airflow out of vent valve i can be written as

$$F_i^{vv} = \dot{m}_i v_{i,out} = c_n \rho_c A_i^l \sqrt{\frac{2(p_0 + \mu(t)p_0)}{\rho_a}} \sqrt{\frac{2(p_0 + \mu(t)p_0)}{\rho_a}}, \tag{2.52}$$

where A_i^l denotes the total leakage area of the respective vent valve, i.e. $A_{0,i} + \Delta A_i$. The first terms on the right hand side of equation 2.52 equals the mass flow going through the leakage area, while the last term denotes it's velocity. Clearly this can be rewritten to yield the net thrust from vent valve i:

$$u_i^{vv} = -n \cdot c_n \cdot \rho_c A_i^l \frac{2(p_0 + \mu(t)p_0)}{\rho_a}, \tag{2.53}$$

where c_n is some thrust-reduction coefficient and the normal vector of the leakage area A^l, n, is defined as positive for air flowing along the positive y-axis. For a vent valve pointing in the negative y-direction, a positive thrust will be generated. For the typical SES setup, there are a total of two vent valves. The thrust from the port and starboard vent valve will, in the following, be denoted $u_y^{port,vv}$ and $u_y^{sb,vv}$, respectively. However, as the section concerning the thrust allocation problem will show, these two thrust forces can be generalised as one thruster. The net force from the vent valves will therefore be denoted u_y^{vv}, and allowed to take positive and negative values in compliance with the defined sign convention. The assumed flow regime of $C\mathcal{V}$ is illustrated in figure 2.6.

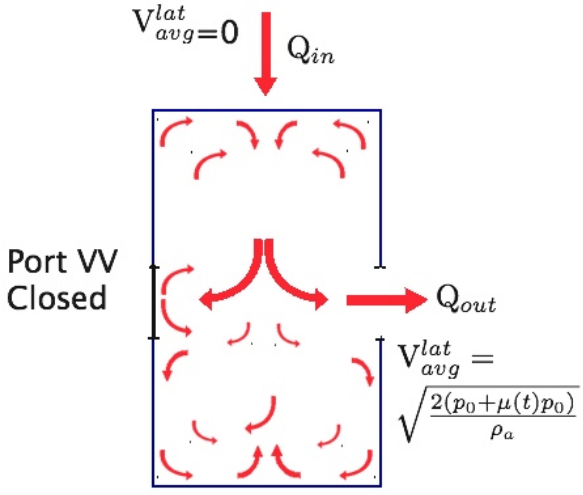

Figure 2.6: Control volume flow velocities

2.2.6 Waterjet Thrust

The most important parts of a water jet pump drive is the intake, drive-shaft, impeller, stator, steering deflector and the reverse duct/deflector. The basic principle is illustrated in figure 2.7.

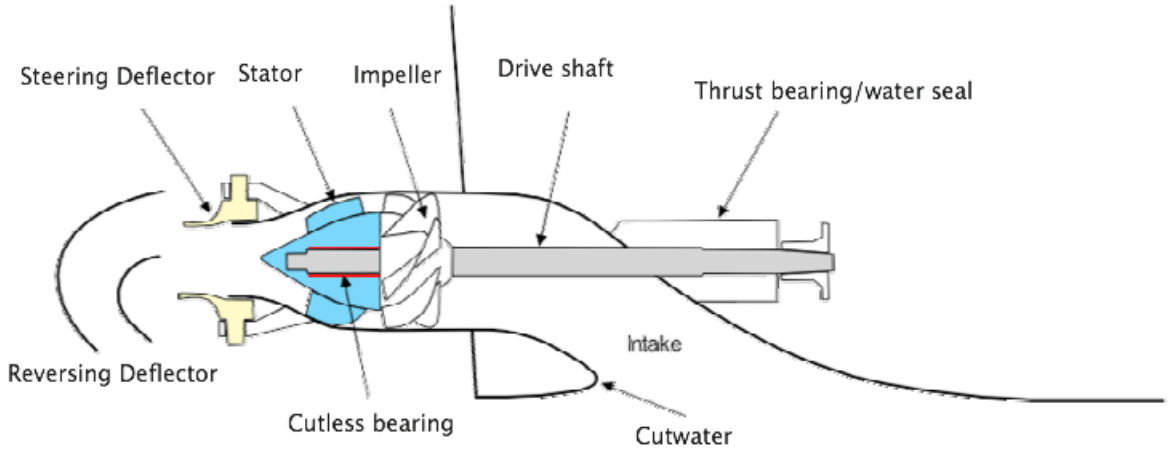

Figure 2.7: Illustration of the Basic Water Jet pump structure, from (Hamilton, 2007) but slightly altered in notation

Water is sucked in through the intake, by the rotating impeller powered by the diesel propulsion engines. The impeller accelerates the water, which is discharged at a high velocity through the discharge nozzle (the steering deflector in figure 2.7). The stator is used to regain energy lost to flow rotations induced by the impeller. According to Newtons 3. law, the accelerated water flow must produce an equally sized, opposite acting, force, which is the propulsive force propelling the vessel. To derive an expression for the thrust provided by the water jets, a similar approach as for the lateral airflow thrust forces can be used, i.e. by starting out with the linear momentum continuity equation (2.47). The amount of thrust provided by the jet flow will be influenced by both frictional- and pressure losses, however at low speeds, and for the qualitative purposes of these derivations, these various loss factors will be conveniently omitted. The derivation of the thrust from the water jets will be done by neglecting any loss terms, and the three characteristic velocities, as given by (Bulten, 2006):

1. Ship speed V_{ship}(=u, ref table 2.1).

2. Mass averaged ingested velocit at duct inlet (V_{in}).

3. Average outlet velocity at the nozzle (V_{out}).

V_{in} accounts for the boundary layer produced by the ships hull, and is defined as

$$V_{in} = \frac{1}{Q_w} \int v_{flow}(z') \cdot v_n dA = \frac{1}{A} \int v_{flow}(z') dA, \tag{2.54}$$

Where v(z') denotes the velocity distribution of the flow, as we move a distance z' away from the hull along the normal vector of the surface. Q_w is the volumetric water flow through the system, and v_n is the normal flow through the area. Due to the boundary layer generated by the ship hull, the mass averaged velocity of the ingested water is lower than the ship speed, and is defined by the *wake fraction* $w = 1 - \frac{v_{in}}{v_{ship}}$. For a flow along a flat plate, a power law describing the velocity profile of the boundary layer is given by

$$\frac{v_{flow}}{U_\infty} = \left(\frac{z'}{\delta}\right)^{\frac{1}{n}}, \tag{2.55}$$

where U_∞ is the flow far away from the plate, δ is the thickness of the boundary layer and n is some curve-shaping integer often set equal to 7. Now, it is obvious that this boundary layer can affect the average velocity of the flow going into the volume. However, as this thesis is to examine a dynamic positioning application of the system, the low velocities of interest make these effects safely negligible, specially if we add the fact that the outlet velocity of such water jet systems is in the order of $10^2[m/s]$. By neglecting the shape of the boundary layer, the inlet velocity can be given by

$$V_{in} = \frac{Q_w}{\frac{\pi}{4} D_{inlet}^2}. \tag{2.56}$$

Similarily, the outlet velocity is given by

$$V_{out} = \frac{Q_w}{\frac{\pi}{4} D_{nozzle}^2}. \tag{2.57}$$

Now we return to the conservation of linear momentum. By defining a control volume cutting through the water intake and the nozzle of the water jet, we can follow the simplifications from equation (2.52) and assume somewhat uniform flow conditions over the cross section of the jet

stream. By neglecting any volumetric forces on the system, the total force is then given by:

$$\sum F = \rho_w Q_w V_{out} - \rho_w Q_w V_{in}. \tag{2.58}$$

If we assume the inlet velocity to be close to zero, which holds for low speed maneuvering, the expression can be further simplified to

$$F_{waterjet} = \rho_w Q_w V_{out}. \tag{2.59}$$

This reveals a linear relationship between the force and the volumetric flow, which simplifies the force vector decomposition when the reversing shield is applied. As the reversing deflector, figure 2.7, is lowered, it intercepts the jet stream after it has left the steering nozzle, and, partially or totally, redirects it back underneath the hull to produce a reversed thrust component. Most such reverse ducts has split passages, which can generate two reversed flow components, by directing parts of the flow to either sides. The jet stream is split into the following three components:

1. The forward thrust component, which goes underneath the deflector. Its direction is only affected by the angle of the steering nozzle, and the magnitude of the component will equal zero when the deflector is fully lowered.

2. The starboard component flowing through the deflector, i.e. it provides a reverse thrust.

3. The port component flowing through the deflector, producing a backwardly directed thrust.

For deflector shields only pivoting in the vertical direction, the two reverse flow components can only be affected in magnitude, not direction. Thus, when the deflector is fully lowered, the relative size of the two reverse flow components can be adjusted by rotating the steering nozzle. Pointing the nozzle to the far starboard side directs the entire flow through the starboard flow component while, correspondingly, directing the nozzle to the far port will channel the entire flow through the port component. If we augment equation (2.59) to consist of three mass flow components $Q_{w,i}$, with corresponding direction in the 3dimensional space denoted by the unit vector n_i, the net force can be obtained

$$|u^{wj}| = \sum_{i=1}^{3} -\rho_w V_{out} n_i Q_{w,i}. \tag{2.60}$$

V_{out} denotes the speed (not the vectorial velocity) of the flow component, which is assumed to be equal for the three components. For a fixed diesel engine RPM, the variable in the net thrust is

simply the distribution of the mass flow among the three components described in the list above. From equation (2.60) we can sum up the different combinations of flow distributions to obtain the thrust region of one single water jet. We denote the longitudinal- and lateral components of the water jet thrust u_x^{wj} and u_y^{wj}, respectively. The water jet has two main modes, the deflector fully lowered and fully opened, however the position can also be adjusted continuously between the two, as illustrated in figure 2.8.

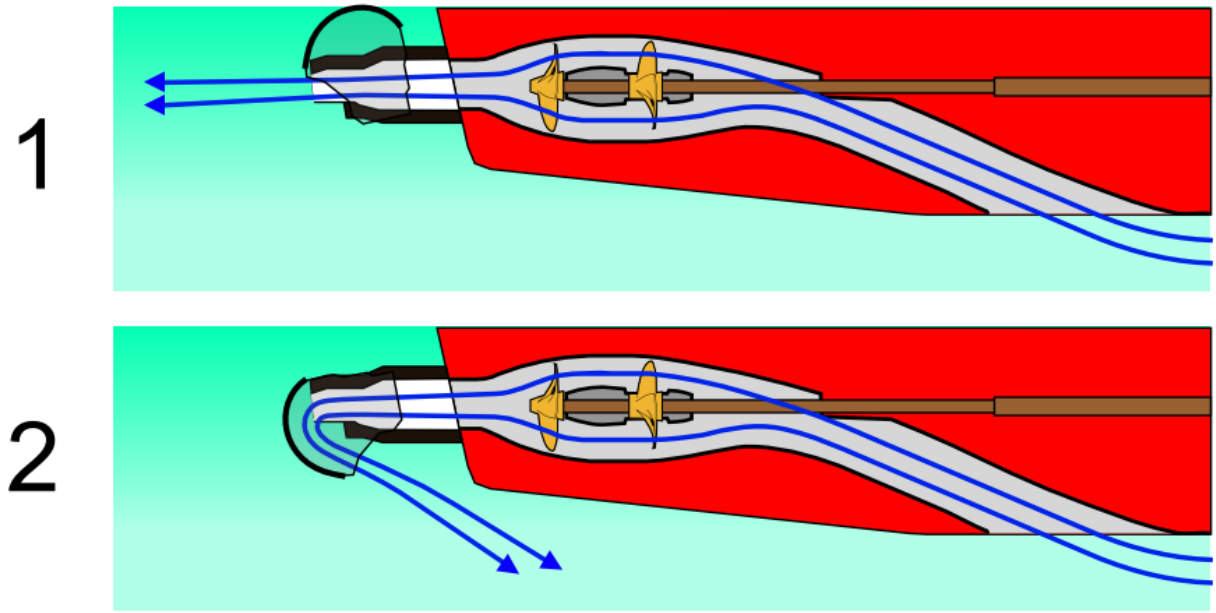

Figure 2.8: Operational modes of water jet drive, taken from (Commons, 2008)

The maximum magnitude of the thrust vector is denoted $U_{100\%}^{wj}$. A common design of water jets is two use a deflector shield which does not rotate with the nozzle, thus the thrust in reverse can be continuously distributed between a port and starboard component. We will assume the water jets for this plant to be of this type. We also assume the deflector shield to direct the jet stream forwards at a $\pm 30°$ angle relative to positive x_b, and $30°$ downwards relative to the $x_b y_b$-plane. The control design chapter will derive a water jet thrust and azimuth controller where these angles are allowed to take arbitrary values. If the deflector is only partially lowered the net forward thrust can equal zero, and pure lateral net thrust components can be achieved. The different water jet/deflector shield configurations are illustrated by figure 2.9.

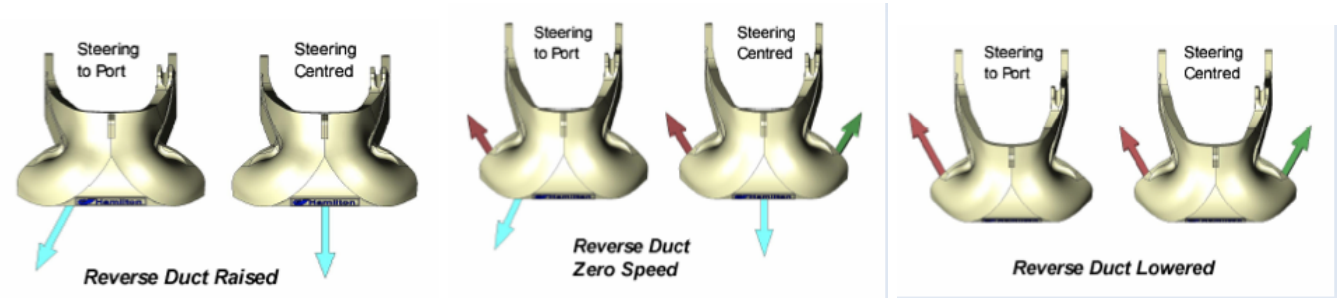

(a) Deflector up (b) Zero Speed (c) Deflector Down

Figure 2.9: Waterjet Configuration from (Hamilton, 2007)

By the assumptions above, the directional components of the maximal reversed port thrust vector are given by:

$$\begin{aligned} u_x^{rev,p} &= U_{100\%}^{wj} \cos 30^\circ \cos 150^\circ = -0.75 U_{100\%}^{wj}, \\ u_y^{rev,p} &= U_{100\%}^{wj} \cos 30^\circ \cos 240^\circ = -0.433 U_{100\%}^{wj}. \end{aligned} \tag{2.61}$$

If the equivalent is done for the starboard component, the two reversed thrust vectors and the set of possible forward thrust vectors of the water jet are illustrated by figure 2.10.

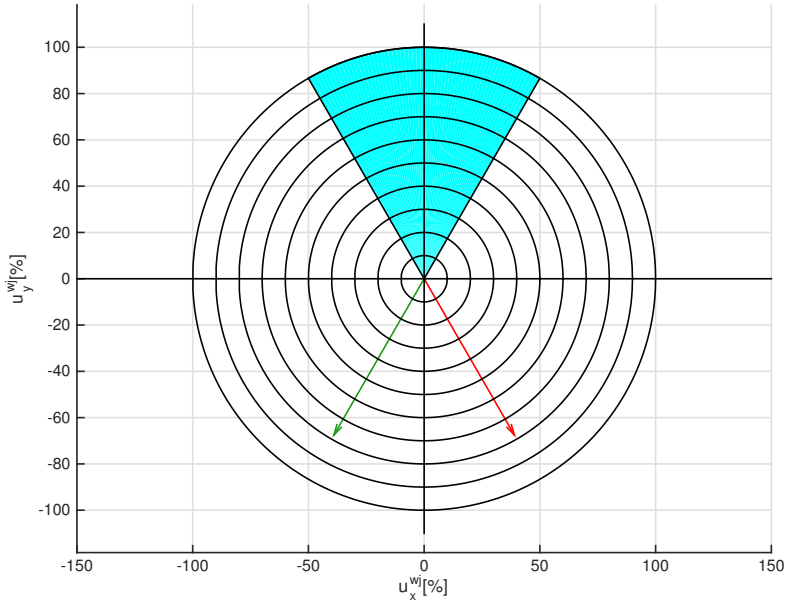

Figure 2.10: Horizontal Components of Waterjet Thrust Vectors

The colours in figure 2.10 are chosen to comply with figure 2.9. Remember that figure 2.10 describes the resulting forces, while figure 2.9 illustrates the water flow. The two quantities will be acting oppositely. From figure 2.10, we derive the full thrust region by looking at the resultant lateral thrust component of one water jet with the deflector at an arbitrary position and the steering

nozzle pointing as far as possible to port (we look at a combination of the blue and red region in figure 2.10). We assume the diesel engine to be running fixed at its maximum RPM, thus the thrust corresponding to the deflected horizontal water flow is $u^{wj}_{100\%}$. If the reversing shield is fully up, the resultant thrust vector will be pointed forwardly at an 30° angle to the $z_b x_b$-plane, it's lateral component equals $U^{wj}_{100\%} \sin 30^\circ$. If we lower the reversing shield, a fraction of the flow will be directed backwardly at an 30° angle relative to the $z_b x_b$-plane in the direction of negative x_b, but it will also be given a 30° angle relative to the $y_b x_b$-plane (downwards), so horizontal thrust is lost. We let u_{rev} denote the magnitude of the backwardly directed flow component, and u_f denote the magnitude of the forwardly directed component. Since, as the shield is lowered, the thrust is transferred from one component to another one, by assuming constant RPM equal to the maximum RPM of the engine we can express the forwardly directed (blue) component as a function of the backwardly directed (red) component in the following way.

$$u_f(u_{rev}) = U^{wj}_{100\%} - \frac{1}{\cos 30^\circ} u_{rev}. \tag{2.62}$$

If we look at the resultant lateral force from these two components, it is given by (2.63)

$$u^{wj}_y = u_f \sin 30^\circ + u_{rev} \sin 60^\circ, \tag{2.63a}$$

$$u^{wj}_y = (u_f - \frac{1}{\cos 30^\circ} u_{rev}) \sin 30^\circ + u_{rev} \sin 60^\circ. \tag{2.63b}$$

This can be rewritten:

$$u^{wj}_y(u_{rev}) = (\sin 60^\circ - \frac{\sin 30^\circ}{\cos 30^\circ}) u_{rev} + U^{wj}_{100\%} \sin 30^\circ, \tag{2.64}$$

which is clearly an affine function in u_{rev}, i.e. the distribution between the forwardly- and the backwardly directed component. This type of argument holds for the entire 360° region. Therefore, the thrust region, i.e. the set of achievable longitudinal and lateral thrust components, obtainable by dividing the flow in the different directions, can be found by drawing straight lines between the directional maxima, given by figure 2.10. We obtain a resulting thrust envelope as the one illustrated by figure 2.11. The red region illustrates the effect of reducing the engine RPMs, the envelope is simply linearly scaled.

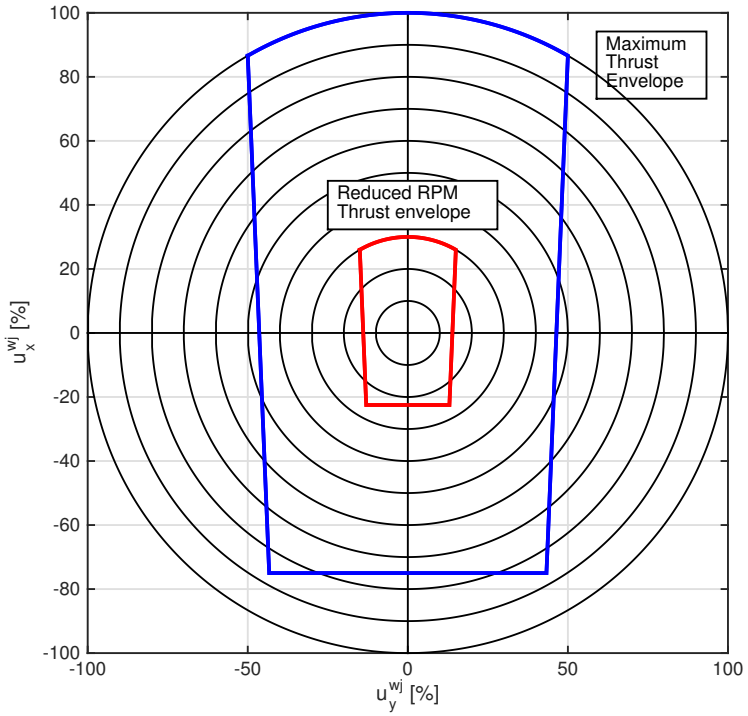

Figure 2.11: Water jet thrust envelope

We notice that figure 2.11 implies that zero net thrust can be achieved even at maximum RPM. This can e.g. be useful in a *Power Management System* (PMS) as part of a thruster-bias configuration which allows for extremely quick load shedding, as described in (Veksler et al., 2012). The downwardly directed flow component will not be utilized in any useful applications for the scope of this thesis, however, we should bear in mind the possibilities and limitations behind phenomenons such as DP-induced pitch oscillations etc. for small water plane area vessels, as described by (Sørensen and Strand, 2000).

2.3 Vessel Dynamics

To derive expressions for the total motions of a marine vessel, it is common to divide the motions into two components, i.e. a Low-Frequency (LF)- and a Wave-Frequency (WF) component, which are, in turn, superposed and the total motion will be the sum of these two components, illustrated by figure 2.12, from (Sørensen, 2013).

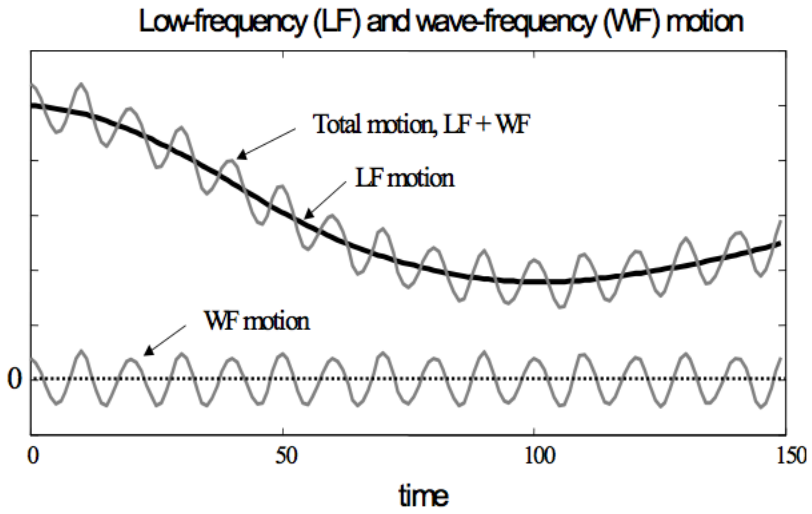

Figure 2.12: Total ship motion as sum of WF and LF components, from (Sørensen, 2013)

.

The subject for this thesis is to investigate the possibilities for combining control of the LF motions (the dynamic positioning problem) with damping of WF motions in heave and sway. Our approach to the problem is to regard this as two individual problems, derive the dynamics independently and superpose the components to obtain the resulting motions. The WF motions are mainly due to first order wave loads, while the LF motions are induced by slowly varying second order loads, as will be explained in section 2.4. The LF motions will only be investigated for the horizontal problem and derived in a similar manner as in (Sørensen, 2013), while the WF motions will be derived in all 6 DOF, in a conventional manner using a linear model in the body-fixed reference frame {b} which investigates the motions relative to the seakeeping frame {s}. We assume small amplitudes of motion for the WF case.

2.3.1 Low Frequency Vessel Model

A generic nonlinear LF vessel model, expressed in {b} can be written as follows

$$M\dot{\nu}_r + C_{rb}(\nu)\nu + C_A(\nu_r)\nu_r + D(\kappa, \nu_r) + G(\eta_n) = \tau, \tag{2.65}$$

where τ represents the forces defined in equation (2.8), and can be split into various components such as forces originating from the vessel actuators, environmental loads, etc. $G(\eta_n)$ represents the generalised restoring forces, which, for this system mainly consists of the hydrodynamic forces originating from Archimedes equations. For other systems, components such as mooring lines etc. could provide restoring forces in the horizontal DOFs. Here, however, the restoring coefficients are only related to the vertical DOFs, thus they will be disregarded for the LF problem. D(κ,ν_r) contains the generalized damping and viscous part of the current forces, which are included in the nonlinear term. ν_r denotes the relative velocity between the vessel and the current, according to

$$\nu_r = \begin{bmatrix} u - u_c & v - v_c & r \end{bmatrix}. \tag{2.66}$$

The damping term can be divided into a nonlinear and a linear component, $D(\kappa, \nu_r) = D_l(\kappa, \nu_r)\nu_r + d_{NL}(\nu_r, \gamma_r)$, whereas the nonlinear component becomes dominating as the speed increases. At low velocities, however, the linear component given by equation (2.67) is dominant and can expressed as:

$$D_l\nu_r = \begin{bmatrix} X_u & 0 & 0 \\ 0 & Y_v & Y_r \\ 0 & N_v & N_r \end{bmatrix}. \tag{2.67}$$

This linear LF damping can be regarded as the vessels added resistance when advancing in waves and is proportional to the square of the significant wave height. This matrix can be rather hard to compute, but approximations can be found by numerical computer programs. For this thesis, ShipX will be used to estimate D_l. Y_r, Y_v respectively denotes the forces in sway due to the rotation rate in yaw and the sway velocity, etc.

$M \in \mathbb{R}^{3\times3}$ is the systems inertia matrix, given by

$$M = M_{RB} - M_A, \tag{2.68}$$

where M_A is the systems added mass matrix. This is on the form

$$M_A = \begin{bmatrix} -X_{\dot{u},0} & 0 & 0 \\ 0 & -Y_{\dot{v},0} & -Y_{\dot{r},0} \\ 0 & -N_{\dot{v},0} & -N_{\dot{r},0} \end{bmatrix} = \begin{bmatrix} -X_{\dot{u},0} & 0 & 0 \\ 0 & -Y_{\dot{v},0} & -Y_{\dot{r},0} \\ 0 & -Y_{\dot{r},0} & -N_{\dot{r},0} \end{bmatrix}, \tag{2.69}$$

where the coupled entries are equal, thus the matrix is symmetrical and the last equality holds. The inputs $X_{\dot{u},0}$ etc. denotes the zero frequency added mass coefficients. u, v and r are the first, second and last input on the vector ν, given by (2.5), which explains the subscripts in the zero frequency added mass coefficient notation. M_{RB} denotes the system mass matrix, and is given by

$$M_{RB} = \begin{bmatrix} m & 0 & 0 \\ 0 & m & mx_g \\ 0 & mx_g & I_z \end{bmatrix}. \tag{2.70}$$

x_g is the arm from the longitudinal position of the centre of gravity, which equals zero if the origin of the {b} frame is set to coincide with the centre of gravity of the body.
$C_{RB}(\nu)\nu$ denotes the forces on the system due to Coriolis and centripetal effects on the rigid body. For the horizontal problem, $C_{RB} \in \mathbb{R}^{3\times 3}$ is given by

$$C_{RB}(\nu) = \begin{bmatrix} 0 & 0 & -m(v + x_G r) \\ 0 & 0 & -mu \\ m(v + x_G r) & mu & 0 \end{bmatrix}. \tag{2.71}$$

$C_A(\nu_r)$ accounts for the Coriolis and centripetal forces of the added mass including the potential part of the current loads due to the relative velocity ν_r, and equals

$$C_A(\nu_r) = \begin{bmatrix} 0 & 0 & X_{\dot{v}} v_r + Y_{\dot{p}} p + Y_{\dot{r}} r \\ 0 & 0 & -X_{\dot{u}} u_r - X_{\dot{w}} w - X_{\dot{q}} q \\ -X_{\dot{v}} v_r - Y_{\dot{p}} p - Y_{\dot{r}} r & X_{\dot{u}} u_r + X_{\dot{w}} w + X_{\dot{q}} q & 0 \end{bmatrix}. \tag{2.72}$$

For low speed applications, such as dynamic positioning, , linear damping and inertial forces will dominate the vessel mode, thus the coriolis and centripetal terms will become negligible for local maneuvering (but should still be considered for a drifting vessel).

2.3.2 Linear Wave Frequency Vessel Model

The WF-model assumes relatively small amplitudes of waves and motions, and calculates the excitation forces with respect to the body fixed frame, however, a seakeeping frame {s} is necessary to be able to examine the displacements of the WF motions. The WF motions can be described according to

$$M(\omega)\ddot{\eta_s} + D_p(\omega)\dot{\eta_s} + G\eta_s = \tau_{wave1} + \tau_c. \tag{2.73}$$

$\eta_s \in {}^6$ is the WF motion vector in the seakeeping frame {s}, τ_c is the actuator control inputs, τ_{wave1} denotes the first order body fixed wave loads and will be explained in section 2.4.
$D(\omega) \in \mathbb{R}^{6\times6}$ is the wave radiation damping matrix. This will be computed using numerical software. It can also be computed by the use of 2 dimensional damping coefficients, for zero forward speed, as in (Faltinsen, 1993), exemplified in equation (2.74), where the diagonal and coupled terms, respectively, are given by:

$$D_{ii} = \int_L D_{ii}^{2D}(\omega, x)dx, \tag{2.74a}$$

$$D_{ij} = -\int_L xD_{ii}^{2D}(\omega, x)dx. \tag{2.74b}$$

It is important to note the strong frequency dependency of the damping coefficients, thus the computed values are only valid for a rather narrow frequency range. The same holds for the matrix M(ω), given by:

$$M = M_{RB} + M_A, \tag{2.75a}$$

$$= \begin{bmatrix} m & 0 & 0 & 0 & 0 & 0 \\ 0 & m & 0 & -mz_g & mx_g & \\ 0 & 0 & m & 0 & -mx_g & 0 \\ 0 & -mz_g & 0 & I_x & 0 & -I_{xz} \\ mz_g & 0 & -mx_g & 0 & I_y & 0 \\ 0 & mx_g & 0 & -I_{zx} & 0 & I_z \end{bmatrix} + \begin{bmatrix} X_{\dot{u}} & \dots & X_{\dot{r}} \\ \vdots & \ddots & \vdots \\ N_{\dot{u}} & \dots & N_{\dot{r}} \end{bmatrix}.$$

M_A contains the strongly frequency dependant added mass coefficients, which explains the frequency dependency of M in equation (2.73). The calculations of A will, as for the rest of the hydrodynamic coefficients, be computed numerically by strip theory using the software ShipX. The calculation of the coefficients based the corresponding 2 dimensional coefficients are done similarly as for the

linear damping, as in(Faltinsen, 1993), for the generic added mass coefficients where subscript ii denotes added mass in DOF i due to acceleration in i, while ij denotes added mass in DOF i due to acceleration in j.

$$A_{ii} = \int_L A_{33}^{2D}(\omega, x)dx, \tag{2.76a}$$

$$A_{ij} = -\int_L xA_{33}^{2D}(\omega, x)dx. \tag{2.76b}$$

The restoring forces are given by the coefficients in the matrix G, and denote the hydrostatic loads on the system due to excitations in the vertical DOFs. G is on the form

$$G = \begin{bmatrix} 0 & 0 & 0 & 0 & 0 & 0 \\ 0 & 0 & 0 & 0 & 0 & 0 \\ 0 & 0 & Z_z & 0 & Z_\theta & 0 \\ 0 & 0 & 0 & K_\phi & 0 & 0 \\ 0 & 0 & M_z & 0 & M_\theta & 0 \\ 0 & 0 & 0 & 0 & 0 & 0 \end{bmatrix}. \tag{2.77}$$

As for the other coefficient matrices, the name of the coefficient denotes the direction of the resulting force, while the subscript denotes the DOF of the displacement that generates the force. The restoring coefficients are given as:

$$Z_z = \rho_w g A_{wp}, \tag{2.78a}$$

$$Z_\theta = M_z = -\rho g \iint_{A_{wp}} x ds, \tag{2.78b}$$

$$K_\phi = \rho g \nabla \overline{GM}_T, \tag{2.78c}$$

$$M_\theta = \rho g \nabla \overline{GM}_L, \tag{2.78d}$$

where A_{wp} is the total water plane area, ∇ is the volumetric displacement and $\overline{GM}_T$ and $\overline{GM}_L$ is the transverse- and longitudinal initial metacentric height. ρ_w is the density of the seawater, roughly equal to 1025[kg/m^3]. The dependency on both frequency and time is strictly speaking not quite trivial, as time series simulations of frequency dependent systems can be hard to generate. This type of system is called a *pseudo-differential equation*. An important method for time-series representation of frequency dependent added mass and wave radiation damping is the so-called

fluid memory effects. To successfully simulate for irregular seas, these effects must be accounted for, which can be done by convolution integrals as in (Cummins, 1962) which in turn can be used to derive a linear state space model for the effect as done in (Fossen, 2011). We will limit our simulations to regular sea states, thus omitting this problem.

2.4 Environmental Loads

This thesis is not meant to provide a thorough study of the aero- or hydrodynamic properties of typical SESs. As far as possible, numerical programs will be used to calculate loads and/or load-coefficients. Only a short introduction of the methods used to obtain and apply the environmental loads for the simulation will be presented here. As we recall from section 1.7, traditional DP-applications are typically concerned with 2nd order wave forces. However, due to some special properties of the SES, we will investigate lateral control of first order motions as well. This is possible due to the bandwidth of some of the SES actuators, which includes the WFs (typically 0.1s to 15s). The WF controller will not be suitable for damping of motions of period much higher than 15s, due to the signal processing which notch-filters the accelerometer signal in order to avoid signal drifting and noise. Waves of periods higher than 15 seconds will also, in general, imply sea states far above the operational window of the vessel. This thesis does also investigate a DP problem, which concerns higher period motions. However, this would, in its final implementation, be based on GPS measurements, not accelerometer signals.

We assume that the wave-induced forces can be represented as the product of two transfer function, as illustrated in figure 2.13

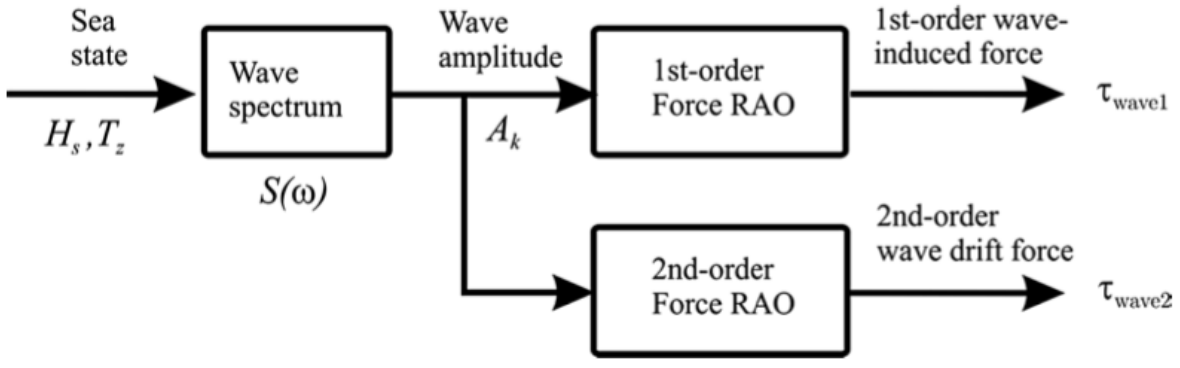

Figure 2.13: Wave-induced loads from sea state, taken from (Fossen, 2011)

2.4.1 1st Order Wave Loads

The 1st order wave loads will be obtained using so called force *Response Amplitude Operators* (RAOs), which for this thesis will be computed by the numerical seakeeping prediction program ShipX, from MARINTEK, and implemented by the method described in (Fossen, 2011). This approach assumes a linear relationship between the wave amplitude and the corresponding force exerted on the vessel, expressed by the means of generalised wave-induced forces as the vector

$$\tau_{wave1} = \begin{bmatrix} X_{wave1} \\ Y_{wave1} \\ Z_{wave1} \\ K_{wave1} \\ M_{wave1} \\ N_{wave1} \end{bmatrix} \tag{2.79}$$

To simulate for irregular waves, the JONSWAP spectrum,(Hasselmann et al., 1973), can for instance be used, and the amplitudes of each individual wave component, A_k, will be superimposed to obtain the resulting response. The relation between the wave spectrum S(ω_k) and the wave amplitude A_k for wave component k can be given as the sum of N harmonic components:

$$\frac{1}{2}A_k^2 = S(\omega_k)\Delta\omega. \tag{2.80}$$

Thus, the surface elevation, assuming *long-crested* seas, is found by:

$$\xi = \sum_{k=1}^{N} A_k \cos(\omega_k + \epsilon_k) = \sum_{k=1}^{N} \sqrt{2S(\omega_k)\Delta\omega}\cos(\omega_k + \epsilon_k). \tag{2.81}$$

Where ϵ_k is the phase-angle of wave component k. This expression assumes zero craft speed in the direction of the wave propagation, and is thus valid for this low/zero-speed problem. If that was not the case the frequency component should be switched to the corresponding frequency of encounter, given by equation (2.18).

The force RAOs are complex variables, and given by:

$$F_{wave1}^{dof}(\omega_k, \beta_i) = \left| \frac{\tau_{wave1}^{dof}(\omega_k, \beta_i)}{\rho_w g A_k} \right| e^{j\angle\tau_{wave1}^{dof}(\omega_k, \beta_i)}, \tag{2.82}$$

for wave directions β_i, and dof $\in \{1,2,3,4,5,6\}$. $\angle\tau^{dof}_{wave1}(\omega_k,\beta_i)$ denotes the angle of the phase of the transfer function at the given frequency and wave direction. If we denote the imaginary and real part of the transfer function: $Im_{wave1}\{dof\}(k,i)$ and $Re_{wave1}\{dof\}(k,i)$, we can find the amplitude and phase of the transfer function according to:

$$\left|F^{dof}_{wave1}(\omega_k,\beta_i)\right| = \sqrt{Im_{wave1}\{dof\}(k,i)^2 + Re_{wave1}\{dof\}(k,i)^2}, \tag{2.83a}$$

$$\angle F^{dof}_{wave1}(\omega_k,\beta_i) = atan2(Im_{wave1}\{dof\}(k,i), Re_{wave1}\{dof\}(k,i)), \tag{2.83b}$$

where atan2 denotes a function that computes the arctangent of two arguments. From this, we can express the wave-induced forces for all 6 DOF in the time-domain, denoted by the vector τ_{wave1}, from the following expression:

$$\tau^{dof}_{wave1} = \sum_{k=1}^{N} \rho_w g \left|F^{dof}_{wave1}(\omega_k,\beta_i)\right| A_k \cos\left(\omega_k t + \angle F^{dof}_{wave1}(\omega_k,\beta_i) + \epsilon_k\right). \tag{2.84}$$

Implementation of fluid memory effects in the vessel state-space model was beyond the scope of the thesis and has not been done. Therefore, we will limit our simulations to regular waves, and only one wave component is necessary in the sea surface realisation of equation (2.81)

2.4.2 Current Loads

The current loads will be simulated in the simplest possible form, 2 dimensional-, non-rotational flows. They will be implemented in the model through the damping matrix, and assumed sufficiently slow so that the linear model still show some validity. We denote the current velocity V_c and the current direction β_c. Thus the components of the current in {n} are given as

$$v^n_c = \begin{bmatrix} V_c \cos\beta_c \\ V_c \sin\beta_c \\ 0 \end{bmatrix}. \tag{2.85}$$

The velocity of the curren, V_c, will be modeled as the sum of a constant term and a fluctuating term modeled as a random, gaussian walk, thus V_c is given according to:

$$V_c = V_{cc} + V_{gc}, \tag{2.86}$$

where

$$\dot{V}_{gc} = -V_{gc} + w_c, \tag{2.87}$$

where w_c is gaussian white noise. The velocities in {n}are transformed to {b} by the relation

$$u_c^b = R_{3d}(\psi)^T v_c^n. \tag{2.88}$$

Since we assume the rotational components of the current to be negligible and the velocity to be without large variations, it suffices to include the relative velocity in the damping term of the LF-vessel model in order to implement the current effects in the simulation model. The relative velocity is given by

$$\nu_r = \nu - u_c^b. \tag{2.89}$$

The state space model given by equation (2.65) and, in particular, the damping term from equation (2.67) already accounts for relative velocity effects, thus this is easily implemented in the model.

2.4.3 Wind Loads

The wind loads on the vessel will be modeled in a similar manner as in (Fossen, 2011). For vessels that are symmetric with respect to the $x_b z_b$-plane, the wind loads can be written as:

$$\begin{aligned} X_{wind} &= -\frac{1}{2}\rho_a V_{rw}^2 c_x \cos(\gamma_{rw}) A_{Fw}, \\ Y_{wind} &= \frac{1}{2}\rho_a V_{rw}^2 c_y \sin(\gamma_{rw}) A_{Lw}, \\ N_{wind} &= \frac{1}{2}\rho_a V_{rw}^2 c_n \sin(\gamma_{rw}) A_{Lw} L_{oa}. \end{aligned} \tag{2.90}$$

A_{Fw} and A_{Lw} are the frontal and lateral projected areas, respectively, and V_{rw} is the effective wind speed. c_x, c_y and c_n are the wind load coefficients, which should be carefully determined for a quantitative analysis. For the qualitative station keeping analysis in this thesis, however, we will set these coefficients equal to the middle values of the rough intervals given by (Fossen, 2011), namely $c_x \in \{0.5, 0.9\}$, $c_u \in \{0.7, 0.95\}$ and $c_n \in \{0.05, 0.2\}$. γ_{rw} is the winds angle of attack, given by

$$\gamma_{rw} = -atan2(v_{rw}, u_{rw}), \tag{2.91}$$

and v_{rw} and u_{rw} are the relative x- and y-velocities are given by

$$\begin{aligned} v_{rw} &= v - v_w = v - V_w \cos(\beta_w - \psi), \\ u_{rw} &= u - u_w = u - V_w \sin(\beta_w - \psi), \end{aligned} \tag{2.92}$$

where ψ is defined in table 2.1 and β_w is the wind direction, defined as the way the wind is heading (not where it is coming from which might be common in other fields). As for the current loads, the windspeed V_w will, in the simulations, be given as a constant value but also as the sum of a constant velocity and a fluctuating component modeled by a gaussian random walk according to:

$$V_w = V_{cw} + V_{gw}, \tag{2.93}$$

where

$$\dot{V}_{gw} = -V_{gw} + w_w, \tag{2.94}$$

where w is gaussian white noise. The effective wind velocity, V_{rw}, is given by

$$V_{rw} = \sqrt{u_{rw}^2 + v_{rw}^2}. \tag{2.95}$$

2.5 Conditional Parametric Sensitivity

Due to the nature of SESs, there are several factors that influence the parameters of the vessel dynamics. The fact that the equilibrium cushion pressure can be chosen within a wide interval and the corresponding variations in equilibrium draft implies that hydrodynamic-, hydrostatic and aerodynamic coefficients are highly sensitive to the operational modes. To obtain reasonable simulation results, it is important to be aware of these differences. If the draft is increased, the hydrodynamic and hydrostatic loads will be larger, while the wind loads will be reduced due to the reduced above-water surface area. Similarly will a reduction of the draft increase the wind loads, with a corresponding reduction in the hydrostatic and hydrodynamic loads induced on the vessel. The variations in pressure will also determine the behavior and relative influence of the cushion dynamics. At maximum pressure, more than 80% of the displacement will be lifted by the cushion pressure which thus, to a large degree, will dominate the vertical behavior of the plant, while the vertical dynamics will rely solely on hydrodynamic- and hydrostatic effects when the fans are turned off. These variations will strongly affect the added mass- and damping terms, and it is therefore

important to specify the actual conditions used in simulations and other quantitative studies.

Further, we would like to pay some attention to the loss factor related to the airflow out of the air cushion, namely c_n. This is a recurring factor in the literature regarding the vertical dynamics of SESs, and is usually set to a fixed value equal to 0.61, as in (Sørensen and Egeland, 1995), (Kaplan et al., 1981) and (Faltinsen, 2005), and believed to be conservative. In the derivations earlier in this chapter we wanted to do a thorough investigation of the dynamic equations of the cushion pressure, and started out with Reynolds Transport Theorem and Euler's equations to derive an accurate nonlinear model of the cushion dynamics to be used in the process plant. Doing so, we investigated what we could find of relevant literature regarding the subject and, rather than a value of $c_n = 0.61$, we found indications that this factor, in reality, is a lot closer to unity. This makes the value of 0.61 indeed conservative, but perhaps unnecessarily conservative, at least if the motivation is to investigate the thrust delivering- and heave compensating capabilities of the cushion dynamics. Liepmann (1961) suggests that a value of c_n equal to 0.85 would be more accurate, while (Kurita, 1988) suggests an even higher value of 0.98 for round edged orificies or short tubes in high Reynolds numbers. $c_n = 0.61$ might be a suitable level for sharp edged orifices, but such geometry can easily be omitted in the design of a SES. There will probably be larger losses than the one suggested by Kurita, mostly due to the Vent Valve Louvers, however experiences from the full-scale tuning of the Wave Craft motion damping system indicated that they will still be significantly smaller than the losses implied by $c_n = 0.61$. Auestad et al. (2015) concludes that the value of $c_n = 0.61$, used in the simulations, was too small. Full scale testing gave significantly better results than what was expected by simulations and model tests, mostly since the increased outflow meant that the pressure could be decreased quicker. In real life, a lower loss coefficient would increase the dynamic pressure operational range, and should therefore also increase the vertical motion damping capabilities. It would also mean that we could expect significantly more thrust from a given directional leakage area at a given pressure, according to equation (2.53).

Chapter 3

Control System Design

3.1 Control Objective

This thesis concerns two main control objectives. The first objective is to use the Dynamical Positioning (DP) algorithm in combination with the different thrusters and actuators in the vessel so that station keeping can be performed. The second objective is to utilize the cushion pressure and the potential airflows related to it in order to, as far as possible, minimize the first order motions. This control objective is denoted the Wave Frequency (WF) motion damping. The problem is illustrated by the flow chart in figure 3.1.

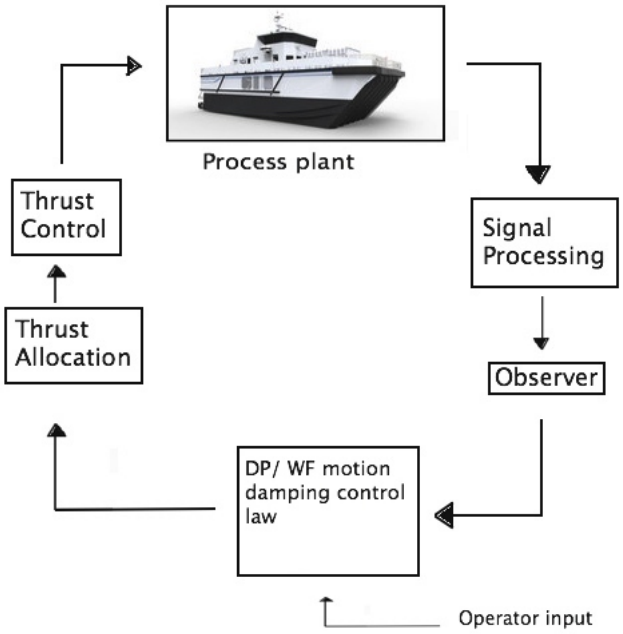

Figure 3.1: Generic marine control problem

The block called 'Process plant' contains the equations derived in chapter 2, and will be used to verify and test the behavior of the DP- and WF motion damping controller, as well as the thrust allocation and thrust control. Note that the vertical part of the WF motion damping controller will be similar, but not identical to the BCS control law presented in (Auestad et al., 2015), as it will feature cushion pressure feedback and different computation of the feedback gains. The signal processing block could typically be used to avoid sensor drifting and to remove noise, by applying a cascaded high- and low pass filter. The observer block usually contains a Kalman algorithm or some nonlinear passive observer, (Strand and Fossen, 1999). These are used to reconstruct unmeasured states and/or perform dead-reckoning when or if a sensor measurement drops out. However, these two blocks are beyond the scope of this thesis and will not be discussed any further. This chapter will concern the remaining three blocks, i.e. the DP/WF motion damping, thrust allocation and thrust control, i.e. the process of going from sufficient information about the states of the plant to an actual output from each individual actuator, as illustrated by figure 3.2. We will not discuss local servo feedback loops, but assume these to be perfect.

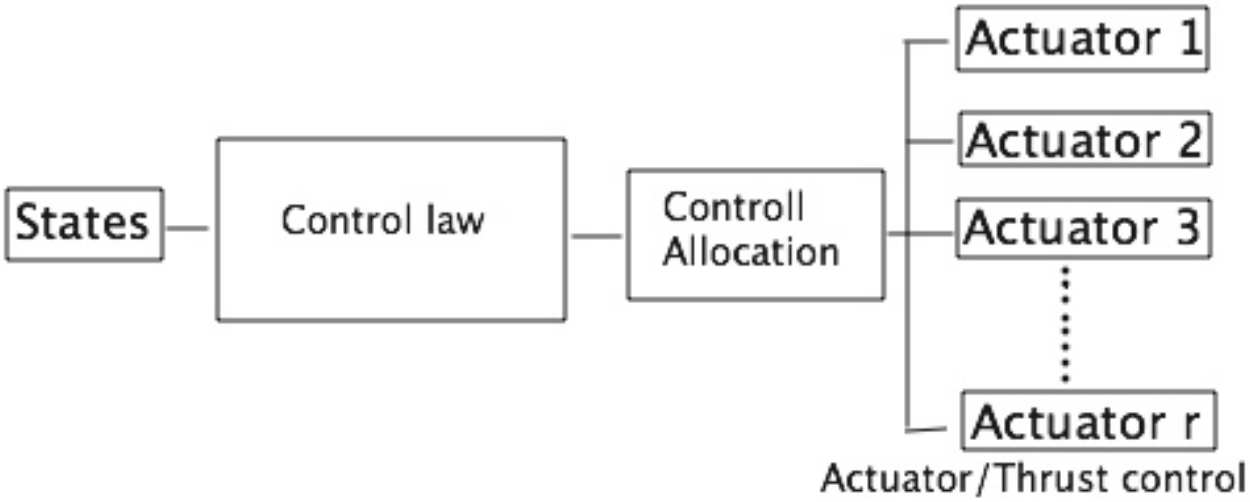

Figure 3.2: Specific control problem

The control laws will be given in Section 3.3 and 3.4, the control allocation problem is described in section 3.5, while the actuator/thrust control is solved in the two last sections of the chapter, i.e., section 3.6 and 3.7. If we summarize the control objective, we wish to obtain full control over the low frequency (LF) horizontal motions, i.e. surge, sway and yaw, which makes up the DP problem. For the WF problem, we wish to damp the motions in heave and sway as far as possible. Further development of the system could probably perform effective damping of the WF trajectories in pitch

and yaw as well, however we will limit the scope of the work to only contain the two translational trajectories for now. The system is defined in all 6 DOF, thus the size of the configuration space, n, equals 6. The order of the system equals 13 since a number of two differential equations are needed to describe the motions in each DOF and the fact that we regard the pressure trajectory as an individual state. We look at the WF and LF as two individual problems. The focus on the LF problem will be limited to show the capacity and potential of such a system on a SES, and the focus here will thus not be on any form for optimal control etc. We denote the size of the LF working space, the space in where the control objective is defined, m_{lf}. We denote the number of independently controlled actuators relevant for this problem r_{lf}=5, by regarding the lateral and longitudinal components of the water jets as individual actuators, and notice that the system is over-actuated in the horizontal plane. I.e., $r_{lf} > m_{lf}$. Strictly speaking, this implies a certain level of redundancy in the system, as full actuation would be achieved even if one of the water jets or the vent valves/lift fans were to fail. For the WF problem, we can reduce the size of the configuration space to a working space of size m_{wf}=3, which includes the cushion pressure state. We have two inputs, leakage area and the vent valve thrust, which control the heave and sway motions, respectively, thus $r_{wf} = 2$. We must remember that, dependent on the longitudinal position of the vent valves relative to the COG, the Vent Valve thrust will induce yaw moments if this distance is different from zero, however this motion is not subject to feedback, and will not be controlled for now. For the existing Wave Craft, the vent valves are located at midships, thus the yaw moment induced will be very small if the controller was to be applied on that system. The DP section assumes the vent valves to be located in the bow. This discrepancy in assumptions is okay due to the fact that horizontal WF motion damping will never be applied simultaneously with the DP controller, and we can therefore simulate for the conceptual effect of both controllers individually. For the WF problem we have $r_{wf} \leq m_{wf}$ and, the problem is therefore under actuated. This implies that $full$ control over all DOFs will be very hard to achieve, however damping of the trajectories is still possible. There is a strong coupling between the vent valve thrust and the cushion pressure, which complicates the problem significantly, and makes perfect control nearly impossible. This will be discussed in section 3.3, and the simulation chapter will show that the WF controller performs large degrees of motion damping on the system. We denote the commanded force vector for the LF

problem (see table 2.1):

$$\tau_{pid} = \begin{bmatrix} X_{lf} \\ Y_{lf} \\ N_{lf} \end{bmatrix} \in \mathbb{R}^3. \tag{3.1}$$

For the WF problem, the commanded control signal will consist of a commanded total leakage area from the vent valves and a lateral thrust in newtons from the vent valves, which in turn will be "translated" to a lateral leakage area, by equation (3.70). We denote this WF control vector u_c^l, where

$$u_c^l = \begin{bmatrix} \sum \Delta A_i^l \\ u_c^{vv} \end{bmatrix}, \tag{3.2}$$

where $\sum \Delta A_i^l$ from now on will be replaced by ΔA_{vert}^l, for better compliance with common conventions of notation. We choose the last input as the commanded force and not a lateral leakage area because the leakage area depends on the pressure, which would have made the control input matrix time- and state dependent, and severely complicated the linearization. Instead the transformation will be regarded as a thrust control problem, and solved later.

3.2 Control Plant Model

The control problem in the thesis is dual, i.e. it can be divided into the dynamic positioning problem and the WF motion compensation problem. The DP controller will feature a simple PID controller to demonstrate the DP capabilities of the vessel. The WF motion damping algorithm, however, will feature a controller derived by linear quadratic minimisation methods, thus the WF-dynamics must be on linear form. The WF vessel dynamics were derived in a linear manner, and need no further alterations. The equations describing the dynamics of the uniform pressure, however, are of a nonlinear nature and must be linearized in order to perform the LQR synthesis.

3.2.1 Linearization

The common convention for linearizing non-linear systems, is to use the second term in the Taylor expansion, and, due to equilibrium arguments, neglect the *constant* term. The generic system of investigation will be given by

$$\dot{x} = f(x, u, t). \tag{3.3}$$

The multivariate Taylor approximation of the k times differentiable function f(x,u,t) of n-coupled differential equations, at the operating point a, is given by:

$$f(x) = \sum_{|a|\leq k} \frac{D^a f(a)}{a!}(x-a)^a + \sum_{|\beta=k+1} R_\beta(x)(x-a)^\beta, \tag{3.4}$$

where the last term is the remainder, and should, together with all terms of second or higher order, be neglected in the approximation. $D^a f$ is defined as

$$D^a f = \frac{\partial^{|a|} f}{\partial x_1^{a_1} \dots \partial x_n^{a_n}}. \tag{3.5}$$

This approach yields an undisturbed linearized system on the form

$$\begin{aligned} \dot{x} &= Ax + Bu, \\ y &= cx. \end{aligned} \tag{3.6}$$

Where A and B at the operating point x_p, are given as in (Balchen et al., 1999):

$$A(t)|_{x_p} = \begin{bmatrix} \frac{\partial f_1(x,u,t)}{\partial x_1} & \dots & \frac{\partial f_n(x,u,t)}{\partial x_n} \\ \vdots & \ddots & \vdots \\ \frac{\partial f_n(x,u,t)}{\partial x_1} & \dots & \frac{\partial f_n(x,u,t)}{\partial x_n} \end{bmatrix}, \text{ and } B(t)|_{x_p} = \begin{bmatrix} \frac{\partial f_1(x,u,t)}{\partial u} \\ \vdots \\ \frac{\partial f_n(x,u,t)}{\partial u} \end{bmatrix}. \tag{3.7}$$

The time dependency can obviously be neglected for time-independent systems. The DOFs that are of concern for the WF motion damping controller are sway and heave, where the vertical trajectories, in turn, are closely related to the uniform pressure, which therefore must be included.

3.2.2 Linear Uniform Pressure Equation - WF motion

The uniform pressure equation is given by

$$\begin{aligned} &\frac{V(p_a + p_0 + \mu(t)p_0)^{\frac{1}{\gamma}-1}}{\gamma(\frac{p_a}{p_0}+1)(p_a+p_0)^{\frac{1}{\gamma}-1}}\dot{\mu}(t) - \sum Q_i + \dots \\ &\dots + c_n(A_0 + A^{fp}(\eta_s) + A^{ap}(\eta_s) + \Delta A^l_{vert})\sqrt{\frac{2(p_0+\mu(t)p_0)}{\rho_a}} = \\ &\qquad -x_{cp}A_c\dot{\eta_5}(t) + A_c\dot{\eta_3}(t) + b\int_{-\frac{L}{2}}^{\frac{L}{2}} \dot{\xi}(x,t)dx. \end{aligned} \tag{3.8}$$

We notice the control input ΔA^l_{vert} and the environmental disturbance in the last term on the right hand side of the equation. By Taylor expanding the nonlinear terms around the operating point $\mu = 0$, we obtain the linearized uniform pressure equation given as

$$\begin{aligned}\frac{V_0}{\gamma(\frac{p_a}{p_0}+1)}\dot{\mu} - Q_0 - \mu\frac{\partial Q}{\partial P}|_{\mu=0} + Q_{out}|_{\mu=0} + p_0\mu\frac{\partial Q_{out}}{\partial P}|_{\mu=0} + \dots \\ \dots + c_n\sum\Delta A_i\sqrt{\frac{2(p_0+\mu p_0)}{\rho_a}} = -x_{cp}A_c\dot{\eta}_5 + A_c\dot{\eta}_3,\end{aligned} \tag{3.9}$$

where Q_0 is the flow from the lift fans at equilibrium and $\frac{\partial Q}{\partial P}|_{\mu=0}$ is the slope of the inverse fan characteristics at equilibrium. The linearized flow of air out of the volume is given as

$$Q^{lin}_{out}(t) = Q_{out}|_{\mu=0} + \mu(t)\frac{\partial Q_{out}}{\partial P}|_{\mu=0}, \tag{3.10}$$

where $Q_{out}|_{\mu=0}$ is given by:

$$Q_{out}|_{\mu=0} = c_n(A_0 + A^{fp}(\eta_s) + A^{ap}(\eta_s))\sqrt{\frac{2p_0}{\rho_a}}. \tag{3.11}$$

Thus, $\frac{\partial Q_{out}}{\partial P}|_{\mu=0}$ equals

$$\frac{\partial Q_{out}}{\partial P}|_{\mu=0} = \frac{c_n}{2}(A_0 + A^{fp}(\eta_s) + A^{ap}(\eta_s))\sqrt{\frac{2p_0}{\rho_a}}. \tag{3.12}$$

At equilibrium $\sum\Delta A$ and $p_0\mu\frac{\partial Q}{\partial P}$ equals zero. It is therefore obvious that Q_0 and $Q_{out}|_{\mu=0}$ should cancel each other out to maintain the equilibrium condition $\dot{\mu} = 0$, (Faltinsen, 2005).

$$Q_{out} = Q_0(1 + \frac{\mu}{2}). \tag{3.13}$$

Summing up equations (3.9), (3.10), (3.12) and (3.13) yields the following linearized uniform pressure equation

$$K^{lin}_1\dot{\mu} + K^{lin}_3\mu + K^{lin}_2\sum\Delta A_i = -x_{cp}A_c\dot{\eta}_{s5} + A_c\dot{\eta}_3, \tag{3.14}$$

where K^{lin}_1, K^{lin}_2 and K^{lin}_3 are given by

$$\begin{aligned}K^{lin}_1 = \frac{V_0}{\gamma(\frac{p_a}{p_0}+1)}, \quad K^{lin}_2 = c_n\sqrt{\frac{2p_0}{\rho_a}}, \\ K^{lin}_3 = \frac{1}{2}(Q_0 - 2P_0\frac{\partial Q}{\partial P}|_{\mu=0}).\end{aligned} \tag{3.15}$$

This linear model is similar to the model used in (Auestad et al., 2015), (Sørensen and Egeland, 1995) and (Faltinsen, 2005).

By including the controlled force from the vent valve louvers, the above derivations can be summed up to the linear control plant model given by

$$\dot{\eta}_{lin} = A_{lin}\eta_{lin} + B_{lin}u_c^l, \tag{3.16}$$

where

$$\begin{aligned}
\eta_{lin} &= \begin{bmatrix} \eta_2 & \eta_3 & \dot{\eta}_2 & \dot{\eta}_3 & \mu \end{bmatrix}^T, \quad u_c^l = \begin{bmatrix} \Delta A_{vert}^l & u_c^{vv} \end{bmatrix}^T \\
A_{lin} &= \begin{bmatrix} 0_{2\times 2} & I_{2\times 2} & 0_{2\times 1} \\ -M^{-1}G_{2\times 2} & -M^{-1}D(\omega)_{2\times 2} & L_{2\times 1} \\ & K_{1\times 5} & \end{bmatrix}, B_{lin} = \begin{bmatrix} 0 & 0 \\ 0 & 0 \\ 0 & 1 \\ 0 & l_x^{vv} \\ -\frac{K_2}{K_1} & 0 \end{bmatrix}, \\
L &= \begin{bmatrix} -A_{cp}p_0 & x_{cp}A_cp_0 \end{bmatrix}^T \quad \text{and} \\
K &= \begin{bmatrix} 0 & 0 & \frac{A_c}{K_1} & \frac{-x_{cp}A_c}{K_1} & \frac{-K_3}{K_1} \end{bmatrix}.
\end{aligned} \tag{3.17}$$

M is the total mass matrix, D is the frequency dependent linear damping matrix and G is the matrix containing the restoring coefficients, the latter three terms are thoroughly explained in section 2.3.2. Note also that $A_{lin} \in \mathbb{R}^{n_{lin}\times n_{lin}}$ and $B_{lin} \in \mathbb{R}^{n_{lin}\times r_{lin}}$, where $n_{lin} = 5$ and $r_{lin} = 2$.

3.3 First Order Wave Load Compensation

This section will derive the WF control law, i.e., the mapping from the states of the system to the control output vector. Later, in Section 3.6, we will show how to go from the commanded signals from the control law to actual actuator commands, which will be regarded as a type of thrust/actuator control, and is, due to saturations and control inflictions, not necessarily quite trivial. Conventional dynamic positioning systems are mostly concerned about counteraction of the slowly varying forces. Due to some very special features, however, SESs are, to a certain degree, also able to counteract the first order wave induced motions. The vast amount of air constantly delivered by the lift fans and the corresponding pressure reservoir provides the system with a significant amount of potential energy, which due to the fast dynamics of their actuators, the vent valve louvers, can be *relased* and redirected in the manner of one tenth of a second. This chapter

will discuss how to utilize these features to, as far as possible, minimize the vessel WF motions. The WF motion damping will be done solely by the means of the variable leakage areas of the vent valves. As explained earlier, by commanding lateral differences in these leakage areas, significant lateral thrust can be achieved in addition to the pressure variations which influences the vertical state trajectories. Since there are a lot of different terms related to these leakage areas, the most important ones will be summarized here, in table 3.1, and later classified.

Definition	Notation
Actual, total leakage area	$A^l = A^l_{port} + A^l_{sb}$
Actual, lateral leakage area	$\Delta A^l = A^l_{port} - A^l_{sb}$
Dynamic lateral leakage area from sway motion damping controller	ΔA^l_{lat}
Commanded dynamic leakage area of all vent valves i=1,2,3, from heave controller	$\sum \Delta A^l_i = \Delta A^l_{vert}$ (the latter will be used in the following)
Bias (equilibrium) leakage area	A_0
Commanded total leakage area	$A^l_c(t) = A_0 + \Delta A^l_{vert}$
Commanded thrust level from sway motion damping controller	u^{vv}_c
Lateral thrust from a given pressure and lateral leakage	$u^{vv}_y = -2n \cdot c_n \cdot \rho_c \Delta A^l_{lat} \frac{p_u(t)}{\rho_a}$

Table 3.1: Summary of important notation regarding the leakage areas

The output from the WF controller will be the vector u^l_c, given by:

$$u^l_c = \begin{bmatrix} \Delta A^l_{vert} \\ u^{vv}_c \end{bmatrix}. \tag{3.18}$$

The reason why we chose to use u^{vv}_c instead of the corresponding lateral leakage area, ΔA^l_{lat}, as the last input in u^l_c is the state dependency of the relation between them. The relation between the lateral leakage area, ΔA^l_{lat}, and the resulting net thrust, u^{vv}_y, depends on one of the system states, $\mu(t)$, thus the subsequent derivations would have been made unnecessarily complicated by this notation. Instead we regard the process of going from a demand for lateral thrust, u^{vv}_c, to the corresponding lateral leakage, ΔA^l_{lat}, as a thrust control problem, which will be discussed in section 3.6 where we also add a saturation handler. We will use a feedback controller as the main control

scheme for this problem, thus we can assume the controller to be given on the following form:

$$u_c^l = \begin{bmatrix} \Delta A_{vert}^l \\ u_c^{vv} \end{bmatrix} = -\underbrace{\begin{bmatrix} k_{11} & k_{12} & k_{13} & k_{14} & k_{15} & k_{16} & k_{17} \\ k_{21} & k_{22} & k_{23} & k_{24} & k_{25} & k_{26} & k_{27} \end{bmatrix}}_{\text{k}} \underbrace{\begin{bmatrix} \eta_2 \\ \dot{\eta}_2 \\ \ddot{\eta}_2 \\ \eta_3 \\ \dot{\eta}_3 \\ \ddot{\eta}_3 \\ \mu \end{bmatrix}}_{\eta_{feedback}}, \tag{3.19}$$

where k, for the scope of this thesis, is a constant coefficient matrix containing the feedback gains. $\eta_{feedback}$ is simply a vector featuring all the terms we have available for feedback in the plant, not all of them will be used. We will assume that the trajectories of all states are available at any given time, however we will not discuss any further the algorithms necessary to obtain this. We also assume the horizontal motion damping to base its control output solely on the horizontal states, while the vertical motion damping will utilize pressure feedback in addition to the velocity and acceleration in heave. From the above, we set $k_{11}, k_{12}, k_{13}, k_{24}, k_{25}$, k_{26} and k_{27}=0. Neither will we be using the positions for feedback in the WF-problem, thus we can also set $k_{14} = k_{21} = 0$. There are multiple sources of motivation for the use of state *derivative* feedback. First of all, by integration and proper filtering of accelerometer outputs, it is possible to obtain decent information about the WF accelerations and velocities. It is, however, quite difficult to obtain accurate information about the WF displacements, especially with the sensors that can be assumed available on a SES today. WF position estimation could hypothetically be performed by some optical measurement system, but these signals will be assumed unavailable for now. It is the WF forces we want to counteract, and since the position trajectory has a 180° phase relative to these, even if accurate information about the positions was available, it would still be a rather inefficient source of feedback given the limited available actuator capacity. We assume that the state trajectories, for regular waves, can

be given as

$$\begin{aligned}
\eta_2 &= |\eta_2| \sin(\omega_w t + \epsilon_2), \\
\dot{\eta}_2 &= \omega_w |\eta_2| \sin(\omega_w t + \dot{\epsilon}_2), \\
\ddot{\eta}_2 &= \omega_w^2 |\eta_2| \sin(\omega_w t + \ddot{\epsilon}_2), \\
\eta_3 &= |\eta_3| \sin(\omega_w t + \epsilon_3), \\
\dot{\eta}_3 &= \omega_w |\eta_3| \sin(\omega_w t + \dot{\epsilon}_3), \\
\ddot{\eta}_3 &= \omega_w^2 |\eta_3| \sin(\omega_w t + \ddot{\epsilon}_3), \\
\mu &= |\mu| sin(\omega_w t + \epsilon_\mu),
\end{aligned} \tag{3.20}$$

where $|\eta_2|$ denotes the amplitude of the sway motion, $|\eta_3|$ is the amplitude of the heave motions ω_w is the angular wave frequency and ϵ_2 denotes the relative phase of the heave displacement, etc. We note that $\dot{\epsilon}_2$=$\epsilon_2 + 90°$. We will base the derivation of the feedback gains on an LQR-like synthesis, however due to the fact that the phases between the various sources of feedback spans a large set and the fact that only one actuator is used to control the trajectories of the entire plant, care must be given in the controller tuning to ensure that the level of infliction between the different control desires is minimized. The next section, 3.3.1, will show how to compute the optimal feedback gains for an arbitrary, quadratic, optimization criterion, while section 3.3.2 will explain the method used by us to ensure that the relative phase between the control signals contributes in minimizing the level of mutual infliction between them.

3.3.1 Optimal State Derivative Feedback Gains

The WF motion compensation control scheme will use a Linear Quadratic optimization algorithm to compute the feedback gains of the controller. Instead of using control action proportional to the state feedback, the WF motion damping controller used in this thesis will feature a *state-derivative-feedback* controller, derived according to a method proposed by (Abdelaziz and Valášek, 2005). The system subject to control is the Linear Time Invariant (LTI) system given by equation (3.16), i.e.

$$\dot{\eta}_{lin}(t) = A_{lin}\eta_{lin}(t) + B_{lin}u_c^l(t), \tag{3.21}$$

where $\eta_{lin}(t) \in \mathbb{R}^5$ is the state vector and $u_c^l(t) \in \mathbb{R}^2$ is the controlled input vector. The two fundamental assumptions for this system in order to derive the state-derivative feedback gains is that it is stabilizable and that the matrix A_{lin} is of full rank, i.e. rank(A_{lin})=n_{lin}=5, which is infact true.

The first assumption, on stabilizability is also valid as will be showed later by the strictly negative eigenvalues of the closed loop system. A full proof of stability for the vertical SES dynamics when subject to state feedback is given by (Auestad et al., 2014).

Linear Quadratic Regulation, with both state- and state-derivative feedback, is a subset of optimal control, and it is based on the idea of minimizing some criterion, or cost function, here denoted J_{LQR}. This is, in its most general form, given by

$$J_{LQR} = \int_0^\infty \dot{\eta}_{lin}(t)' Q \dot{\eta}_{lin}(t) + u_c^l(t)' R u_c^l(t) dt, \tag{3.22}$$

where Q is a $n_{lin} \times n_{lin}$ positive semidefinite state-derivative weighting matrix and R is an $m_{lin} \times m_{lin}$ positive definite symmetric control weighting matrix. R determines how strongly the controlled input is to be weighted in the minimization. Large value of the inputs in R means that the most effective way to decrease J_{LQR} is to employ a small input, at the expense of a large controlled output. In contrast, a relatively small value of R means that J_{LQR} is most effectively decreased by allowing a large control input, with a corresponding small controlled output. The solution to the Linear Quadratic problem is a gain matrix k_{lqr}, which yields the controller

$$u_c^l = -k_{lqr} \dot{\eta}_{lin}. \tag{3.23}$$

$k_{lqr} \in \mathbb{R}^{r_{lin} \times n_{lin}}$ is the control input gain that minimizes the quadratic cost criterion. Substituting (3.23) into (3.22) yields the updated cost function given by

$$J_{LQR} = \int_0^\infty (\dot{\eta}_{lin}(Q + k_{lqr}^T R k_{lqr}) \dot{\eta}_{lin}) dt. \tag{3.24}$$

We then obtain the closed-loop dynamics given by

$$\dot{\eta}_{lin}(t) = A_c \eta_{lin}(t), \quad A_c = (I_n + B_{lin} k_{lqr})^{-1} A_{lin}. \tag{3.25}$$

$I_n \in \mathbb{R}^{n_{lin} \times n_{lin}}$ is the identity matrix. Rearranging the terms in equation (3.25) yields

$$\eta_{lin} = A_c^{-1} \dot{\eta}_{lin}, \quad A_c^{-1} = A_{lin}^{-1}(I_n + B_{lin} k_{lqr}). \tag{3.26}$$

This requires A_{lin} to be invertible, which is strictly speaking not the case due to the lack of restoring forces in sway. We omitted this by slightly altering the dynamics to ensure that A_{lin} was invertible. We did this by adding a negligible small restoring coefficient in sway, with a relative order of magnitude when compared to the restoring coefficient in heave of 10^{-5}, thus the dynamics should not have been severely affected. We note that the final result yielded a very strongly performing controller. Now we assume that there exists some constant positive-semidefinite symmetric matrix P, such that

$$\dot{\eta}_{lin}(Q + k_{lqr}^T R k_{lqr})\dot{\eta}_{lin} = -\frac{\partial}{\partial t}(\eta_{lin}^T P \eta_{lin}) = -\dot{\eta}_{lin}^T P \eta_{lin} - \eta_{lin}^T P \dot{\eta}_{lin}. \tag{3.27}$$

By inserting (3.27) into the original cost criterion, this can be evaluated as

$$\begin{aligned} J_{LQR} = \int_0^\infty (\dot{\eta}_{lin}(Q + k_{lqr}^T R k_{lqr})\dot{\eta}_{lin})dt = -\eta_{lin}^T P \eta_{lin}\big|_0^\infty = \\ = -\eta_{lin}^T(\infty) P \eta_{lin}(\infty) + \eta_{lin}^T(0) P \eta_{lin}(0). \end{aligned} \tag{3.28}$$

By the assumption of closed-loop stability, the first term on the right hand side of the last equality will vanish, thus the cost criterion is given by the initial condition and the matrix P, and converges to

$$J_{LQR} = \eta_{lin}^T(0) P \eta_{lin}(0). \tag{3.29}$$

By equation (3.26), we rewrite equation (3.27) such that,

$$\dot{\eta}_{lin}^T(Q + k_{lqr}^t R k_{lqr})\dot{\eta}_{lin}^T = -\dot{\eta}_{lin}^T(P A_c^{-1} + A_c^{-1^T} P)\dot{\eta}_{lin} \tag{3.30}$$

which yields the following relation

$$P A_c^{-1} + A_c^{-1^T} P + k_{lqr}^T R k_{lqr} + Q = 0. \tag{3.31}$$

This is recognized as the *Lyapunov* equation. By Lyapunovs method, which is thoroughly explained e.g. in (Hespanha, 2009), (3.31) is solvable with respect to P if and only if the closed loop system is stable, thus P should be found. By inserting (3.26) into (3.31), and noting that since R is a

positive-definite symmetric matrix it can be written R=$T^T T$, we rewrite equation (3.31) such that

$$PA_{lin}^{-1} + A_{lin}^{-1^T} P + (Tk_{lqr} + T^{-1^T} B_{lin}^T A_{lin}^{-1^T} P)^T (Tk_{lqr} + T^{-1^T} B_{lin}^T A_{lin}^{-1^T} P) - \ldots \\ \ldots PA_{lin}^{-1} B_{lin} R^{-1} B^T A_{lin}^{-1^T} P + Q = 0. \tag{3.32}$$

From this we note that the LQR criterion is minimized with respect to K by the minimization of

$$\dot{\eta}_{lin}^T (Tk_{lqr} + T^{-1^T} B^T A_{lin}^{-1^T} P)^T (Tk_{lqr} + T^{-1^T} B^T A_{lin}^{-1^T} P) \dot{\eta}_{lin}, \tag{3.33}$$

thus we obtain the optimal gain matrix k_{lqr}:

$$k_{lqr} = -R^{-1} B^T A_{lin}^{-1^T} P \in \mathbb{R}^{2\times 5}, \tag{3.34}$$

which yields the following control law

$$u_c^l(t) = R^{-1} B^T A_{lin}^{-1^T} P \dot{\eta}_{lin}(t) \in \mathbb{R}^{2\times 1}. \tag{3.35}$$

P is found as the solution to the algebraic Riccati equation (ARE), which is given by

$$PA_{lin}^{-1} + A_{lin}^{-1^T} P - PA_{lin}^{-1} B_{lin} R^{-1} B^T A_{lin}^{-1^T} P + Q = 0. \tag{3.36}$$

The conditions for existence of a symmetric matrix P, which satisfies the ARE are, in short, given by the following statements:

1. The pair (A_{lin}, B_{lin}) is stabilizable
2. The pair (A_{lin}, Q) is detectable
3. A_c is a stability matrix, i.e. for each eigenvalue λ_i of A_c, then Re[λ_i]<0

These conditions are further explained in (Hespanha, 2009). For a more thorough investigation of the derivation of the optimal state derivative feedback gain, the reader is referred to (Abdelaziz and Valášek, 2005).

For all reasonable parameter values used in the model, the above conditions hold. The stabilizability of the pair (A_{lin}, B_{lin}) is implied by the exponential stability of the closed-loop dynamics given by A_c, which in turn is proofed by the closed loop eigenvalues and the following equivalent statements (Hespanha, 2009).

1. The system A_c is exponentially stable.

2. All the eigenvalues of A_c have strictly negative real parts

And the vector of the eigenvalues λ_c corresponding to the closed loop dynamics A_c, given below for the parameters given in Appendix B.

$$\lambda_c = \begin{bmatrix} -0.0000001255 + 0.0i \\ -0.000045 + 0.0i \\ -0.0000085 + 0.0i \\ -0.008344 + 2.39i \\ -0.0083447 - 2.39i \end{bmatrix} \tag{3.37}$$

We note that the eigenvalues have, even though some of them being close to the imaginary axis, strictly negative real values. The detectability of the system is shown by the Popov-Belevitch-Hautus [PBH] test for detectability which states:

PBH test for detectability 1. *A continuous-time LTI system is detectable if and only if*

$$rank \begin{bmatrix} A_{lin} - \lambda I \\ Q \end{bmatrix} = n_{lin}, \qquad \forall \lambda : Re[\lambda] \geq 0 \tag{3.38}$$

which does hold for our linearized system, thus detectability is shown, and we know that the solution P to the ARE exists, thus the optimal state derivative feedback gains can be computed, and will be used for the WF motion damping. Note that these derivations are valid for linear systems only, and the result will only be applied for the small perturbations occurring within the range of the WF motions, where we assume the nonlinearities of the process plant to be somewhat restricted.

3.3.2 Control Signal Phase Shift by Proper Feedback Gains

The preceding section provides us with a set of feedback gains, optimal with respect to the different weighting matrices used, i.e. Q and R. However, due to the nature of this plant we need a way in determining what weighting matrices to use. This plant exhibit some quite unusual actuator properties, which were briefly explained in the beginning of section 3.3. Both the available lateral thrust needed for sway motion damping and the vertical forces used for control of the heave trajectories

depends on one of the system states, i.e. the pressure, normalized by $\mu(t)$. The only controlled input for the pressure state is the total leakage area of the vent valves, A^l, while the lateral thrust is controlled by the means of the lateral difference in leakage area, i.e. ΔA^l_{lat}, thus they are, strictly speaking, controlled by the exact same set of actuators. If we look at the two WF control problems individually, the conflict of interest which will be described in the following is irrelevant, however since we also will investigate the potential in performing simultaneous motion damping of both heave and sway motions, a problem arise. The desires for total- and lateral leakage areas will, if not proper precaution is taken, strongly inflict on each other. Maximum total leakage, A^l_{max}, is obtained by fully opening both vent valves, while maximum lateral leakage, $\frac{A^l_{max}}{2}$, is achieved by fully opening one vent valve, while fully closing the other one. Both of these desires can obviously not be achieved at the same time, and if the system *tries* to achieve them simultaneously, the performance of one or both of the control objectives will be severely harmed. Therefore, strong precaution must be taken in the design of the system, so that proper weighting of the various state trajectories in the feedback gains ensures the two control signals to be in such a phase relative to each other that the conflict mentioned above is, as far as possible, avoided. To ensure that the phase of these control signals is within the requirements, we derive a simple method to determine the relative weighting of the lateral state trajectories, necessary in order to force the resulting lateral control signal to a 90° phase relative to the vertical motion damping control signal. The reason why we need 90° phase becomes apparent by studying figure 3.3. In that way, the maximum absolute value of one signal will coincide with the minimum absolute value of the other signal (since both ΔA^l_{vert} and ΔA^l_{lat} oscillates somewhat sinusoidal around 0), and the level of infliction is reduced.

We will assume all state trajectories, phases and amplitudes, to be known, and derive a set of "phase-optimal" feedback gains which will be used for iteration of the state weighting matrix, Q, in order to obtain the properties described above. By the gains from equation (3.19), we can find the relative phase, ϵ_{shift}, due to superposition of two sinusoidal components of amplitude $k_{22}\left|\dot{\eta}_2\right|$ and $k_{23}\left|\ddot{\eta}_2\right|$, and phase $\dot{\epsilon}_2$ and $\ddot{\epsilon}_2$, given by

$$\epsilon_{shift} = arctan\frac{k_{22}\left|\dot{\eta}_2\right|\sin\dot{\epsilon}_2 + k_{23}\left|\ddot{\eta}_2\right|\sin\ddot{\epsilon}_2}{k_{22}\left|\dot{\eta}_2\right|\cos\dot{\epsilon}_2 + k_{23}\left|\ddot{\eta}_2\right|\cos\ddot{\epsilon}_2}. \tag{3.39}$$

We can also relate the feedback gains to the amplitude of the resulting control signal. The level we choose for the resulting control signal amplitude should relate the known motion amplitudes with

the maximum obtainable thrust levels, in a manner so that saturation is avoided. We must also remember that as the controller is applied, the motion amplitudes should be reduced, thus the size of the feedback gains can be increased, when compared to the undamped motion trajectories, while still keeping the control signal within the saturation limits. Megretski (1996) presents interesting work regarding motion damping of strongly saturated systems by a gain scheduling like scheme, however their results will not be applied for the work in this thesis. We relate the state trajectory amplitudes to the control amplitude by:

$$|u_c^{vv}| = \sqrt{A_{amp}^2 + B_{amp}^2}, \tag{3.40}$$

where

$$\begin{aligned} B_{amp} &= [k_{22}\,|\dot{\eta}_2|\cos\dot{\epsilon}_2 + k_{23}\,|\ddot{\eta}_2|\cos\ddot{\epsilon}_2] \quad \text{and} \\ A_{amp} &= [k_{22}\,|\dot{\eta}_2|\sin\dot{\epsilon}_2 + k_{23}\,|\ddot{\eta}_2|\sin\ddot{\epsilon}_2]. \end{aligned} \tag{3.41}$$

From the above we now possess two equations relating the phase and amplitude of the state trajectories with the phase and amplitude of the resulting control signal. It is the phase of this control signal we want to ensure to be of the optimal value. By solving (3.39) and (3.40) for the two respective feedback gains, k_{21} and k_{22}, we obtain the "phase-optimal" velocity feedback gain given implicitly by:

$$\begin{aligned} A_{amp}^2 + B_{amp}^2 = k_{22}^2\,|\dot{\eta}_2^2|\underbrace{(\sin^2\dot{\epsilon}_2 + \cos^2\dot{\epsilon}_2)}_{=1} + k_{23}^2\,|\ddot{\eta}_2^2|\underbrace{(\sin^2\ddot{\epsilon}_2 + \cos^2\ddot{\eta}_2)}_{=1} + \ldots \\ \cdots + k_{22}\,|\dot{\eta}_2|\,k_{23}\,|\ddot{\eta}_2|\underbrace{(\cos\dot{\eta}_2\cos\ddot{\epsilon}_2 + \sin\dot{\epsilon}_2\sin\ddot{\eta}_2)}_{=\cos(\dot{\epsilon}_2 - \ddot{\epsilon}_2) = 0} \\ \Downarrow \\ k_{22} = \sqrt{\frac{|u_c^{vv}|^2 - k_{23}^2\,|\ddot{\eta}_2|^2}{|\dot{\eta}_2|^2}}. \end{aligned} \tag{3.42}$$

The "phase optimal" acceleration feedback gain is in turn found by inserting the expression from (3.42) into (3.39), and solving for k_{23}.

$$\begin{aligned}
\tan(\epsilon_{shift}) &= \frac{k_{22}\left|\dot{\eta}_2\right|\sin\dot{\epsilon}_2 + k_{23}\left|\ddot{\eta}_2\right|\sin\ddot{\epsilon}_2}{k_{22}\left|\dot{\eta}_2\right|\cos\dot{\epsilon}_2 + k_{23}\left|\ddot{\eta}_2\right|\cos\ddot{\epsilon}_2} \\
&= \frac{\sqrt{\left|u_c^{vv}\right|^2 - k_{23}^2\left|\ddot{\eta}_2\right|^2}\sin\dot{\epsilon}_2 + k_{23}\left|\ddot{\eta}_2\right|\sin\ddot{\epsilon}_2}{\sqrt{\left|u_c^{vv}\right|^2 - k_{23}^2\left|\ddot{\eta}_2\right|^2}\cos\dot{\epsilon}_2 + k_{23}\left|\ddot{\eta}_2\right|\cos\ddot{\epsilon}_2} \\
&\Downarrow \\
k_{23} &= sign(\epsilon_{shift})\frac{\left|u_c^l\right|}{\left|\ddot{\eta}_2\right|\sqrt{\left(1+\left[\frac{-\cos\ddot{\epsilon}_2\tan\epsilon_{shift}+\sin\ddot{\epsilon}_2}{\cos\dot{\epsilon}_2\tan\epsilon_{shift}-\sin\dot{\epsilon}_2}\right]^2\right)}}.
\end{aligned} \tag{3.43}$$

The process is now explained; By investigating the phases between the two WF control signals, ΔA_{vert}^l and u_c^{vv}, for some arbitrary state weighting matrix, Q, we can find a desired phase, ϵ_{shift} of u_c^{vv} necessary in order for the relative phase between ΔA_{vert}^l and u_c^{vv}, to be $\pm 90°$. The derivations are only valid for a desired phase of $-90° \leq \epsilon_{shift} \leq 90°$, thus the signs above should by chosen in order fulfill that and is not otherwise important as it is, for the sake of controller performance, irrelevant in which direction the shift occurs. The desired shift is found by defining a phase scale, relative to the phases of the lateral motion trajectories where $\epsilon_2 = -90°$, $\dot{\epsilon}_2 = 0°$ and $\ddot{\epsilon}_2 = 90°$, and investigating the phase of the two control signals relative to this scale. This should reveal the desired phase of the final lateral control signal in order to obtain the desired relative phase between them. For instance, if we see that the phase of ΔA_{vert}^l, $\angle\Delta A_{vert}^l$, equals $-30°$, then we would want the phase of u_c^{vv}, $\angle u_c^{vv}$, to be $-30° + 90° = 60°$, thus $\epsilon_{shift} = 60°$. This value is then set as ϵ_{shift} in equation (3.43). In general, a positive phase shift would imply a relatively stronger weighting on the acceleration signal. By using the *updated* state weighting matrix indicated by relative weighting of the acceleration and velocity signals, given by the equations above, the phase of the resulting signal should approach $90°$, perhaps after a few iterations. A perfect match with these valuees is not necessary, however, the closer we are the smaller the degree of infliction of the two control signals will be. The computed gains can also be used directly, which, by experiences from the simulations, yields a strong performing controller. An example of the two control signals obtained by using the gains computed above is given in figure 3.3 for regular seas of $\omega_w = 0.78$ and a generic, 25m SES.

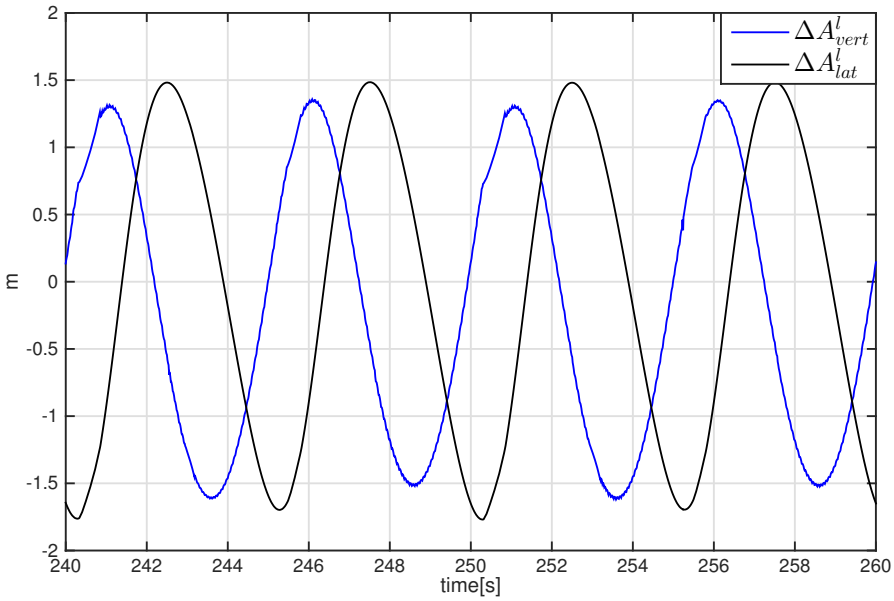

Figure 3.3: Timeseries of u_c^l, which illustrates the phase shift

We see that the relative phase between the two signals is a perfect 90° offset. Even though the signal phase is as good as it gets, there will still be inflictions, which cannot be avoided. Due to the relative low thrust of the vent valves, it must be performing consistently close to the edge of its capacity to obtain decent motion damping. Therefore there will also be saturations in the lateral thrust and an infliction in the performance of the vertical motion damping is, unfortunately, inevitable. Because of this, the gains should be scaled according to the current sea states to avoid too large saturation levels. Interesting work on automatic sea state-dependent, tuning of controller gains is done by (Nguyen et al., 2007) who proposes a hybrid, sea state dependent control scheme where the gains are chosen to comply with the current sea state.

3.4 Dynamic Positioning Control

The horizontal plane DP-controller used for the simulations and concept-proving in this thesis will be a simple PID-controller, proportional to the low frequency vessel motions. The controller output is given by the vector τ_{pid}, defined in equation (3.1). We define the error e_n as the difference between a reference point in {n}, denoted η_d and the actual position η_{3n}, so that

$$e_n(t) = R_{3d}(\psi)(\eta_{3n}(t) - \eta_d(t)). \tag{3.44}$$

The control law is then given by

$$\tau_{pid}(t) = -k_p e_n(t) - k_d \dot{e}_n(t) - k_i \int_0^T e_n(t)dt, \tag{3.45}$$

where $k_p \in \mathbb{R}^{3\times3}$, $k_d \in \mathbb{R}^{3\times3}$ and $k_i \in \mathbb{R}^{3\times3}$ are the feedback gain matrices of the proportional, derivative and integral term, respectively. These are chosen to be diagonal matrices and their different inputs are given in the appendix for the simulations where they are relevant.

3.5 Control Allocation

Control allocation defines the process of going from a demand for directional thrust and/or, in this case, leakage area of the vent valve louvers, given by the respective controllers, to an actual commanded level sent to each individual actuator. In a fully actuated and unsaturated system, i.e. the number of actuators equal the size of the working space, this process is trivial because the number of possible ways to achieve the desired actuator states equals 1. For an over-actuated system, such as the LF dynamical positioning problem of this plant, the number of possible solutions increases the possible ways to solve the problem. As emphasized above, the WF motion control allocation is also non-trivial as the different control desires potentially can conflict with each other and saturation is reached quite often. The control allocation of the horizontal- and the vertical plane will be treated individually. For the DP problem, the commanded thrust levels of each actuator, expressed by the vector u_c, is related to the commanded body fixed force/moment vector τ_c^h through the relation given by equation (3.46)

$$\tau_{lf} = \begin{bmatrix} X_{lf} \\ Y_{lf} \\ N_{lf} \end{bmatrix} = T_{tc} u_c \in \mathbb{R}^{m_h}, \tag{3.46}$$

where $T_{tc} \in \mathbb{R}^{m\times r}$ is the *thrust-configuration* matrix. T_{tc} will take the following form:

$$T_{tc} = \begin{bmatrix} 0 & 1 & 0 & 1 & 0 \\ 1 & 0 & 1 & 0 & 1 \\ l_x^{vv} & -l_x^{wj,p} & l_y^{wj,p} & -l_x^{wj,sb} & -l_y^{wj,sb} \end{bmatrix}, \tag{3.47}$$

where l_x^{vv} is defined as the longitudinal distance (subscript x) of the vent valves (superscript vv) from the centre of gravity, $l_y^{wj,sb}$ denotes the lateral distance (subscript y) of the starboard water jet (superscript wj, sb). Superscript wj,p denotes port water jet pump. Normally, the actuator thrusts are given on the form $f = Ku_c$, where u_c is the control input depending on the actuator considered and K is some force coefficient matrix, whose nature depends on the type of thruster. However, such a linear relationship between actuator control input and resulting force is not as easily achievable for the pressure dependent thrust from the vent valves, thus this notation is omitted here.

We notice that the rank of $T_{tc} \in \mathbb{R}^{m_{lf} \times r_{lf}}$ equals $m_{lf} < r_{lf}$, thus there are no unique solutions to the problem, as it is *under-determined*, i.e. the number of equations, m_{lf}, is less than the number of variables, r_{lf}. However, according to the Rouch-Capelli theorem, (Schrimpf, 2013), a system of linear equations with r_{lf} variables has a solution if and only if the rank, i.e. the size of the largest collection of linearly independent columns or rows, of its coefficient matrix, here: T_{tc}, is equal to the rank of its augmented matrix $T_{aug} = \left[T_{tc}^{m_{lf} \times r_{lf}} : \tau_{lf}^{r_{lf}}\right] \in \mathbb{R}^{m_{lf} \times (r_{lf}+1)}$.

For this case, we have

$$rank(T_{tc}) = rank(T_{aug}) = 3, \tag{3.48}$$

thus, we can guarantee that a solution *exists* and that the control allocation problem is solvable if we neglect saturations and limitations in the actuators, i.e., there will still be maximum levels of achievable thrust from the respective thrusters. The problem of thrust allocation has been subject to strong investigation the last years. (Fossen and Johansen, 2006) provides a survey of some of the different methods used. There are several methods to solve under-determined problems, and it is often done with respect to some function, which is subject for minimization, which leads us to the field of optimal thrust allocation. Since there are an infinite number of solutions, the most favorable one is picked according to some criterions, e.g. a minimization of fuel consumption etc. De Wit (2009) describes a method of fuel optimal thrust allocation based on Lagrange Multipliers. However, this method fails to effectively and directly account for the different saturations and limitations implied by the nature of this (or any) real system, as will be described in section 3.5.2. For this thesis, we will solve the thrust allocation problem with a method based on *quadratic programming*, which is generally described in (Johansen et al., 2004), as this method is highly effective in accounting for the strong limitations in the magnitude and direction of the thrust from both the water jets and the vent valves.

3.5.1 Quadratic Programming

Quadratic programming is a subset of constrained optimization, where the latter concerns all problems where the aim is to minimize some function, say f for generality, called the *objective* function with respect to some equality and inequality constraints. If we let the objective function be quadratic then the problem is a quadratic program which can be stated on the following form:

$$\min_{u_c \in \mathbb{R}^{r_h}} f(u_c) \quad \text{subject to the constraints} \quad \begin{matrix} A_{tc}u_c \leq b_{tc} \in \mathbb{R}^q \\ T_{tc}u_c = \tau_c^h \in \mathbb{R}^{m_{LF}} \end{matrix}, \tag{3.49}$$

where q is the number of inequalities used to define the achievable *thrust region* of the different actuators and u_c is a vector containing the commanded thrust levels from each thruster, which are sent to the $thrust-control$ block. A_{tc} and b_{tc} is a matrix and a vector, respectively, used to describe the thrust constraints as will be explained in section 3.5.2. T_{tc} is the thrust-configuration matrix defined in section 3.5, τ_{pid} is the commanded body-fixed thrust levels from the DP controller and m_{lf} is the size of the LF-working space. For a quadratic program, the objective function f(x) can be on the form:

$$f(u_c) = u_c^T G u_c + u_c^T c. \tag{3.50}$$

Where $G \in \mathbb{R}^{r_{lf} \times r_{lf}}$ and $c \in \mathbb{R}^{r_{lin}}$ are the weighting matrices/arrays of the objective function. If a linear function would suffice for the objective function, a linear programming solver could be used, which normally demands less computational power. Dependent on what is the objective of minimization, $f(u_c)$ could be designed in several ways, e.g. to reduce power consumption or to reduce the use of specific thrusters. For this problem, the use of the vent valves as the source of thrust would imply less fuel consumption than if the same thrust was provided by the water jets, as the fans has to run at a fixed RPM anyways to provide the necessary lift. Therefore, channeling the airflow to either directions does not lead to any extra fuel consumption. For the water jets, however, the fuel consumption is nearly an affine function of the thrust, with minimum equal to the zero thrust idle consumption, given that RPM control is used to regulate the thrust magnitude, as will be thoroughly explained in section 3.7. Therefore, to reduce fuel consumption, the minimization objective could weight the thrust from the water jets heavily, through the matrix G, thus forcing the algorithm to reduce the use of these as far as possible. A reasonable starting point of implementing this is to start out with the matrix G on diagonal form, and weight the inputs appropriately. All parameters used in the thrust allocation will be given in the Appendix

and referred to in the simulations where it is appropriate. Since this is a thrust allocation problem, the solution to the optimization problem will be a row vector u_c, where the entries correspond to the commanded longitudinal and lateral components of the different thrusters, i.e.

$$u_c = \begin{bmatrix} u_y^{vv} \\ u_x^{wj,p} \\ u_y^{wj,p} \\ u_x^{wj,sb} \\ u_y^{wj,sb} \end{bmatrix}. \tag{3.51}$$

The inputs in this vector are given in newtons. The method to achieve the desired levels of thrust from the respective thrusters will be investigated in section 3.6 and 3.7. There are numerous quadratic programming solvers available, based on different algorithms which will not be further discussed in this thesis. Neither will there be much focus on different minimization objectives in the following. For this thesis, the problem is solved using the built in *quadprog* solver in MATLAB.

3.5.2 Thrust Region - Inequality Constraints

The inequality constraints in the optimization problem are implemented because there are strong saturations in the different thrusters, i.e. the water jets are unable to provide a larger volumetric water flow than the one defined by the maximum RPM of the diesel engines and the maximum thrust from the vent valves is limited by the cushion pressure. There are 3 thrusters relevant for the DP problem, where the two water jets can be decomposed into longitudinal and lateral components. To ensure that the solutions of the problem do not demand thrust levels which exceeds the capacities, we implement the restrictions as a set of linear inequalities describing the achievable thrust regions. For the vent valves, this process is quite trivial as the thrust is one-dimensional and only limited by the maximum thrust. For the two water jets, however, the thrust region spans 360°, where the maximum thrust magnitude is dependent on its azimuth (angular direction). The thrust region of the vent valves is of a purely unidirectional nature, and will be modeled much similar to conventional tunnel thrusters. Strictly speaking, as for the traditional set up with one vent valve on each side of the vessel, the vent valves will act as two individual thrusters. However, if we do not look at the individual thrust from each single vent valve, but rather consider the net force, we can assume them to be located at the same longitudinal distance from the COG, and instead regard them as one unidirectional, thruster. However, there are a couple of important differences, which must be

remembered. One is the limited thrust capacity. The maximum thrust force is a function of the pressure inside the cushion and the maximum lateral leakage areas. It is also only for the thrust allocation the similarities between the vent valves and conventional tunnel thrusters are valid. For the thrust *control*, for instance, the approach should be quite dissimilar. Dependent on maximum available thrust force T_{max}, the vent valve thrust region can be illustrated by figure 3.4.

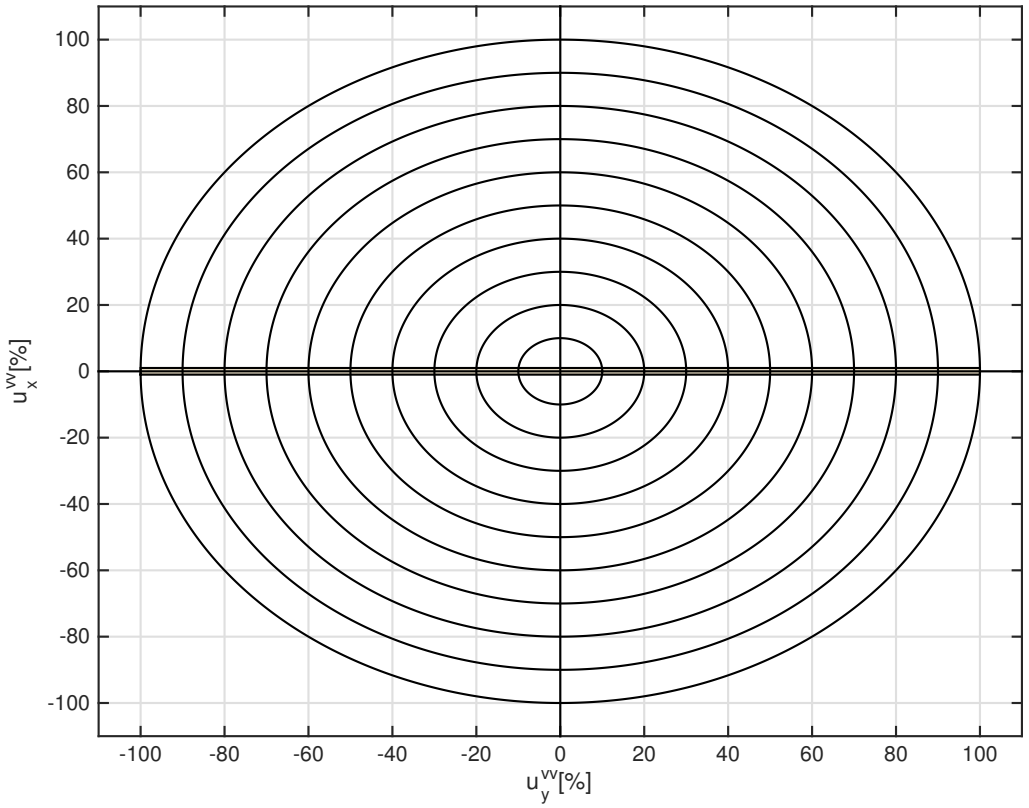

Figure 3.4: Vent valve thrust region in percents of maximum

The numeric value of the maximum thrust force can be found from equation (2.53).

$$u_y^{vv}(t) = -nc_n\rho_c\Delta A_{lat}^l(t)\frac{2(p_0+\mu(t)p_0)}{\rho_a}[Newtons], \tag{3.52}$$

from section 2.2.5, where the different parameters are defined. If we, as a case-study, assume that a vessel has a maximum total leakage area of $x[m^2]$, then the maximum lateral leakage area, from equation (3.67), equals $\frac{x}{2}[m^2]$, which, in a matter of total leakage areas, corresponds to a 50% bias opening. If we assume the equilibrium cushion overpressure to be y[Pa], then the lateral thrust force can be computed directly according to (3.52). However, as the will be shown in the following,

the maximum constant vent valve thrust force made available for the thrust allocation will have a large impact of the heave compensating capacities of the system, dependent on how the two desires are weighted, and the priorities should be weighted thereafter.

The thrust region of the water jets will be implemented in the thrust allocation algorithm by describing it with a set of linear inequalities, i.e., on the form $Ax \leq b$. As the thrust envelope of the water jets is nonlinear, due to the rotatable discharge nozzle, it has to be linearized. The linearization is done by constructing multiple polygons to comprise the entire thrust region. By defining points around the periphery of the thrust region, which will make up the vertices of the polygons used to linearize the regions, we can obtain a set of linear implicit inequalities which will describe the region. Each inequality will describe a region beneath or above some line, running between two of the vertices. These can be found by starting with a generic expression for a straight line through two points (x_1, y_1) and (x_2, y_2).

$$(y - y_1) = \frac{y_2 - y_1}{x_2 - x_1}(x - x_1) \tag{3.53}$$

We will use a thrust region much similar to the one illustrated in figure 2.11. By defining vertices around the periphery of the thrust region, and in a clockwise manner labeling them (x_1, y_1), (x_2, y_2) etc. as illustrated in figure 3.5, we can obtain the linearized region.

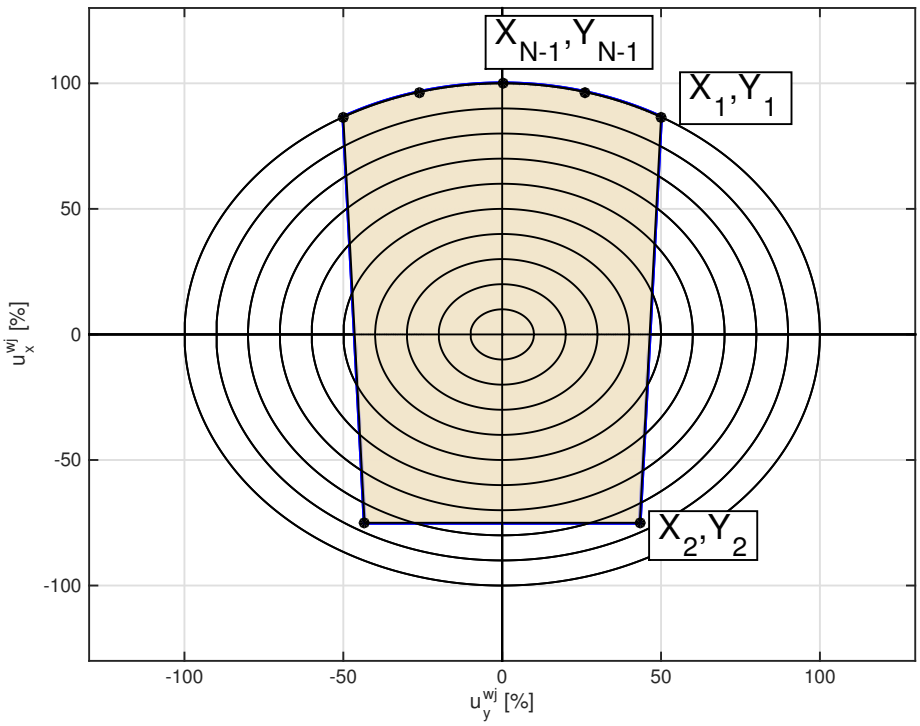

Figure 3.5: Labelling of vertices

To do so, we start out with equation (3.53), and solve it for the two variables, now u_x and u_y, which in this case, and here care must be given, corresponds to the y- and x-axis in figure 3.5, respectively.

$$(y - y_1)(x_2 - x_1) \leq (x - x_1)(y_2 - y_1) \tag{3.54a}$$

$$y(x_2 - x_1) - x(y_2 - y_1) \leq y_1(x_2 - x_1) - x_1(y_2 - y_1) = y_1x_2 - x_1y_2 \tag{3.54b}$$

$$a_1y + a_2x \leq b \tag{3.54c}$$

$$a_1u_x + a_2u_y \leq b \tag{3.54d}$$

Where $a_1 = x_2 - x_1$, $a_2 = y_2 - y_1$ and $b = y_1x_2 - x_1y_2$. If we apply the fact that, $x = u_y$ and $y = u_x$, and assume that the N polygon vertices are ordered clockwise, the hyperplanes defining the thrust region are given by

$$[a_{k,1}a_{k,2}] \begin{pmatrix} u_x \\ u_y \end{pmatrix} \leq b_k \tag{3.55}$$

Where

$$a_{k,1} = (x_{k+1} - x_k) \tag{3.56a}$$

$$a_{k,2} = (y_{k+1} - y_k) \tag{3.56b}$$

$$b_k = x_{k+1}y_k - y_{k+1}x_k \tag{3.56c}$$

Note that if we want a closed polygon, then $(x_N, y_N) = (x_1, y_1)$. If we apply the above to all the vertices defined in figure 3.5 we obtain the thrust region for a single water jet defined by the following set of inequalities

$$\begin{bmatrix} a_{1,1} & a_{1,2} \\ a_{2,1} & a_{2,2} \\ \vdots & \vdots \\ a_{N,1} & a_{N,2} \end{bmatrix} \begin{pmatrix} u_x \\ u_y \end{pmatrix} \leq \begin{bmatrix} b_1 \\ b_2 \\ \vdots \\ b_N \end{bmatrix} \tag{3.57}$$

Which defines the region illustrated in figure 3.6, for N=8.

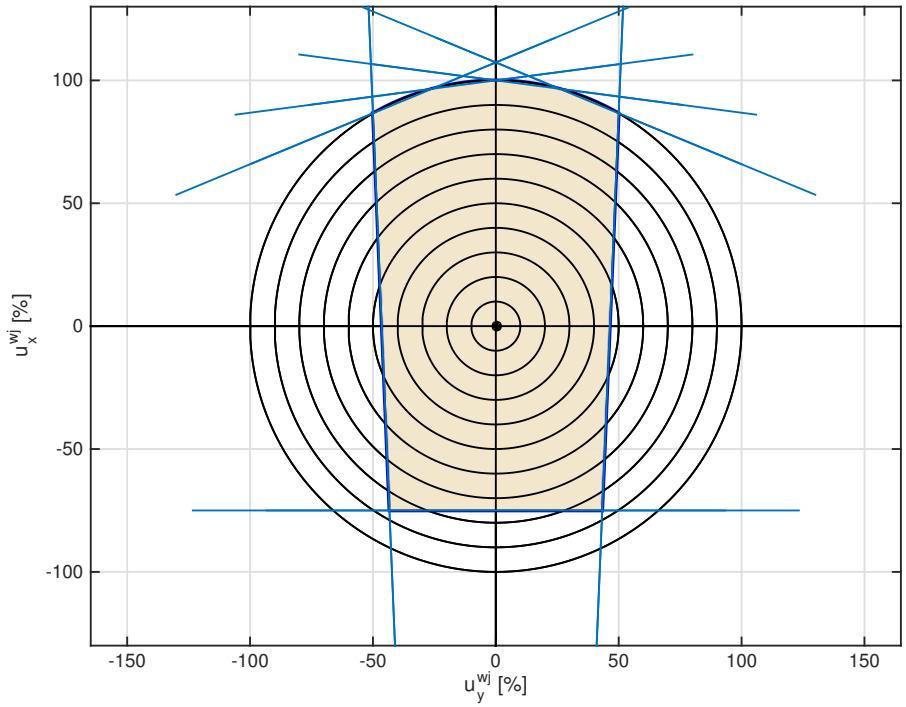

Figure 3.6: Linearized thrust region

Figure 3.7 illustrates the error obtained by approximating the circle-sector shaped water jet thrust region for N=8.

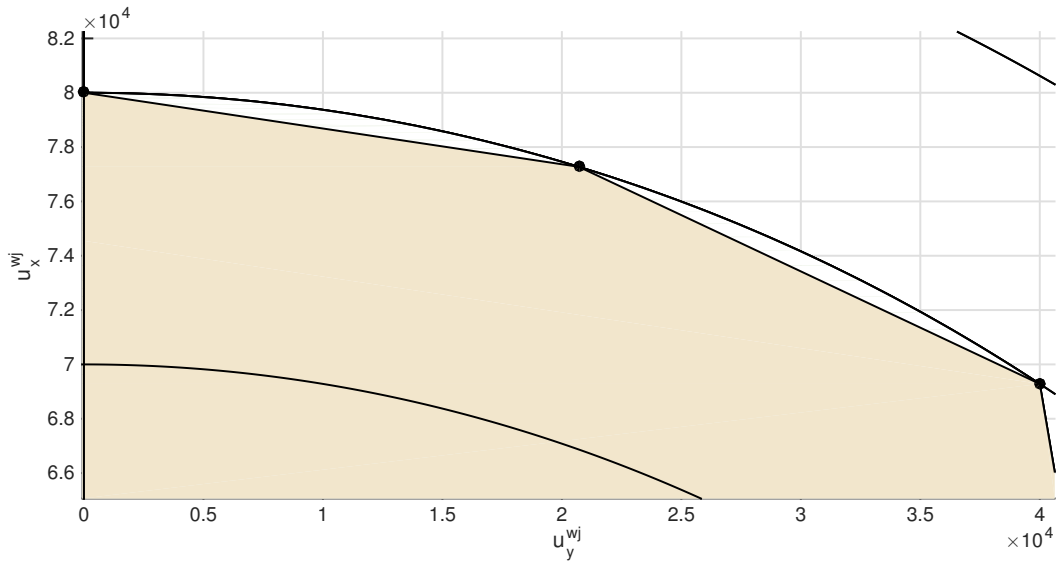

Figure 3.7: Linearization error

This resolution (number of vertices) should, by far, suffice for our applications, and we notice that the result will be conservative because the linearized thrust region is smaller than the real one, as illustrated in figure 3.7. The computational time needed for most of the common Quadratic Programming solvers depend on the number of inequality constraints implemented, thus it is favorable to keep these at a minimum. If we include the limitations of the vent valve thrusters, and look at the global system with two water jets and the *Vent Valve Thruster*, equation (3.57) can be augmented to:

$$\underbrace{\begin{bmatrix} 1 & 0 & 0 & 0 & 0 \\ -1 & 0 & 0 & 0 & 0 \\ 0 & a_{1,1} & a_{1,2} & 0 & 0 \\ 0 & a_{2,1} & a_{2,2} & 0 & 0 \\ \vdots & \vdots & \vdots & \vdots & \vdots \\ 0 & 0 & a_{N,1} & a_{N,2} & 0 \\ 0 & 0 & 0 & 0a_{1,1} & a_{1,2} \\ \vdots & \vdots & \vdots & \vdots & \vdots \\ 0 & 0 & 0 & a_{N,1} & a_{N,2} \end{bmatrix}}_{A_{tc}} \begin{pmatrix} u_y^{vv} \\ u_x^{wj,p} \\ u_y^{wj,p} \\ u_x^{wj,sb} \\ u_y^{wj,sb} \end{pmatrix} \leq \underbrace{\begin{bmatrix} T_{max} \\ T_{max} \\ b_1 \\ b_2 \\ \vdots \\ b_N \\ b_1 \\ b_2 \\ \vdots \\ b_N \end{bmatrix}}_{b_{tc}} \tag{3.58}$$

For a quadratic solver to be able to search for and find a solution within a set, that set must be convex, i.e., the problem is a subset of convex optimization. A convex set is a set of points such

that, given any two points A, B in that set, the line AB joining them lies entirely within that set. Intuitively, this means that the set is connected and has no dents in its perimeter. Thus, you can pass between any two points within the set, without ever leaving it. As we can se, the thrust region of the water jets is indeed convex, and the inequality set need no further alterations. As all straight line segments will be convex, the thrust region of the vent valves is also convex.

3.5.3 Equality Constraints

The equality constraints for this problem is given as in equation (3.46).

$$T_{tc}u_c = \tau_{pid} \tag{3.59}$$

The relation equates the resultant thrusts and yaw momentum provided by the thrusters, with the demanded levels from the DP-controller. τ_{pid} will thus contain the commanded levels of thrust in surge and sway, and yaw momentum, and be on the form:

$$\tau_{pid} = [X_{lf}\ Y_{lf}\ Z_{lf}]^T \tag{3.60}$$

Where we refer to equation (2.7a), section 2.1. Subscript lf indicates that these are the commanded levels from the LF-DP controller. Since each thruster, i, is decomposed into its longitudinal and lateral components, u_x^i and u_y^i, respectively, T must be on the form

$$T_{tc} = \begin{bmatrix} 0 & 1 & 0 & 1 & 0 \\ 1 & 0 & 1 & 0 & 1 \\ l_x^{vv} & -l_y^{wj,port} & l_x^{wj,port} & -l_y^{wj,sb} & -l_x^{wj,sb} \end{bmatrix} \tag{3.61}$$

In order to obtain an answer from the optimization algorithm, even if the demanded thrust levels are infeasible due to actuator saturations, the system should be augmented by *slack variables*, i.e., allowing the resulting thrust to deviate from the commanded levels by some variable which is subject to heavy weigthing in the objective function, such as done by (De Wit, 2009). For the conditions used in the simulations, however, we did not experience infeasible thrust vectors, thus the problem was omitted.

3.6 Thrust Control - Vent Valves

As shown in the mathematical modeling in chapter 2, the thrust from the air accelerating through the vent valve ducts, due to the pressure drop, is proportional to both the overpressure inside the cushion, $p_u(t)$, and the leakage area. If the difference between the lateral leakage areas through starboard and port vent valve equals zero, there will be no net-thrust. A net thrust is obtained by commanding a larger leakage area from one of the vent valves, as the pressure drop over both them will be equal anyway. As for the heave compensation, the total pressure differences in the cushion does not at all depend on the direction of air flowing out of it, but only on the total amount, i.e. the total leakage area. For the following derivations we will define two more entities concerning the leakage areas of the vent valves, where we will try to keep some of the similarities with common practice for notation within the subject. First we recall the generic WF feedback control scheme defined in Section 3.3, given by:

$$u_c^l = \begin{bmatrix} \Delta A_{vert}^l \\ u_c^{vv} \end{bmatrix} = - \begin{bmatrix} k_{11} & k_{12} & k_{13} & k_{14} & k_{15} & k_{16} & k_{17} \\ k_{21} & k_{22} & k_{23} & k_{24} & k_{25} & k_{26} & k_{27} \end{bmatrix} \begin{bmatrix} \eta_2 \\ \dot{\eta}_2 \\ \ddot{\eta}_2 \\ \eta_3 \\ \dot{\eta}_3 \\ \ddot{\eta}_3 \\ \mu \end{bmatrix}, \tag{3.62}$$

The gain matrix k_{lqr} was derived by an LQR-synthesis, which yielded the feedback gain matrix given by:

$$k_{lqr} = -R^{-1}B^T A^{-1^T} P \in \mathbb{R}^{2\times 5}, \tag{3.63}$$

where the different terms are thoroughly explained in Section 3.3.1. This yields the final WF control law, given by

$$u_c^l = \begin{bmatrix} \Delta A_{vert}^l \\ u_c^{vv} \end{bmatrix} = -k_{lqr}\dot{\eta}_{lqr}, \tag{3.64}$$

where η_{lqr} is given by $\eta_{lqr} = \begin{bmatrix} \eta_2 & \eta_3 & \dot{\eta}_2 & \dot{\eta}_3 & \mu \end{bmatrix}^T$. From table 3.1, we remember that the WF control law signals implies the commanded total- and lateral leakage areas given by:

$$\begin{aligned} A_c^l(t) &= A_0 + \Delta A_{vert}^l \\ \Delta A_{lat}^l &= \frac{\rho_a u_c^{vv}}{-2nc_n\rho_c p_u(t)} \end{aligned} \tag{3.65}$$

We note that this control law strictly speaking yields an algebraic loop, however by using the values from the preceding time step this problem is omitted in the simulations. For the actual plant, the state derivative signals in (3.64) are taken from onboard accelerometer signals which are appropriately filtered. Thus, for instance, $\ddot{\eta}_2$ will then correspond to the y-values from the accelerometer sensor, while $\dot{\eta}_2$ is the integral of $\ddot{\eta}_2$. Now, this section will concern how to actually obtain the commanded leakage areas from the vent valve louvers, from equation (3.65) and (3.64), and propose a saturation handler to cope with the situations where the desires can not be achieved. First we will define the total leakage area A^l as the sum of the leakage areas of the port and starboard vent valves, i.e.

$$A^l = A_{sb}^l + A_{port}^l \tag{3.66}$$

Then we define a lateral leakage area ΔA^l, so that

$$\Delta A^l = A_{port}^l - A_{sb}^l \tag{3.67}$$

These are the actual levels. The commanded levels are given by ΔA_{lat}^l. The sign convention is chosen in such a way that a positive ΔA^l corresponds to a positive net thrust, which is noticed by the fact that a larger port leakage area will provide a net thrust in the positive y-direction (positive y is directed to starboard side), we refer to equation (2.53). The lateral leakage area, ΔA^l does not affect the heave compensation directly, neither is there an explicit relationship between the total leakage area A^l and the lateral thrust. Therefore, the problem boils down to satisfying two desires, which are the commanded levels of lateral- and total leakage area, ΔA_{lat}^l and A_c^l, respectively. We refer to table 3.1 for the definitions behind this notation. The commanded lateral leakage area is found from equation (2.53) from section 2.2.5, which gives the thrust from an arbitrary leakage area A_i.

$$u_y^{vv,i}(t) = -2n \cdot c_n \cdot \rho_c A_i(t) \frac{p_u(t)}{\rho_a} \tag{3.68}$$

If we use the fact that the normal vector along the y-axis of the port leakage area is equal to negative 1, and that the corresponding normal vector of the starboard vent valve equals 1, we can obtain the net force from the airflow through the port and starboard vent valves.

$$\begin{aligned} u_y^{vv} &= 2c_n\rho_c(A_{port}(t) - A_{sb}(t))\frac{p_u(t)}{\rho_a} \\ &= 2c_n\rho_c\Delta A_{lat}^l(t)\frac{p_u(t)}{\rho_a} \end{aligned} \tag{3.69}$$

We combine this with equation (3.67), and solve for the commanded lateral leakage area ΔA_c^l.

$$\Delta A_c^l = \frac{\rho_a u_c^{vv}}{2c_n\rho_c p_u(t)}, \tag{3.70}$$

where $u_c^{vv}(t)$ denotes the commanded thrust level from the vent valves. The actual leakage area is controlled by a hydraulic linear actuator, which in turn is controlled by an internal feedback loop and a PID-controller. This internal loop has a very low time-constant, far below the dynamics of the global system, thus these actuator dynamics can safely be neglected here.

As the above definitions result in two equations with two unknowns, given by equation (3.67) and (3.66), the problem should be easily solvable. However, the nature of this plant makes this a bit more complicated. The actuators for this system are the leakage areas, which in turn are controlled by a linear hydraulic actuator. The problem with this is that the actuators reach saturation quite fast, as they can neither be more than fully opened nor less than fully closed. In addition to the physical limitations, we must also keep in the back of our minds the fact that the thrust is proportional to the excess cushion pressure as well, which is not at all constant. The maximum total leakage area is denoted A_{max}^l, and we add the extra conditions which must be fulfilled, i.e. due to the limitations in the design they are physically impossible to circumpass. We assume the vent valves of both sides to be of equal size.

$$0 \leq A_{sb}^l + A_{port}^l = A^l \leq A_{max}^l \tag{3.71a}$$

$$0 \leq A_{sb}^l \leq \frac{A_{max}^l}{2} \tag{3.71b}$$

$$0 \leq A_{port}^l \leq \frac{A_{max}^l}{2} \tag{3.71c}$$

By solving the set of inequalities defined by equations (3.67), (3.66) and (3.71), we obtain the following relations between the leakage area of each individual vent valve, and the total- and lateral

leakage area.

$$A^l_{port} = \frac{A^l_c + \Delta A^l_{lat}}{2} \tag{3.72a}$$

$$A^l_{sb} = \frac{A^l_c - \Delta A^l_{lat}}{2} \tag{3.72b}$$

This is in compliance with the sign convention of the lateral leakage area. If we combine equation (3.72) with equation (3.71), an explicit expression for the saturation conditions of the system arise by equation (3.73):

$$\begin{aligned} 0 \leq A^l_c + \Delta A^l_{lat} \leq A^l_{max}, \\ 0 \leq A^l_c - \Delta A^l_{lat} \leq A^l_{max}. \end{aligned} \tag{3.73}$$

This shows that even if the system should be able to handle both the desires for heave compensation and lateral thrust, individually, it does not necessarily have enough capacity to satisfy both the demands at the same time. This suggests that, when the capacity is exceeded, some kind of weighting between the two desires is necessary. The approach we will use is to, when saturated, let one of the desires, either the total- or the lateral leakage area, determine the distribution. I.e., if saturation is reached, totally neglect one of the desires and as far as possible prioritize the other. To do so we must add a *saturation handler* to the expressions in equation (3.72). We define *opening* saturation as the situation where the leakage areas computed by (3.72) exceeds the maximum leakage area, A^l_{max}, of the system, and *closing*-saturation as the counterpart where the leakage computed by (3.72) is lower than the minimum leakage area, 0. We correct the leakage areas computed by (3.72) by adding or subtracting the amount of m^2 the capacity would have been exceeded by, according to equation (3.73), if the leakage areas were as given by (3.72). We only show the derivations for the port vent valves, but the expressions for the starboard vent valves follow somewhat similarly. In the case of opening saturation, we must reduce the commanded leakage area by subtracting the amount exceeding A^l_{max} equally from each of the commanded areas. We denote the "excess area" A^l_δ, and the corrected leakage signal, which is the one that will be sent to the hydraulic actuator

loop (this is beyond the scope of this thesis), $A^l_{port,c}$.

$$\begin{aligned}
0 \leq A^l + \Delta A^l_{lat} &\leq A^l_{max} \\
&\Downarrow \\
A^l_\delta &= A^l + abs(\Delta A^l_{lat}) - A^l_{max} \\
A^l_{port,c} &= A^l_{port} - \frac{A^l_\delta}{2} \\
&= \frac{A^l + \Delta A^l_{lat}}{2} - \frac{A^l + abs(\Delta A^l_{lat}) - A^l_{max}}{2} \\
&\Downarrow \\
A^l_{port,c} &= \frac{\Delta A^l_{lat} - abs(\Delta A^l_{lat}) + A^l_{max}}{2}
\end{aligned} \tag{3.74}$$

The corrected term for the case of closing saturation is given as:

$$\begin{aligned}
0 \leq A^l + \Delta A^l_{lat} &\leq A^l_{max} \\
&\Downarrow \\
A^l_\delta &= -A^l - abs(\Delta A^l_{lat}) \\
A^l_{port,c} &= A^l_{port} - \frac{A^l_\delta}{2} \\
&= \frac{A^l + \Delta A^l_{lat}}{2} - \frac{-A^l - abs(\Delta A^l_{lat})}{2} \\
&\Downarrow \\
A^l_{port,c} &= \frac{\Delta A^l_{lat} + abs(\Delta A^l_{lat})}{2}
\end{aligned} \tag{3.75}$$

By a similar synthesis, the expressions for the starboard vent valve correction term can also be found. We assume that the signals in, i.e., A^l and ΔA^l_{lat}, are already saturated so that they are within the intervals $[0, A^l_{max}]$ and $[-\frac{A^l_{max}}{2}, \frac{A^l_{max}}{2}]$, respectively. By those assumptions the controller prioritizing the lateral leakage areas, denoted *Controller* 1, can be summarized by:

$$A^l_{port,c1} = \begin{cases} \frac{A^l + \Delta A^l_{lat}}{2} & \forall (A^l, \Delta A^l_{lat}) \in [0\,, A^l_{max}] \times [-\frac{A^l_{max}}{2}, \frac{A^l_{max}}{2}] : 0 \leq A^l + \Delta A^l_{lat} \leq A^l_{max} \\ \frac{\Delta A^l_{lat} - abs(\Delta A^l_{lat}) + A^l_{max}}{2} & \forall (A^l, \Delta A^l_{lat}) \in [0\,, A^l_{max}] \times [-\frac{A^l_{max}}{2}, \frac{A^l_{max}}{2}] : A^l + \Delta A^l_{lat} \geq A^l_{max} \\ \frac{\Delta A^l_{lat} + abs(\Delta A^l_{lat})}{2} & \forall (A^l, \Delta A^l_{lat}) \in [0\,, A^l_{max}] \times [-\frac{A^l_{max}}{2}, \frac{A^l_{max}}{2}] : A^l + \Delta A^l_{lat} \leq 0 \end{cases}, \tag{3.76}$$

$$A^l_{sb,c1} = \begin{cases} \frac{A^l - \Delta A^l_{lat}}{2} & \forall (A^l, \Delta A^l_{lat}) \in [0\,, A^l_{max}] \times [-\frac{A^l_{max}}{2}, \frac{A^l_{max}}{2}] : 0 \leq A^l + \Delta A^l_{lat} \leq A^l_{max} \\ \frac{-\Delta A^l_{lat} - abs(\Delta A^l_{lat}) + A^l_{max}}{2} & \forall (A^l, \Delta A^l_{lat}) \in [0\,, A^l_{max}] \times [-\frac{A^l_{max}}{2}, \frac{A^l_{max}}{2}] : A^l + \Delta A^l_{lat} \geq A^l_{max} \\ \frac{-\Delta A^l_{lat} + abs(\Delta A^l_{lat})}{2} & \forall (A^l, \Delta A^l_{lat}) \in [0\,, A^l_{max}] \times [-\frac{A^l_{max}}{2}, \frac{A^l_{max}}{2}] : A^l + \Delta A^l_{lat} \leq 0 \end{cases}, \tag{3.77}$$

Controller 1 bases the saturation handling on adjusting the *total* leakage area when the capacity is exceeded. Now we will present a vent valve controller which instead bases the correction on adjusting the lateral leakage area. This controller is denoted *Controller* 2, and is based on letting the total leakage area signal from the vertical motion damping controller get priority, and then distribute remaining leakage area capacity in a manner such that the desire for lateral leakage area is fulfilled as far as possible. We do this by correcting the lateral leakage term in equation (3.72) in the following manner for *opening* saturation, of the port vent valve.

$$\begin{aligned} & 0 \leq A^l + \Delta A^l_{lat} \leq A^l_{max} \\ & \qquad \Downarrow \\ & \qquad A^l_{\delta} = -A^l - abs(\Delta A^l_{lat}) \\ & A^l_{port,c} = A^l_{port} - \frac{A^l_{\delta}}{2} \\ & \qquad\quad = \frac{A^l + sign(\Delta A^l_{lat})(\Delta A^l_{lat} - A^l_{\delta})}{2} \\ & \qquad \Downarrow \\ & A^l_{port,c} = \frac{A^l + sign(\Delta A^l_{lat})(A^l_{max} - A^l)}{2} \end{aligned} \tag{3.78}$$

The expression for starboard vent valve follows by changing the sign in front of the $sign(\cdot)$-function, while *closing* saturation is done by adding, instead of subtracting, the correction term in the last parenthesis, where A^l_{max} is replaced by $A^l_{min} = 0$. *Controller* 2 can be summarised as follows:

$$A^l_{port,c2} = \begin{cases} \frac{A^l + \Delta A^l_{lat}}{2} & \forall (A^l, \Delta A^l_{lat}) \in [0\,, A^l_{max}] \times [-\frac{A^l_{max}}{2}, \frac{A^l_{max}}{2}] : 0 \leq A^l + \Delta A^l_{lat} \leq A^l_{max} \\ \frac{A^l + sign(\Delta A^l_{lat})(A^l_{max} - A^l)}{2} & \forall (A^l, \Delta A^l_{lat}) \in [0\,, A^l_{max}] \times [-\frac{A^l_{max}}{2}, \frac{A^l_{max}}{2}] : A^l + \Delta A^l_{lat} \geq A^l_{max} \\ \frac{A^l + sign(\Delta A^l_{lat}) A^l}{2} & \forall (A^l, \Delta A^l_{lat}) \in [0\,, A^l_{max}] \times [-\frac{A^l_{max}}{2}, \frac{A^l_{max}}{2}] : A^l + \Delta A^l_{lat} \leq 0 \end{cases}, \tag{3.79}$$

$$A^l_{sb,c2} = \begin{cases} \frac{A^l - \Delta A^l_{lat}}{2} & \forall (A^l, \Delta A^l_{lat}) \in [0\,, A^l_{max}] \times [-\frac{A^l_{max}}{2}, \frac{A^l_{max}}{2}] : 0 \leq A^l + \Delta A^l_{lat} \leq A^l_{max} \\ \frac{A^l - sign(\Delta A^l_{lat})(A^l_{max} - A^l)}{2} & \forall (A^l, \Delta A^l_{lat}) \in [0\,, A^l_{max}] \times [-\frac{A^l_{max}}{2}, \frac{A^l_{max}}{2}] : A^l + \Delta A^l_{lat} \geq A^l_{max} \\ \frac{A^l - sign(\Delta A^l_{lat}) A^l}{2} & \forall (A^l, \Delta A^l_{lat}) \in [0\,, A^l_{max}] \times [-\frac{A^l_{max}}{2}, \frac{A^l_{max}}{2}] : A^l + \Delta A^l_{lat} \leq 0 \end{cases}, \tag{3.80}$$

The differences between the two approaches are illustrated in figure 3.9 & 3.8. The thrust achieved for a desired vent valve thrust signal of 6000N is plotted together with a time series of the heave motions, which illustrates the heave compensation capabilities. The control is turned on at t=200s. First for Controller 1, and secondly for Controller 2. The condition is a regular sea state with wave amplitude of 0.75m, and some vessel which achieves an overpressure of 2200Pa at a 50% bias opening of $2.5m^2$. Other relevant simulation parameters are given in Appendix A.2.

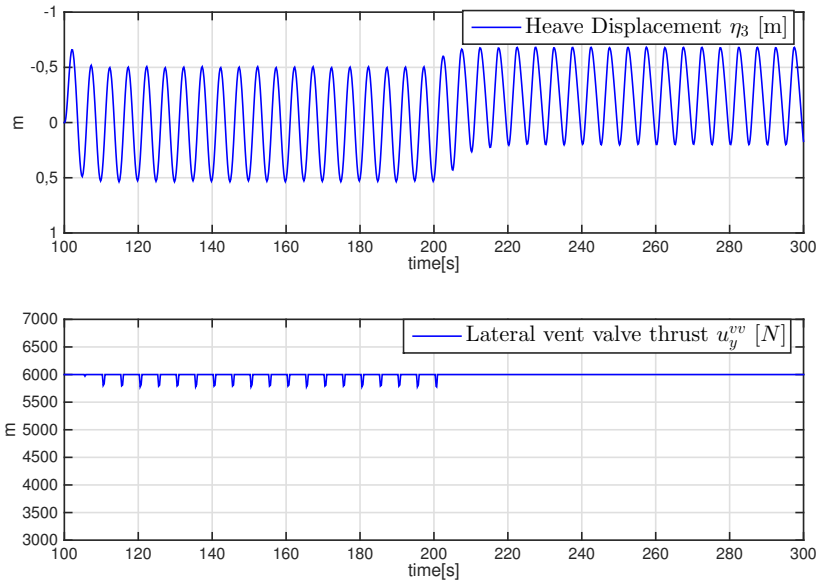

Figure 3.8: Timeseries in heave and thrust, controller 1

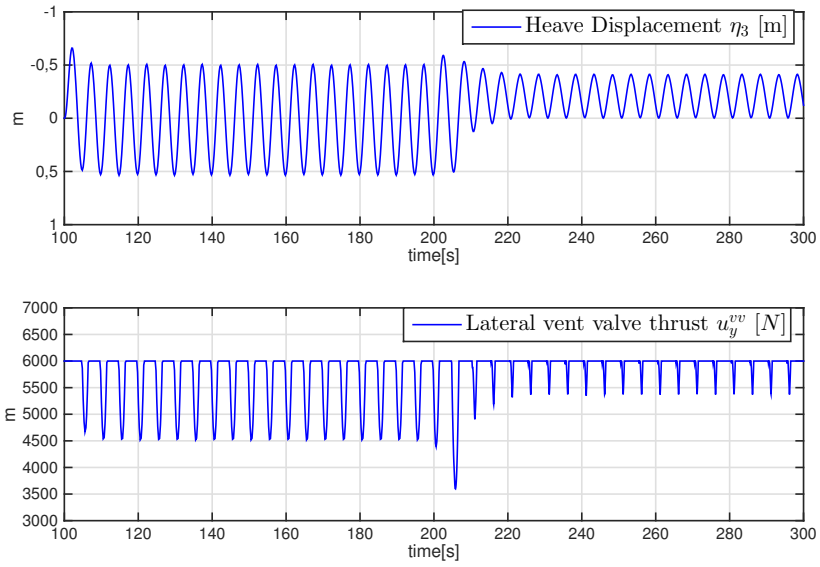

Figure 3.9: Timeseries in heave and thrust, controller 2

The time series shown in figure 3.8 and 3.9 illustrates the effect of fully prioritizing one of the control objectives. We see that both the controllers fulfill the other objective to some degree; however in this thesis it is the lateral thrust that is of greatest importance. The simulation chapter will show that even by prioritizing thrust, significant vertical motion damping can be achieved. Due to the relatively low thrust capacity, the system is more sensitive to losses in thrust than it is for losses in total leakage area (vertical motion damping). The heave compensating capacity of controller 1 is somewhat adjustable through the means of the allocated lateral thrust, i.e. by reducing the demanded thrust, more capacity can be used for total leakage area/vertical motion damping, which is illustrated by the simulation in section 4.7. Section 4.5 and 4.7 will feature controller 1 for the vent valve capacity allocation, while there is no need, in the remaining simulations, for such saturation handling as none of them feature combined heave compensation and lateral vent valve thrust.

3.7 Thrust Control - Water Jets

Section 2.2.6 provides a qualitative description of the thrust providing mechanisms in a water jet drive system. This section will be an extension of that, and explain, qualitatively, how to obtain a desired thrust from a water jet system. By slightly rewriting equation 2.58, we find that the thrust from a water jet drive is given by

$$u^{wj} = \sum_{i=1:3} (-n_i \rho_w Q_{w,i} v_{out} + n_{i,out} \rho_q Q_w v_{in}), \tag{3.81}$$

where n_i and $n_{i,out}$ are unit vectors pointing in the direction of the water flow in- and out of the jet drive, respectively. i spans from 1 to 3, which is the number of components the flow can be divided into, as explained in 2.2.6. The signs differ from equation 2.58 due to the fact that the equation is dependent on the direction of the water flow, whereas the resulting thrust is acting in the opposite direction. If the vessel speed is restricted within a small region around zero, we can safely assume the vessel wake to be insignificant and thus disregard the last term in the equation above. We obtain the simplified expression:

$$u^{wj} = \sum_{i=1:3} -n_i \rho_w Q_{w,i} v_{out}. \tag{3.82}$$

This leaves us with only two parameters we are able to influence with the thrust control, the outlet velocity v_{out} and the flow distribution, $Q_{w,i}$. Note that v_{out} denotes the speed of the fluid flow immediately after the stator, shown in figure 2.7, but before any fluid is redirected by the rotatable nozzle and/or the deflector shield. We will disregard any losses in the deflector and stator, and regard the vectorial fluid flow as a thrust potential we can distribute arbitrarily, within the mechanic restrictions of the construction, and thereby obtain the desired thrust- magnitude and direction.
v_{out} is mainly influenced by one variable factor only, i.e. the engine speed. The relation between the engine speed and the outlet velocity further depends on the *impeller characteristics*, which are known by the water jet manufacturer through experiments. This is a somewhat diffuse relation, of which it is hard to obtain an analytic expression. Typical relations between boat speed and provided thrust for different power outputs are shown in figure 3.10.

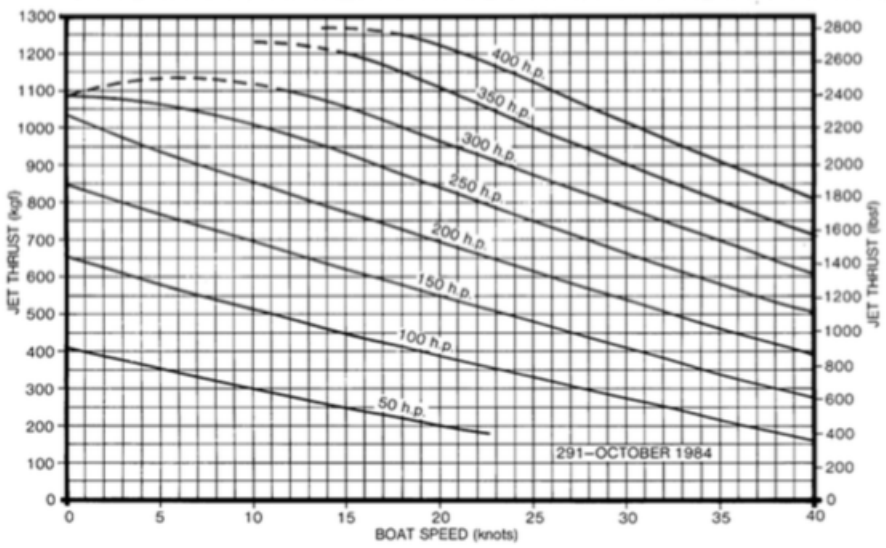

Figure 3.10: Thrust vs. boat speed, as in (Bulten, 2006)

We remember that due to the reversing deflector shield, the water flow is given a vertical component, as illustrated by figure 2.8. This is done in order to avoid the water flow from hitting the transom. We therefore denote the magnitude of the water jet thrust $|u_{3d}^{wj}|$, and it will be shown later why it is important to differ between the horizontal and the 3-dimensional magnitude in the thrust control. If we assume the mapping between impeller rpm, n_{wj}, and the discharge velocity at a given vessel speed to be a known function, denoted $v_{out}(n_{wj})$, we can combine this with equation (3.82), and we obtain an expression for the rpm of the impeller necessary in order to obtain the desired thrust $|u_{3d}^{wj}|$. If the machinery features a reduction gearbox, further mapping is necessary in order to find

the desired engine speed.

$$
\begin{aligned}
|u_{3d}^{wj}| &= \left| \sum_{i=1:3} -n_{i,in} \rho_w A_{nozzle} v_{out}^2(n_{wj}) \right|, \\
&\Downarrow \\
n_{wj} &= v_{out}^{-1} \left(\sqrt{\frac{|u_{3d}^{wj}|}{\rho_w A_{nozzle}}} \right)
\end{aligned}
\tag{3.83}
$$

We use the thrust magnitudes here, in order to specify that this expression is not related to the direction of the desired thrust. The direction of the thrust is controlled solely through the means of the angle of the discharge nozzle and the state of the deflector shield.

The thrust allocation algorithm provides the decomposed thrust from the water jets in their lateral and longitudinal components, u_y^{wj} and u_x^{wj} respectively. The magnitude of the commanded horizontal thrust is found by

$$
|u_c^{wj}| = \sqrt{{u_y^{wj}}^2 + {u_x^{wj}}^2} \tag{3.84}
$$

The *azimuth*-angle α_a is found from:

$$
\alpha_a = \tan^{-1} \left(\frac{u_x^{wj}}{u_y^{wj}} \right) \tag{3.85}
$$

Due to the limited domain of the $\tan(\cdot)$-function, which spans the interval $[-90°, 90°]$, we need to know in which quadrant the resultant thrust is located, which is is easily found by the signs of the lateral- and longitudinal components. The azimuth region of the water jet is divided in four. $\alpha_a = 0$ is set to be in the direction parallel with x_b, and positive clockwise according to the right hand screw rule. We denote the angle of the discharge nozzle α_{nozzle}, and denote the mode of the deflector, d_{rev}, 0 when it is fully open and 1 when it is fully lowered. d_{rev} is allowed to take any value within this interval, which allows the thrust to be distributed arbitrarily in the two directions. To obtain a generic expression for the thrust control, we will denote the maximum angle of the discharge nozzle and the angle of the reversed flow component from the deflector α_f and α_{rev}, respectively. We will assume the construction to be somewhat symmetric with respect to its longitudinal centerline, thus the nozzle is able to turn equally much to both sides, and the two components of the divided reverse flow from the deflector are discharged at the same angle relative to x_b. We will also differ between the port- and starboard components, thus $\alpha_{f,port} = 360° - \alpha_{f,sb}$, etc. The 4 regions are illustrated

in figure 3.11, and explained below.

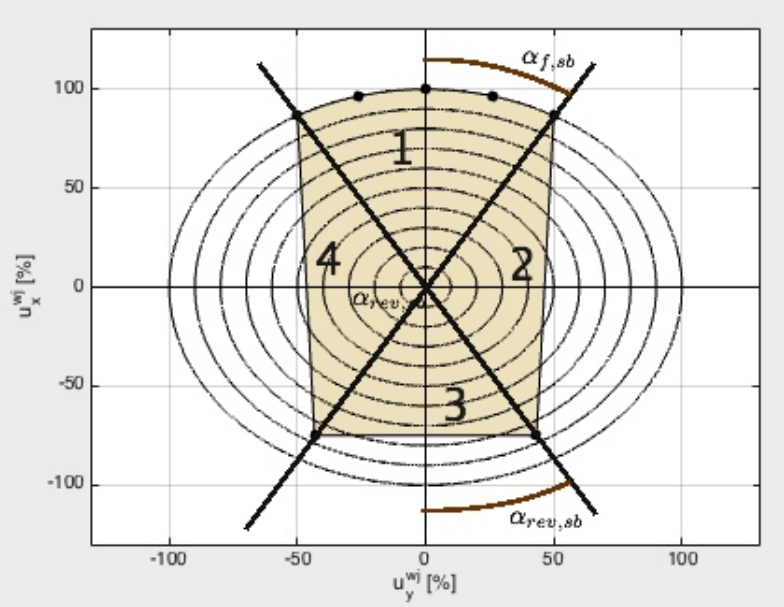

Figure 3.11: The four regions of the Water Jet thrust envelope

1. $\alpha_{f,port} \leq \alpha_a \leq \alpha_{f,sb}$: The direction of the thrust is, in this region, controlled solely by the means of the discharge nozzle. d_{rev}=0.

2. $\alpha_{f,sb} \leq \alpha_a \leq \alpha_{rev,sb}$: In this region, the discharge nozzle is pointing at the angle $\alpha_{f,port}$. The angle of the resultant thrust is controlled by partly-, or totally lowering the deflector in order to distribute thrust between the outer line of the blue region and the red vector in figure2.10.

3. $\alpha_{rev,sb} \leq \alpha_a \leq \alpha_{rev,port}$: To provide a net thrust in this region, the deflector must be fully lowered, i.e. d_{rev}=1. The angle is adjusted solely by the angle of the discharge nozzle, α_{nozzle}.

4. $\alpha_{rev,port} \leq \alpha_a \leq \alpha_{f,port}$: Similar to region 2, only difference is that here, the angle of the discharge nozzle $\alpha_{nozzle} = \alpha_{f,sb}$.

Summing up the above, the water jet control should satisfy two desires, the magnitude of the horizontal thrust, $|u_c^{wj}|$, and the direction α_a. As for the magnitude of the thrust, we remember that the water jet thrust is of a 3-dimensional nature, as the flow going through the deflector has a downwardly directed component, which complicates the control slightly. We denote, as before the thrust in all three planes $|u_{3d}^{wj}|$, and this is the one that actually needs to be generated by the jet pump and diesel engine. For generality we denote the downward angle of the water flow through the deflector, relative to the $x_b y_b$-plane, α_{vert}, however in the simulations and in most jet drives

$\alpha_{vert} \approx 30°$. This means that in order to get the horizontal, reversed thrust component, commanded from the thrust allocation, the 3-dimensional thrust actually produced by the water jet must be slightly higher, to compensate for the fact that $(1 - \cos\alpha_{vert})$ is lost in the downwardly directed flow. For the flow which does not pass through the deflector, the process is more trivial, as this flow is discharged strictly in the $x_b y_b$-plane. Therefore, in region 1, the thrust control process is simply a matter of setting the angle of the discharge nozzle α_{nozzle} equal to negative α_a, and the rpms of the engines equal to the revs computed according to equation (3.83). For the remaining regions, it becomes slightly more complicated. We start out with region 2, and since the problem is on vectorial form we denote the vectors coinciding with the right borderline of the blue region and the red arrow in figure 2.10 $\vec{u}_f$ and $\vec{u}_{rev}$, respectively, in compliance with equation (2.63). The respective subscripts are chosen to denote the forward and reversed thrust components. There are two objectives that needs to be fulfilled by the thrust controller, the angle α_a of the net thrust, and the horizontal magnitude $|u^{wj}|$. The thrust vectors can be written on the following form:

$$\begin{aligned} \vec{u}_f &= \begin{bmatrix} u_{f,1} & u_{f,2} \end{bmatrix}, \\ \vec{u}_{rev} &= \begin{bmatrix} u_{rev,1} & u_{rev,2} \end{bmatrix}, \end{aligned} \tag{3.86}$$

where the first and last entries correspond to the x- and y-components of the thrust, in compliance with the definitions from the body-fixed reference frame {b}, thus $u_{f,1}$ and $u_{f,2}$ is the projections along x_b and y_b respectively. The magnitude of these two vectors can be expressed by the means of the magnitude of the 3-dimensional thrust:

$$\begin{aligned} |\vec{u}_f| &= |u_{3d}^{wj}|(1 - d_{rev}) \\ |\vec{u}_{rev}| &= |u_{3d}^{wj}|(d_{rev})\cos\alpha_{vert}. \end{aligned} \tag{3.87}$$

The various inputs in (3.86) are given by:

$$\begin{aligned} u_{f,1} &= \cos\alpha_{f,sb}|\vec{u}_f| = \cos\alpha_{f,sb}|u_{3d}^{wj}|(1 - d_{rev}) \\ u_{f,2} &= \sin\alpha_{f,sb}|\vec{u}_f| = \sin\alpha_{f,sb}|u_{3d}^{wj}|(1 - d_{rev}) \\ u_{rev,1} &= \cos\alpha_{rev,sb}|\vec{u}_{rev}| = \cos\alpha_{rev,sb}\cos\alpha_{vert}|u_{3d}^{wj}|d_{rev} \\ u_{rev,2} &= \sin\alpha_{rev,sb}|\vec{u}_{rev} = \sin\alpha_{rev,sb}\cos\alpha_{vert}|u_{3d}^{wj}|d_{rev} \end{aligned} \tag{3.88}$$

The angle of the horizontal net thrust, α_a, and its magnitude $|u^{wj}|$ is now related by:

$$\alpha_a = \tan^{-1}\left(\frac{u_{f,2} + u_{rev,2}}{u_{f,1} + u_{rev,1}}\right), \tag{3.89a}$$

$$|u^{wj}| = \sqrt{(u_{f,1} + u_{rev,1})^2 + (u_{f,2} + u_{rev,2})^2}. \tag{3.89b}$$

The two unknowns, d_{rev} and $|u_{3d}^{wj}|$ necessary in order to obtain the thrust desires can now be found. By inserting (3.88) into (3.89) we notice that the angle of the resultant thrust in region 2 and 4, i.e. for a fixed nozzle angle, depends on the state of the deflector only. We solve equation (3.89a) for the deflector state, and obtain:

$$\begin{aligned} \tan\alpha_a &= \frac{|u_{3d}^{wj}|(\sin\alpha_{f,sb}(1-d_{rev}) + \sin\alpha_{rev,sb}\cos\alpha_{vert}d_{rev})}{|u_{3d}^{wj}|(\cos\alpha_{f,sb}(1-d_{rev}) + \cos\alpha_{rev,sb}\cos\alpha_{vert}d_{rev})} \\ &\Downarrow \\ d_{rev} &= \frac{\sin\alpha_{f,sb} - \tan\alpha_a\cos\alpha_{f,sb}}{\tan\alpha_a\cos\alpha_{rev,sb}\cos\alpha_{vert} - \cos\alpha_{f,sb} - \sin\alpha_{rev,sb}\cos\alpha_{vert} + \sin\alpha_{f,sb}} \end{aligned} \tag{3.90}$$

Due to the fact that the tangent function is only valid in the interval $(-90°, 90°)$, the entire system must be shifted 90° in order to obtain valid results from equation (3.90). With the deflector state, d_{rev}, known, we solve for the required 3-dimensional thrust u_{3d}^{wj}, by inserting equation (3.88) into (3.89b).

$$|u_{3d}^{wj}| = \sqrt{\frac{|u^{wj}|^2}{(c(\alpha_{f,sb})(1-d_{rev}) + c(\alpha_{rev,sb})c(\alpha_{vert})d_{rev})^2 + (s(\alpha_{f,sb})(1-d_{rev}) + s(\alpha_{rev,sb})c(\alpha_{vert})d_{rev})^2}}, \tag{3.91}$$

where we denote the $sine(\cdot)$ and $cosine(\cdot)$-functions $s(\cdot)$ and $c(\cdot)$, respectively, in order to save some space. This approach is also valid for region number 4, however the angles used must be shifted differently. Region 3 is less complicated. Since the deflector state, d_{rev} must equal 1 in this region, the only unknown is the 3 dimensional thrust, which can be found by setting d_{rev}=1 in equation (3.91). The angle of the discharge nozzle equals $\alpha_{nozzle} = \alpha_a - 180°$ for region 3. This leaves us with the answer to all the unknowns, and equation (3.91) can be used in combination with equation (3.83) to obtain the necessary speed of the diesel engine. The simulations in this thesis will use the angular values $\alpha_f = 30°$, $\alpha_{rev} = 150°$ and $\alpha_{vert} = 30°$, which are realistic values roughly equal to

what is being used in most commercial water jet drives nowadays. The states of the discharge nozzle and the deflector shield as functions of the azimuth angle, computed according to the derivations above are shown in figure 3.12.

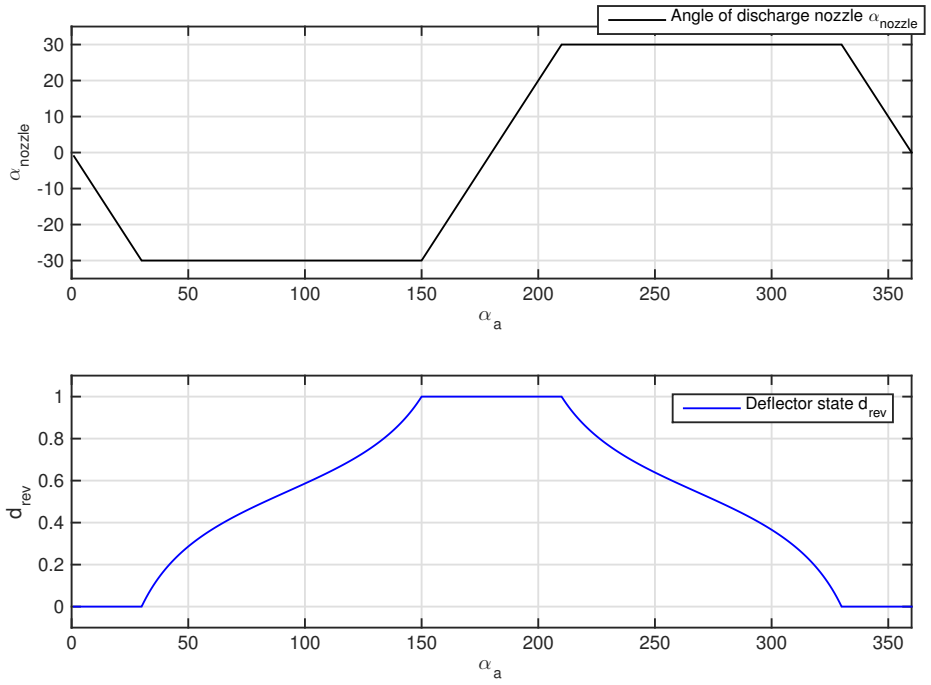

Figure 3.12: State of discharge nozzle α_{nozzle} and deflector shield d_{rev} vs. α_a

Chapter 4

Results and Discussion

This chapter will present the results of the preceding work by simulations that illustrates the behavior of the model and the derived controllers. The simulations are done in the time-domain, and we will display time series of the quantities we find relevant for each plot. There is a set of conditions which are used multiple times during the different simulations. We denote these *runs*, and each of these will be explained in the next section. The various vessel- and control parameters used are given in the appendix, and will be referred to when it is relevant. We will run simulations illustrating the following: behavior of the uncontrolled WF- system, step responses of the vertical plant and cushion pressure, performance of the heave compensation controller, performance of the sway compensation controller, performance of simultaneous sway- and heave compensation, DP-controller when subject for various disturbances and one run showing simultaneous station keeping and heave compensation. The simulations are done for a generic SES vessel, which is similar sized, but not identical to the Wave Craft, hence the results given does not represent the real Wave Craft performance or design, but is, in some aspects, somewhat similar. In order to achieve high performance for the lateral thrust controller, we choose a high total vent valve leakage area of $5m^2$. Due to the sign conventions from chapter 2.1, positive heave motion is defined downwards. For the WF motions, this represent a counter intuitive representation of the actual motions, thus the y-axis will be inverted for the heave motions in the WF simulations. All hydrodynamic parameters are calculated for a direction of wave propagation, β_{wa}, of $5\pi/4$ relative to x_b.

4.1 Simulation Conditions

The conditions and parameters of the different simulations are given by their corresponding *run*, which will be explained individually in the following subsections.

4.1.1 Run 1

Run 1 is a sea state with wave frequency $\omega_w = 0.785[rad/s]$ and wave period $T_w = 8s$. We use regular waves, of amplitude 1m (significant wave height=2m). These conditions are higher than the limiting sea state for most wind farms, i.e. in such conditions the operations are usually called off for conventional, similar sized vessels. This run is meant to illustrate the capacity of the controllers on the very border of their capacity, thus the damping ratio of the motion damping controllers is slightly reduced. There are no other loads present than the wave loads acting on the system. The hydrodynamic coefficients and control parameters used are given in appendix A.

4.1.2 Run 2

Run 2 has regular waves with angular frequency $\omega_w = 1.25[rad/s]$, and amplitude=0.5m. These conditions represent a lower wave height than in run 1, however, due to the high frequency of the waves, the velocities and accelerations becomes larger relative to the wave height, thus the inertial forces are still relatively high. As for run 1, the only loads acting on the system are due to 1st order wave effects. The simulation parameters used are given in appendix B.

4.1.3 Run 3

The wave frequency in this run is similar to run 2, but the wave height is reduced further to correspond to a significant wave height of 0.5m. This is done to show the effect of the sway compensation controller when not subject to the large saturation levels of run 1 an 2. Since the frequency is the same as for run 2, the hydrodynamic and hydrostatic coefficients will be similar, however the controller feedback gains are altered thus the parameters for this run is given in Appendix C.

4.1.4 Run 4

Run 4 is a Dynamic Positioning run, with zero disturbing forces. This is only to show the effect of the DP controller, and does provide any indications regarding the conditional capacity of the

system. The relevant simulation parameters, including DP-feedback gains, are given in appendix D.

4.1.5 Run 5

Run 5 is another station keeping run, differing from run 4 by the fact that there are external disturbances present. We also simulate with regular waves, to illustrate the behavior of the vent valve thrust while subject for non zero surface elevations. The waves are similar to those in run 2, and there is, in addition, a constant wind load, i.e., constant as in there are no fluctuating components. At simulation start, the wind speed, V_w, is 10m/s, with direction $\beta_w = 5\pi/4$. At t=500s, the wind gradually turns to an angle of $\beta_w = 3\pi/4$, and $V_w = 15m/s$. There is no current present. The parameters used are the same as for run 4.

4.1.6 Run 6

This run will show the capacity of the system in conditions where normal operation of conventional, similar sized vessel is usually called off. The windspeed is 12m/s and the velcoty of the current is 1.5m/s. There is, in addition, a sea state similar to that of run 1, which is quite large for this vessel type. The second order loads are pointing in the south-west direction. In addition to the constant loads, the velocity of the wind and current is fluctuating, as modeled by a random walk, gaussian process, described in section2.4.2. This run is meant to show that the vessel should be able to handle quite severe conditions, within the accuracy of the derived model.

4.2 Model Verification

This section will show that various inputs to the simulation plant generates intuitive outputs and responses, both for the cushion- and the vessel dynamics. We will simulate for step responses in the vent valve louver control signals, both for the total and the directional leakage area, for undisturbed conditions, i.e. flat seas. We will also include an uncontrolled run in {s}, when the system is subject to first order wave loads.

4.2.1 Step Response of Heave- and Pressure Trajectory

We simulate for the Vessel Parameters given in Appendix A, to show qualitatively how the system reacts to a step response in the total leakage area for zero seas. The simulation starts with a total leakage area equal to $\frac{A^l_{max}}{2}$, which will be the *bias* leakage for all runs unless otherwise stated. At t=25s, the vent valves are fully closed, and at t=75s they are fully opened. The plot in figure 4.1 shows the response of heave- and pressure position and velocity, together with the corresponding total leakage area.

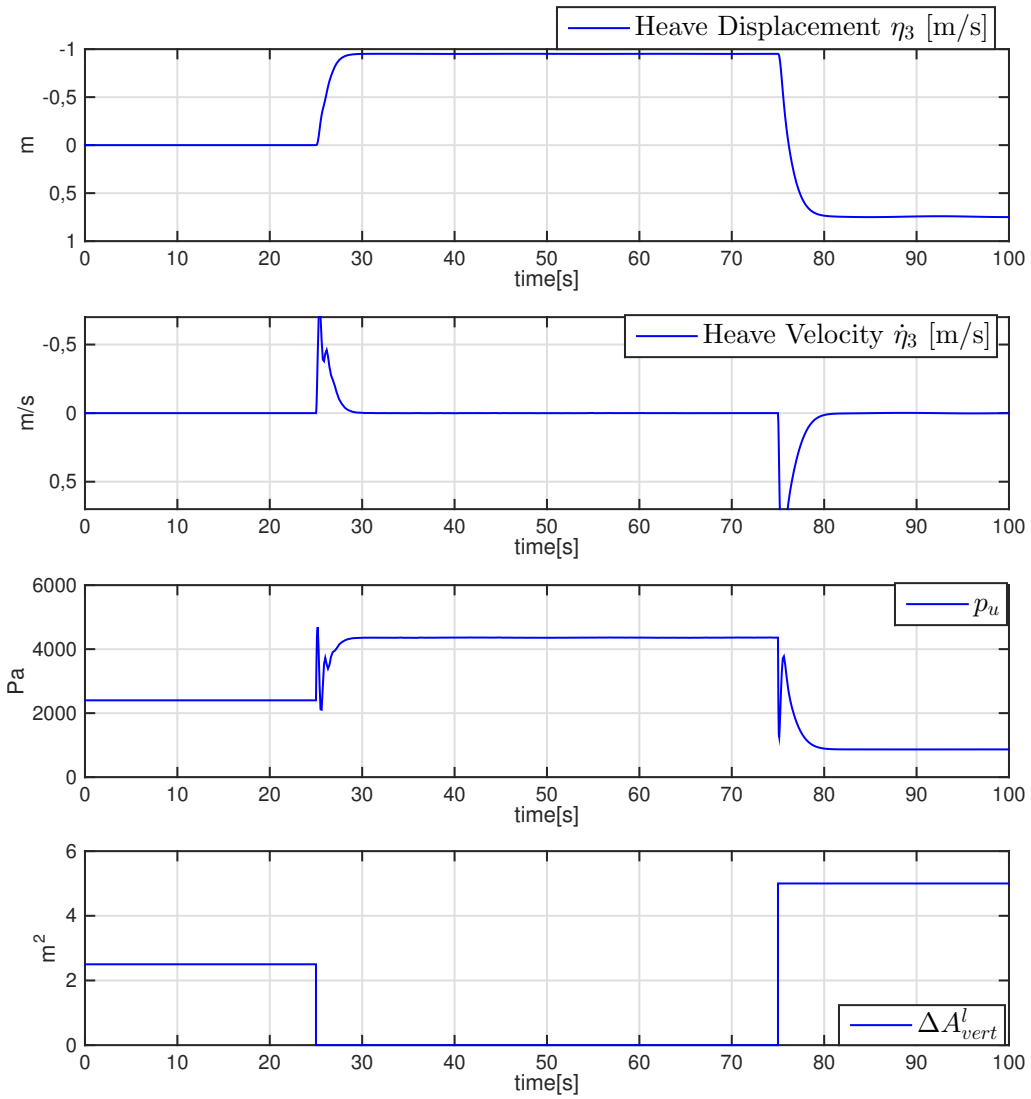

Figure 4.1: Response in Heave and Pressure Due to Step in Total Leakage Area

We notice that there are transient effects in the pressure response due to the steps in the control input. These are recurring and we can not seem to find any good explanations to them. However they only occur for steps, and does not affect the system under regular conditions. We performed some parameter tuning to find possible explanations; the transients are strongly reduced if the added mass of the vessel is increased, however we chose to use the parameters given by the seakeeping estimation program ShipX, as these were the most reasonable estimates of these parameters that we could find. The transients are probably due to several, minor, simplifications or unmodeled dynamics in the uniform pressure equation. Fluid inertia, for instance, is neglected, which, even though extremely low, hypothetically could affect the response slightly. The remaining state trajectories looks highly plausible. The heave position at minimum leakage equals, roughly, -1m, which indicates that the polynomial used to simulate the state dependency of the passive leakage areas is reasonable tuned as this corresponds well with experiences from model tests.

4.2.2 Undamped Regular Waves in {s}

This is a WF simulation, without any controller action. The system is simulated for regular seas of 0.5m amplitude and angular frequency $\omega_w = 1.26[rad/s]$, i.e. the conditions given by run 2. The relevant parameters are given in Appendix B. The initial conditions are the zero states, which explains the transient behavior at simulation start as the velocities and positions would not be zero at the same time for the steady state motions.

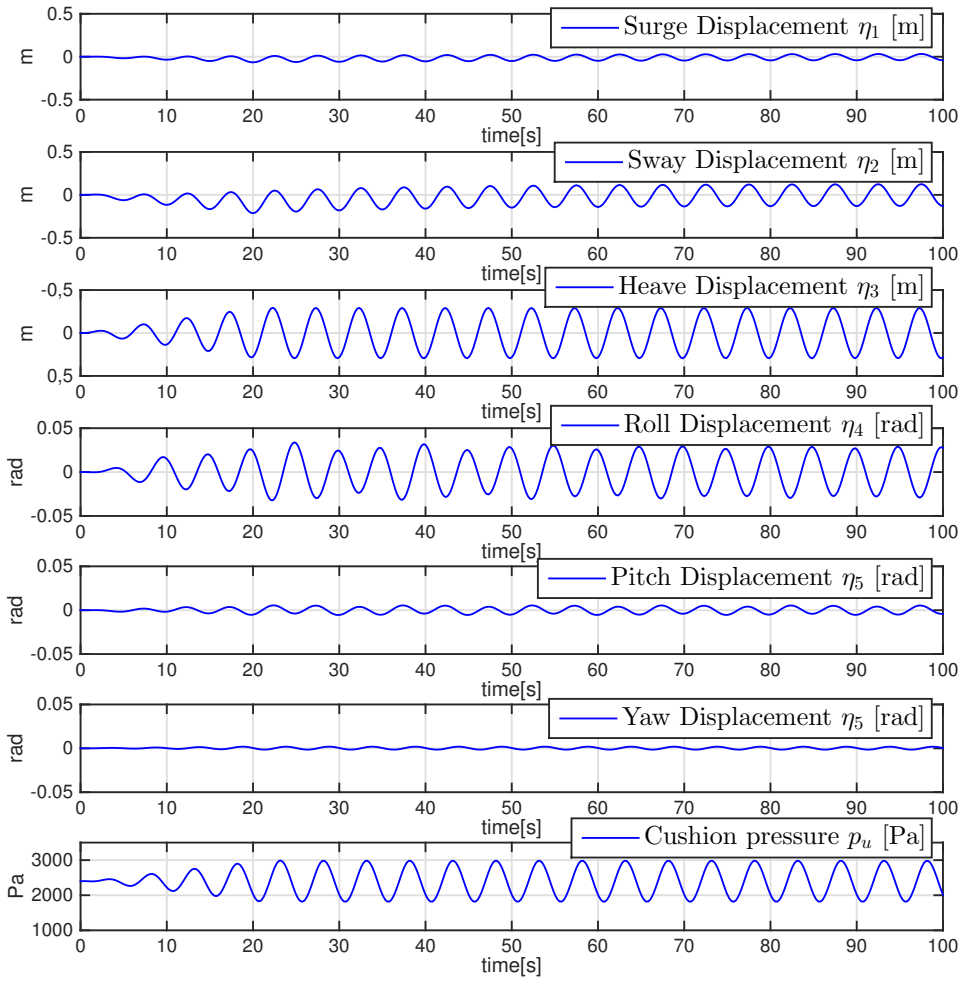

Figure 4.2: Undamped WF Motions

4.3 Heave Compensation

This section will demonstrate the effect of the vertical motion damping system for two runs, run 1 and 2, which are thoroughly explained in the beginning of the chapter, together with reference to the relevant parameters. In run 1, the controller is switched on at t=200s while we apply it at t=100s in run 2. We will only investigate the motions in {s}, in addition to the pressure trajectory, which is presented by the uniform pressure component $p_u(t)$, which holds for all the simulations done in this chapter.

4.3.1 Heave Compensation Run 1

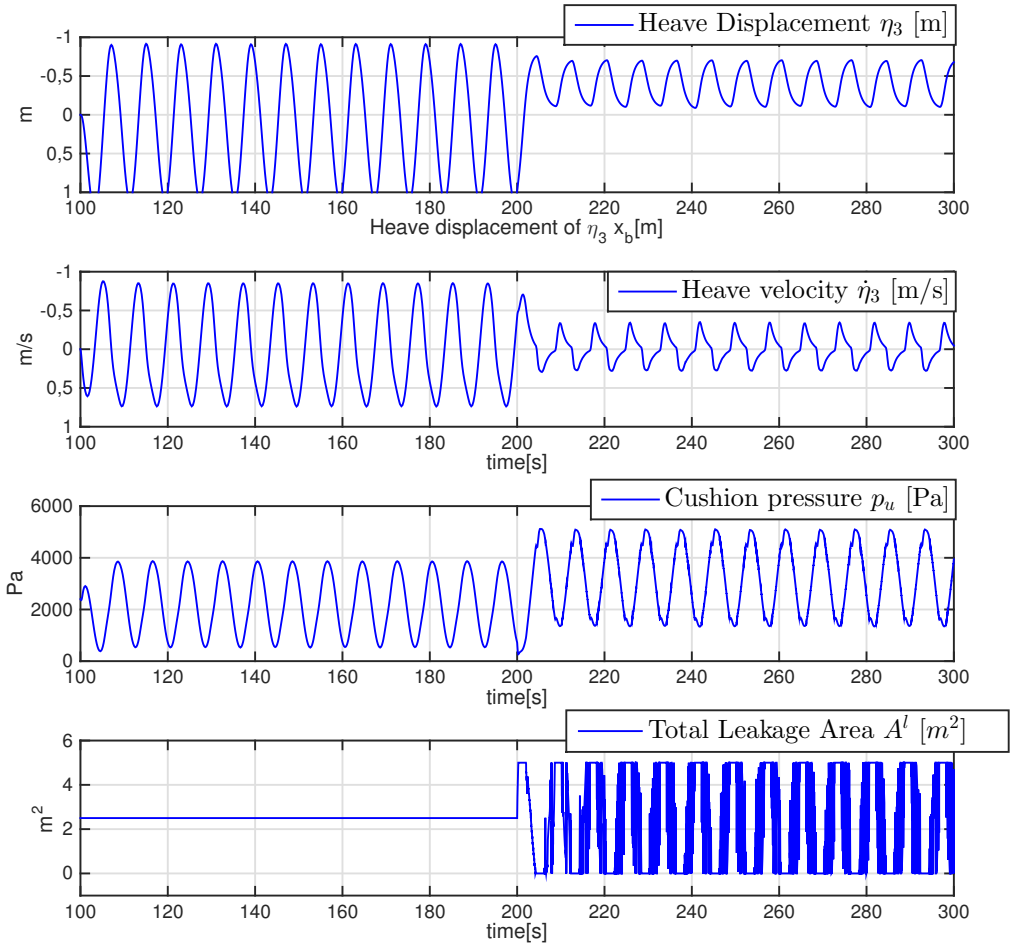

Figure 4.3: Heave displacement and acceleration + cushion pressure and leakage area, run 1

4.3.2 Heave Compensation Run 2

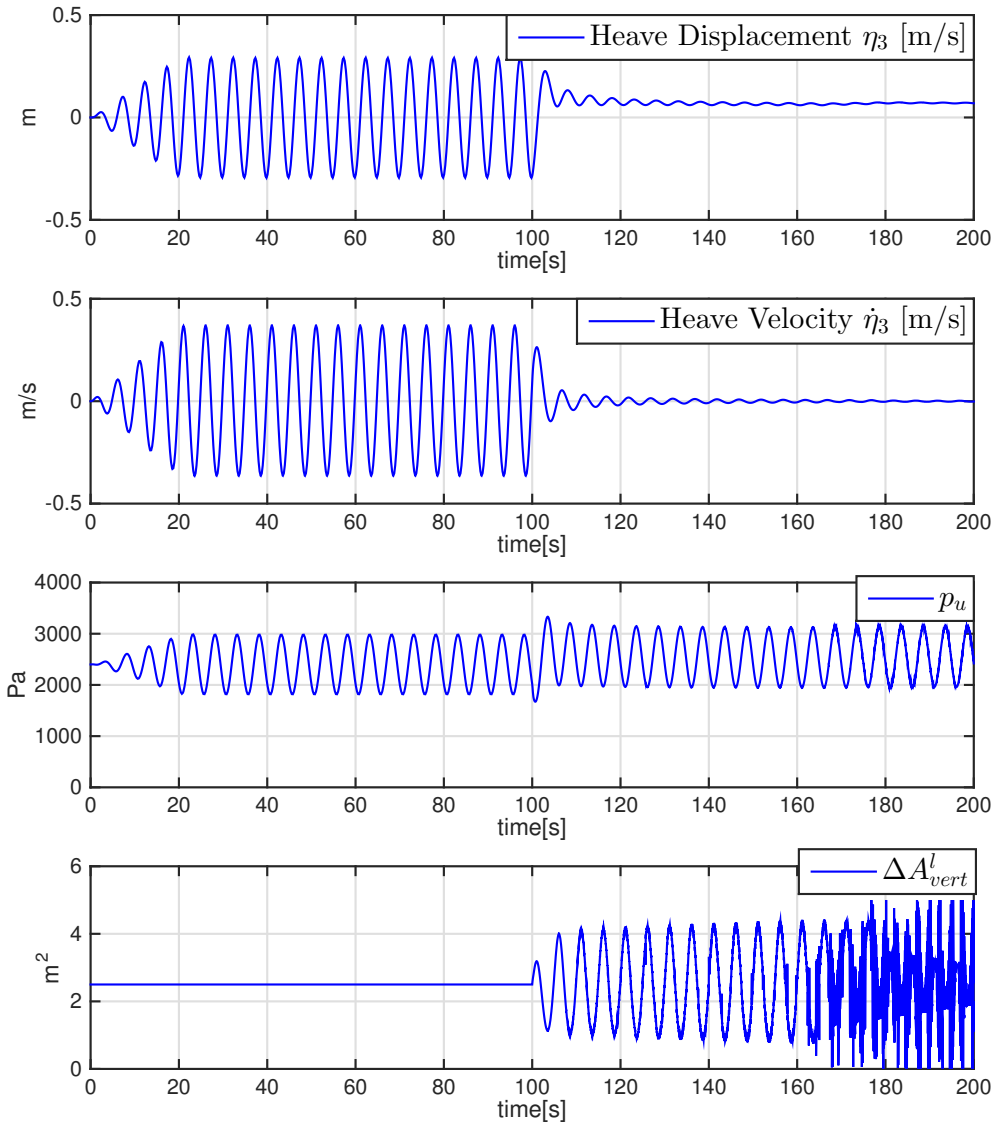

Figure 4.4: Heave- displacement and acceleration + Control Input run 2

4.3.3 Discussion on Heave Compensation Performance

These simulations indicates that the heave controller will exhibit strong performance with the feedback gains computed in chapter 3. Run 1 is simulated for higher seas, and we see that the damping ratio in run 1 is lower than in run 2. This is due to saturations in the actuators, and we can conclude that these sea states are close to the border of the system capacity. The damping is still significant, however. Run 2 shows very strong performance, and there are almost no vertical motions left when the controller is applied. The actuator displacements are well within the capacity for run 2, and the sea state could probably have been even higher, while still maintaining the high damping ratio. This vertical motion controller feature feedback on the pressure state in addition to the two vertical translative trajectories, as opposed to existing zero speed, vertical motion controllers, which seems to work well.

4.4 Sway Compensation

This chapter will show the effect of the sway motion damping controller, and will illustrate it by plots of the velocity and acceleration in sway. We will show simulations for run 1, 2 and 3, in addition to a parameter study where we investigate the behavior of the system if the loss coefficient c_n is increased to 0.9 (as recommended by (Liepmann, 1961) and (Kurita, 1988)). Note that this does not necessarily allow the achieved thrust to be scaled linearly as the increased flow also leads to a reduced pressure for given leakages. We did, however, achieve a significantly increased performance of the sway motion damping, as will be shown in section 4.4.4.

4.4.1 Sway Compensation - Run 1

Conditions are given in the beginning of the chapter. The controller is turned on at t=100s. The waves are large in this run, and it is on the border of the sway damping capacity, thus the damping ratio is rather low compared to the following runs. We achieved a motion damping of about 20%, which is, even though less significant than for the vertical motion damping, still a strong contribution.

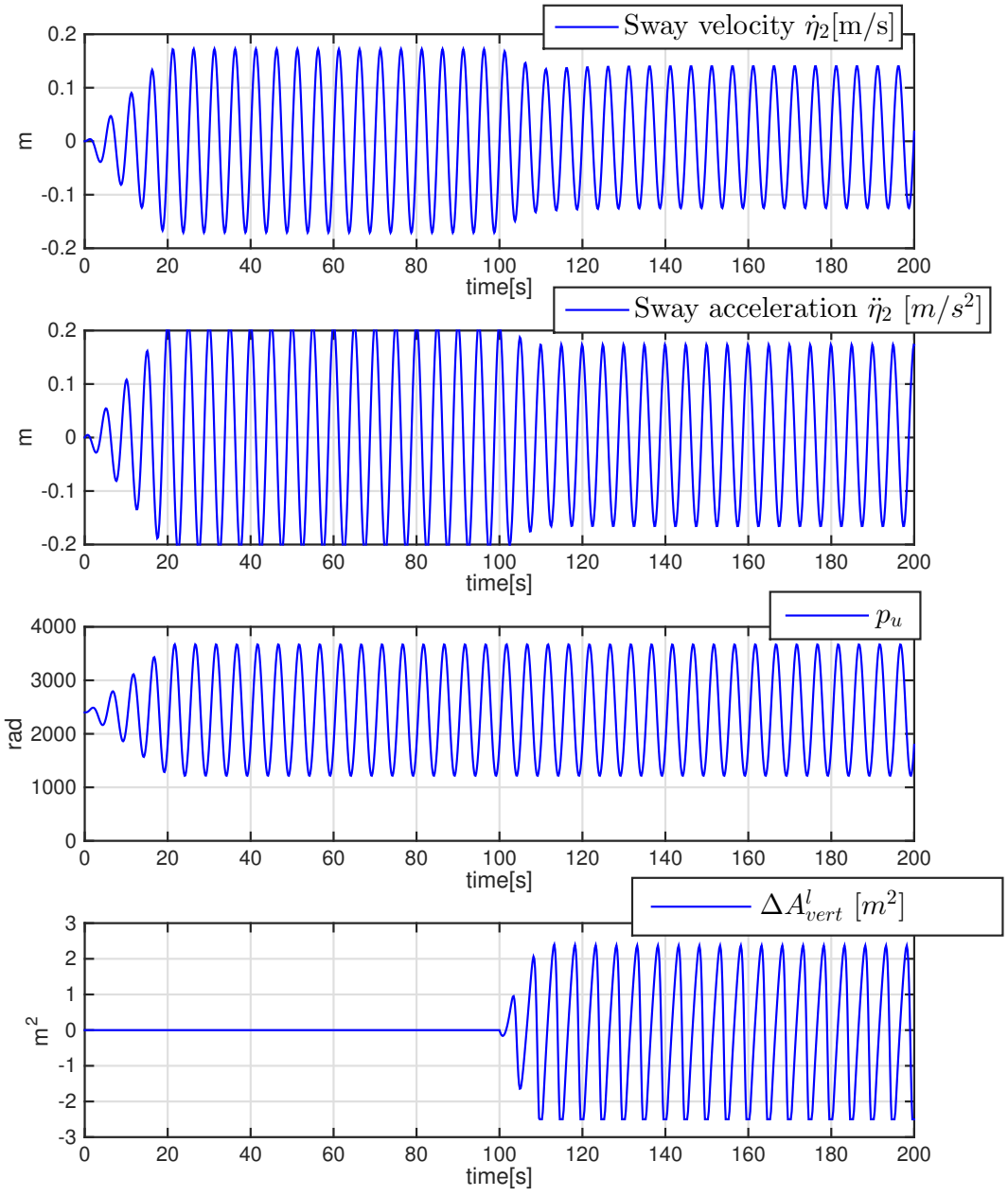

Figure 4.5: Sway compensation, run 1

4.4.2 Sway Compensation - Run 2

Similar conditions as described in the beginning of the chapter. The controller is turned on at t=200s. We notice that the motion damping amounts to about 22%. The wave frequency is a lot higher in this run compared to the previous one, which implies higher accelerations and velocities, relative to the wave height, thus the damping levels are not that much higher than for run 1. The damping is still significant.

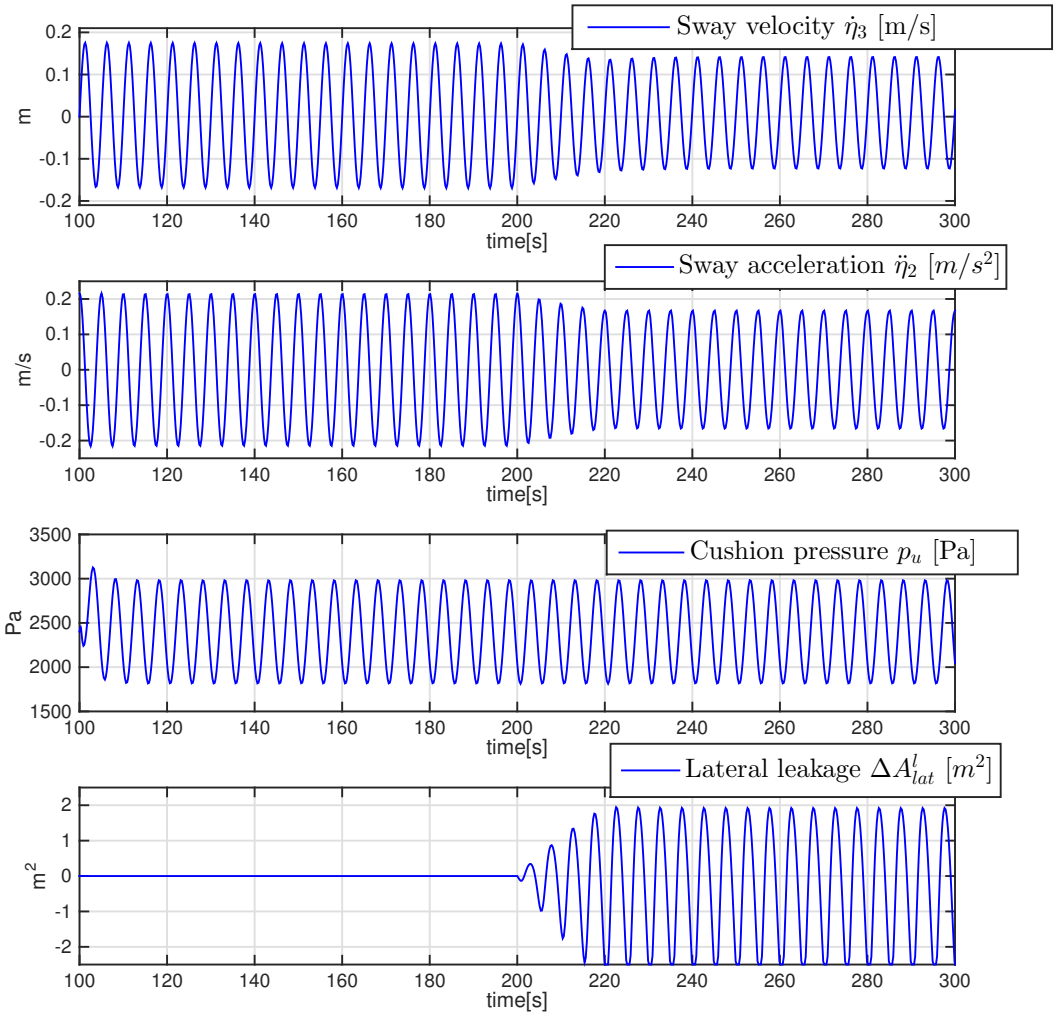

Figure 4.6: Sway compensation, run 2

4.4.3 Sway Compensation - Run 3

The conditions are given in the start of the chapter. The controller is turned on at t=200s. The preceding conditions have had relatively large waves. To put them in context; operations are normally called of for conventional wind service vessels if the sea states exceed 1.5m (0.75m amplitude). Here we simulate the system behavior for 0.5m wave height, to illustrate the effect of the sway motion damping when the saturation levels are lower.

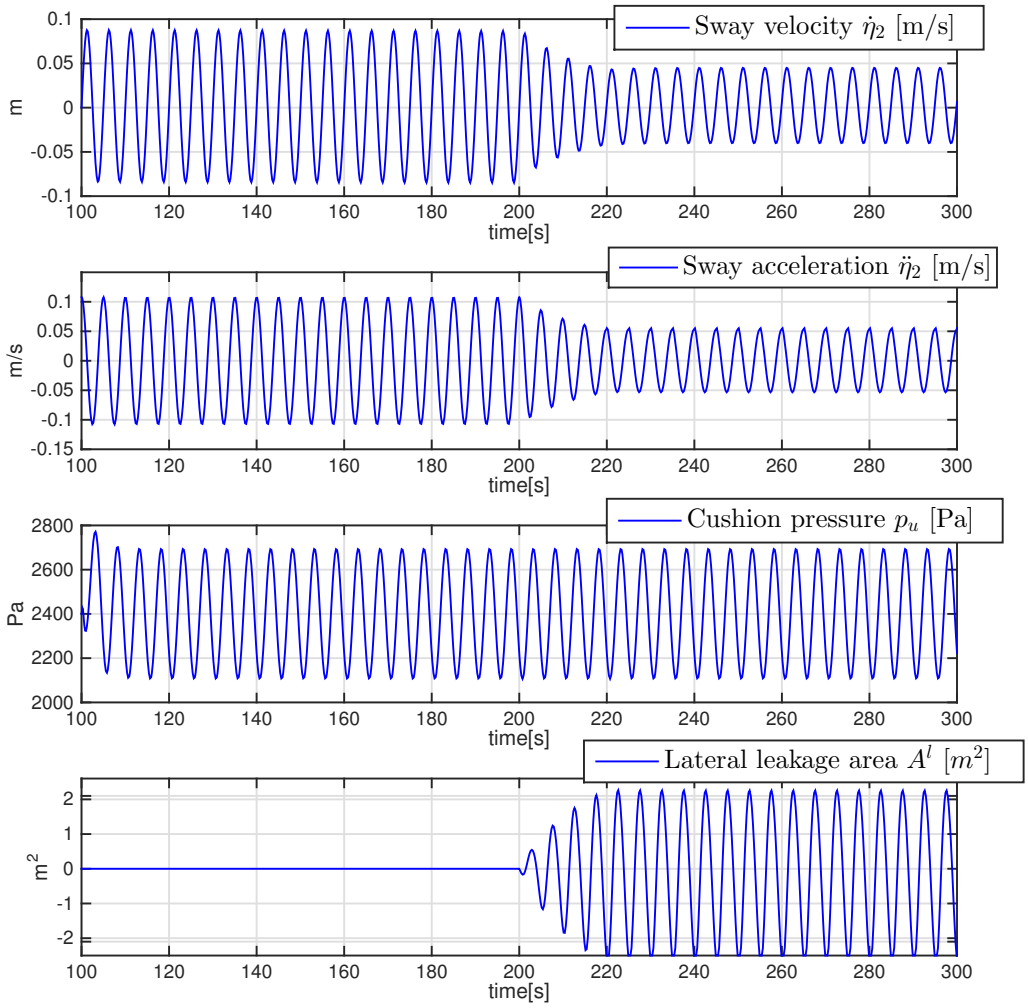

Figure 4.7: Sway compensation, run 3

We note that the damping levels are close to 50%, while saturation of the actuators is still avoided.

4.4.4 Sway Compensation - Run 2 - Parameter Study

This run was done with the same simulation parameters as in chapter 4.4.2, with one difference; c_n is changed to 0.9. This is done to investigate how conservative the results done with $c_n = 0.61$ really are. We found that the sway compensating capabilities are slightly improved, however the decreased losses also means that the pressure will decrease more for a given leakage area. The achieved damping levels amount to around 32%, which is a significant increase compared to run 2. The controller is switched on at t=200s.

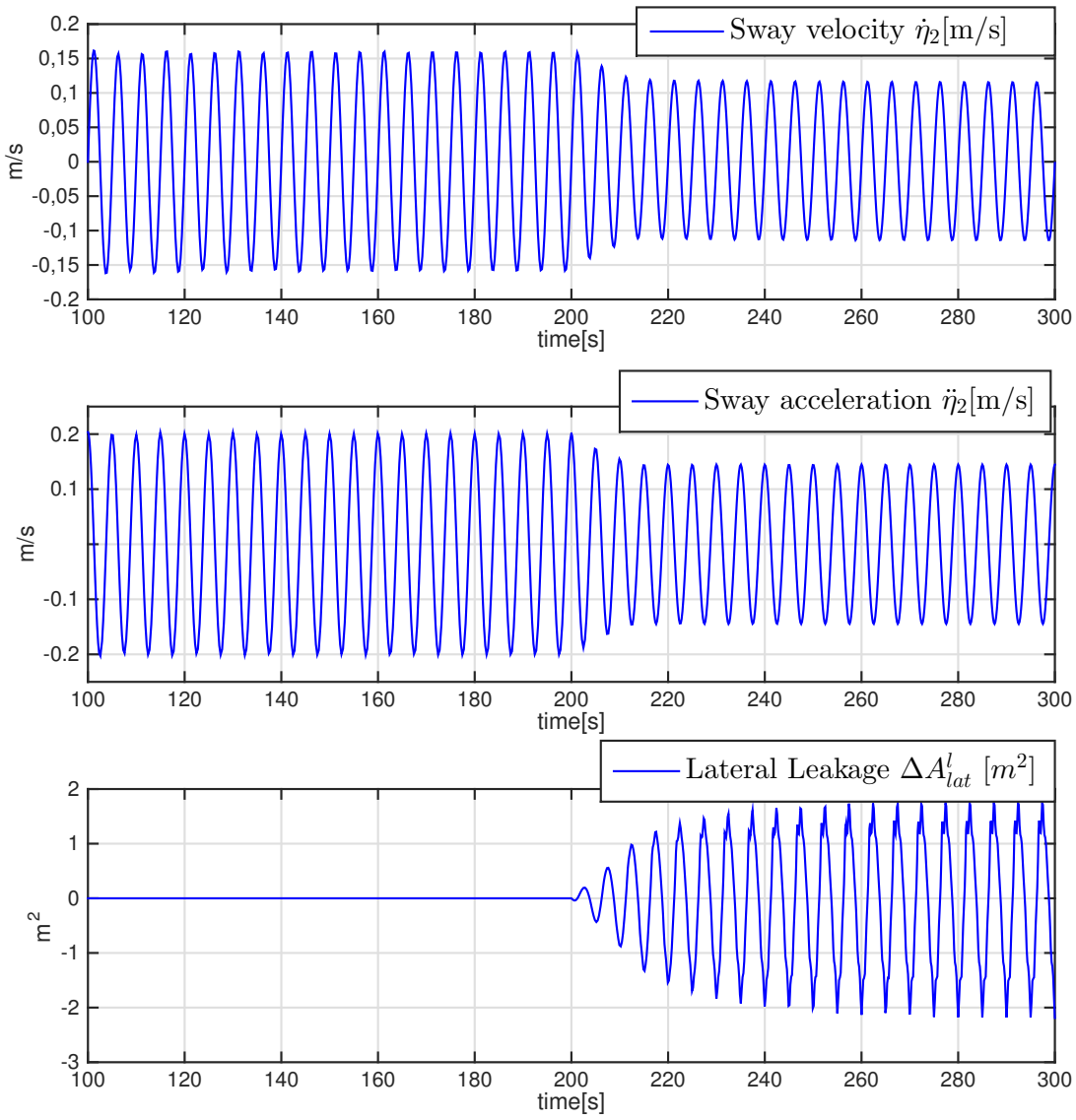

Figure 4.8: Parameter study of loss coefficient $c_n = 0.9$, for sway compensation

4.4.5 Discussion on Sway Compensation Performance

Due to the relatively limited available thrust from the vent valves, the capacity for damping of the first order sway motions is limited. However, we have still shown, by this section, that significant reduction of the motions scan be achieved, albeit less than for the vertical motion damping problem. High waves and/or high frequency waves imply large inertial- and first order wave induced forces, which somewhat limits the achieved damping ratio. It is still above 20%, thus it is significant. For run 3 we note that the damping amounts to as much as 50%, and the system would probably have shown really strong performance in swells as well, however we did not simulate for such conditions. We have, as mentioned earlier, found several factors suggesting that the value $c_n = 0.61$ is too conservative for the results to serve as good indications regarding the actual capacity of the system, however this value seems to be the common convention within the field. Still, it is the authors opinion, that more attention should be paid to the capacity indicated by figure 4.8, as we feel this provides a better indication of the actual system performance.

4.5 Combined Heave and Sway motion damping

WF motion damping scenarios were simulated for waves, in the conditions of run 2 and 3. The controller is turned on at t=200s for both runs. The trajectories of the heave and sway motions are presented as time series, together with the relevant control signals. In run 3 we also include the positions in sway. The vessel parameters used are presented in appendix B for run 2 and C for run 3. The feedback gains of the control input and the relevant parameters used in the derivations, such as LQR weighting matrices etc. are also given there.

4.5.1 Combined WF Damping - Run 2

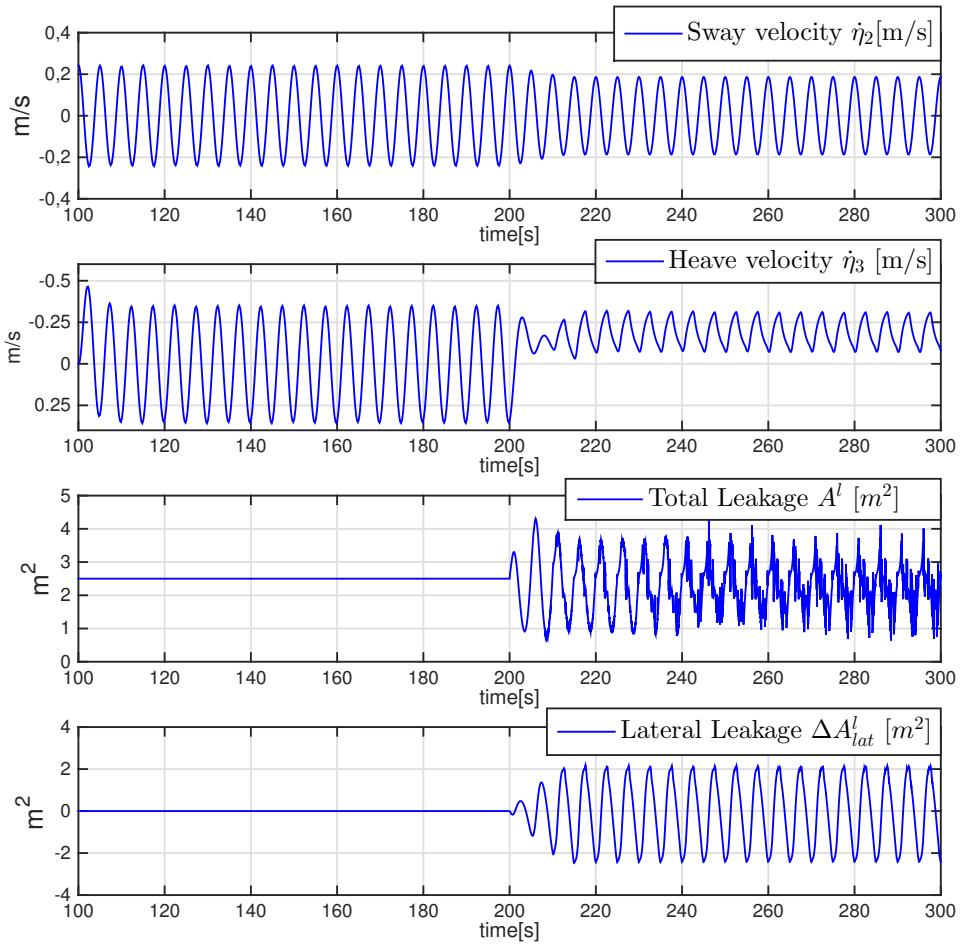

Figure 4.9: Motions in heave- and sway + Control inputs for run 2

4.5.2 Combined WF Damping - Run 3

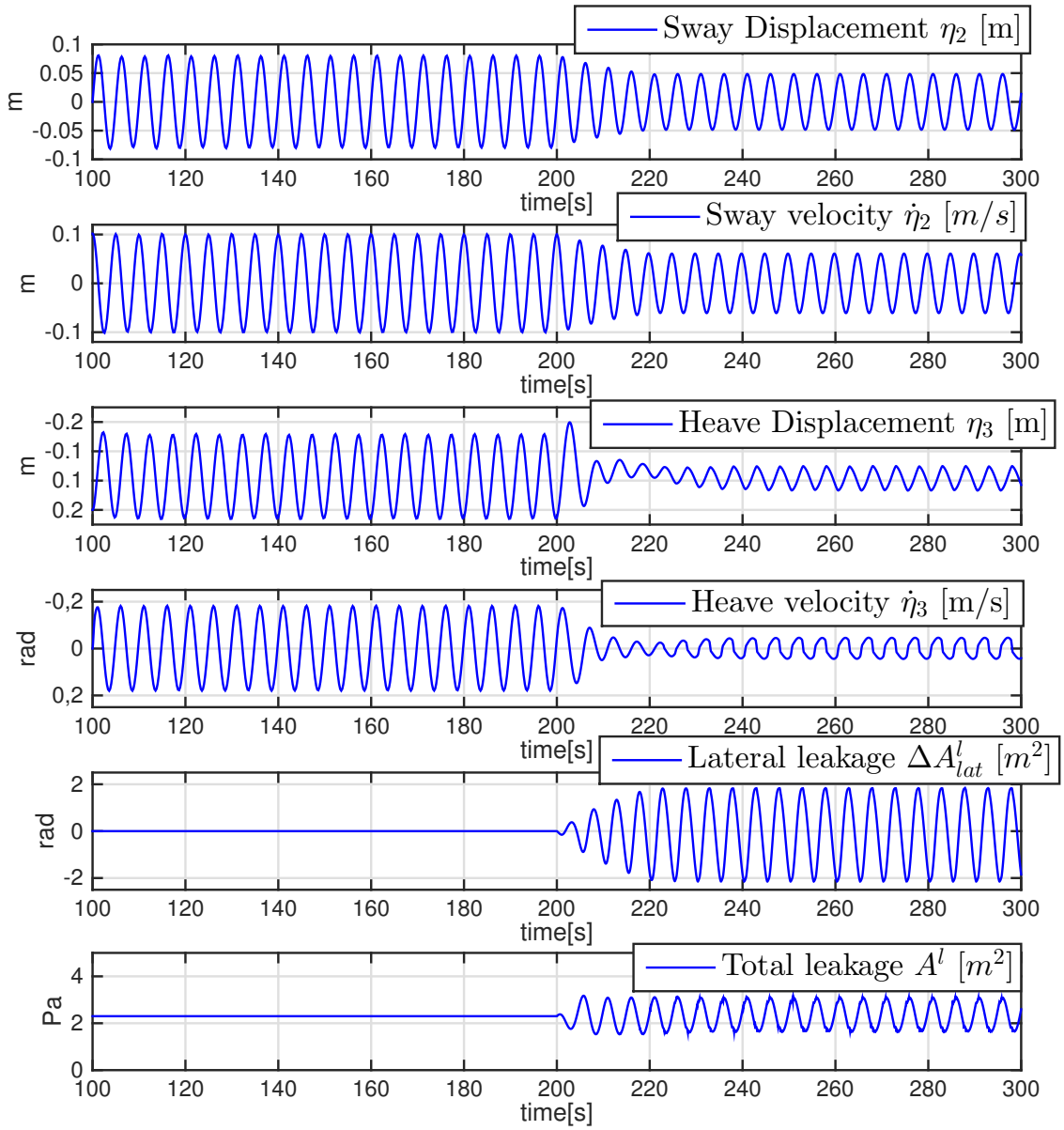

Figure 4.10: Motions in heave and sway + Control inputs for run 3

4.5.3 Discussion on Combined Heave- and Sway Compensation

The simulations above indicate that the potential for damping the motions in both sway and heave, simultaneously, is limited, due to the nature of the only actuator involved, i.e. the vent valve louvers and the cushion pressure. There are simply too many dependancies, and if you reach actuator saturation due to one of the control outputs, the other state will be strongly influenced. To provide any significant sway damping, the lateral thrust needs to be at the limit of its capacity all the time, which does not leave much room for the total leakage area, which in turn controls the vertical motion damping. Even though the phase shifting approach proposed in chapter 3.3.2 improves the matter, there will still be some levels of mutual infliction between the two desires which complicates the process. For the 0.5m wave run, in run 3, we did see significant damping of both trajectories, and the sway motions were damped by, about, 32%, with the damped motions in heave being of an almost negligible magnitude. The sway damping in run 2 amounts to about 18%, where the corresponding heave motions are still damped by around 60%. The 1m wave height in run 2 does, after all, correspond to quite common condition in the areas the vessel is likely to operate, thus, even though the potential of such simultaneous motion damping is limited, we have shown that it is still, to some degree, possible, especially for the less severe environmental conditions. Even though not crucial for normal operation, the motion damping shown in run 3 would still, most likely, provide a significant simplification of a boarding process, and make the operation of the vessel a lot more comfortable for the crew.

4.6 Station Keeping

This section will feature simulations of run 4, 5 and 6, which are thoroughly elaborated in the beginning of the chapter. The vessel parameters used in both the WF- and LF plants, when relevant, are given in Appendix D, which also includes the feedback gains for all relevant controllers used. Initial conditions, set points and further relevant information regarding the different simulations are given in the respective subsections when relevant.

4.6.1 Station Keeping - Run 4

The initial conditions are $\eta_{3d,0} = \begin{bmatrix} 0 & 0 & 0 \end{bmatrix}^T$. The initial position reference is $\eta_d = \begin{bmatrix} 1 & 1 & \pi/4 \end{bmatrix}^T$. At t=100s the heading reference is changed from $\psi_d = \pi/4$ to $\psi_d = -\pi/4$. The plot will include the three NED-coordinates as well as the thrust levels of all thruster components, including the directional leakage area of the vent valves. The directional leakage area and the vent valve thrust will be linearly proportional for this run as there are no external disturbances, thus the pressure remains constant since the system will strive to maintain the equilibrium total leakage bias opening. The station keeping plots given later in the chapter will not include the thrust components from each individual thruster, as the qualitative nature of their behavior is illustrated good enough here. The state of the discharge nozzle and the deflector shield of the water jets will not be presented here, but the relevant mappings from the lateral- and longitudinal thrust components are given chapter 3.7.

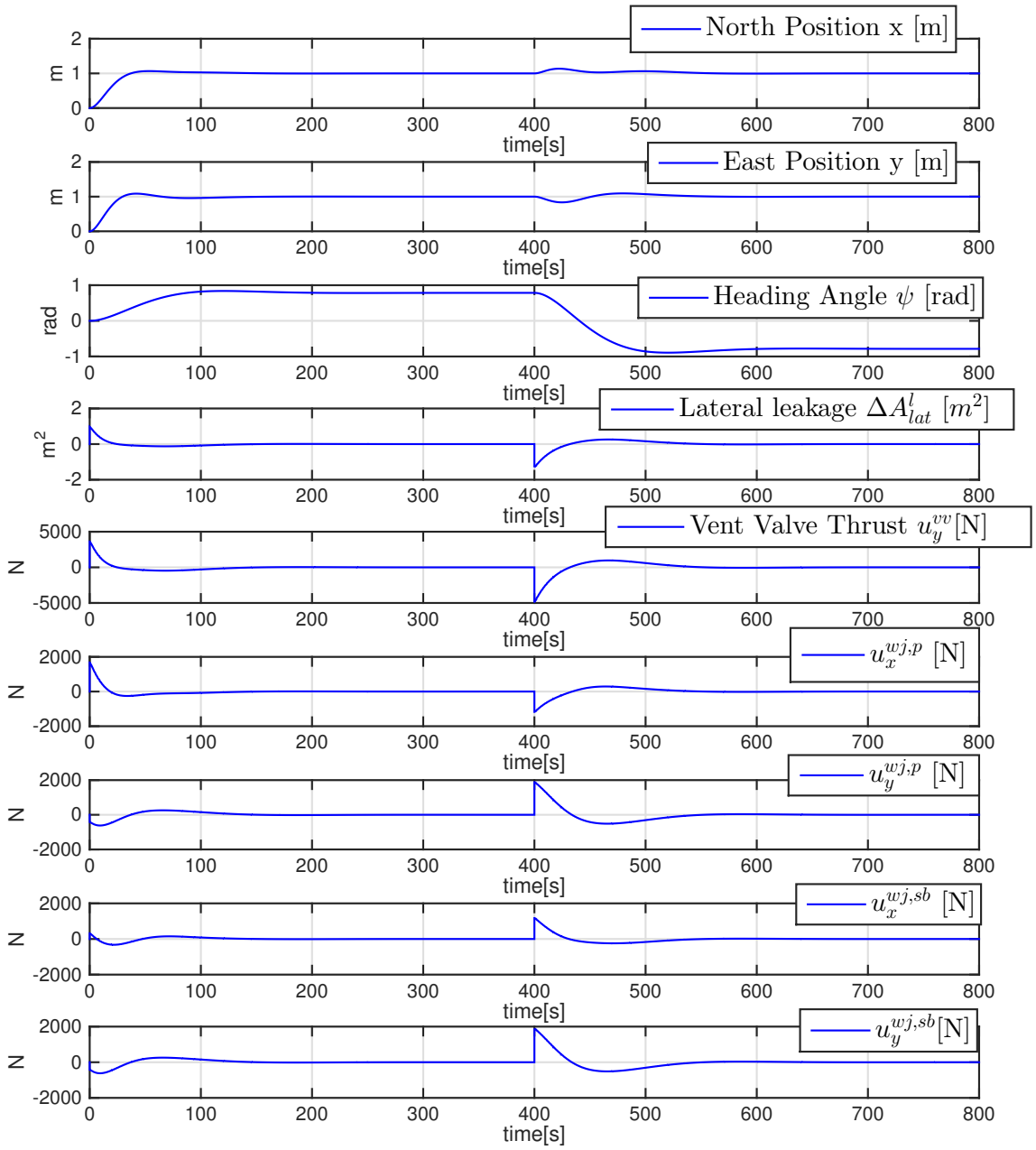

Figure 4.11: Run 4 Station keeping

4.6.2 Station Keeping - Run 5

We will investigate station keeping only, thus the initial conditions are the same as the initial reference position and heading, $\eta_{3d,0} = \eta_d = 0$. This run will show the behavior of the system when subject to non-fluctuating disturbances and nonzero surface elevations. The effect of the integrator term in the controller is also verified. As explained in the beginning of the chapter, the environmental loads will change direction at t=500s.

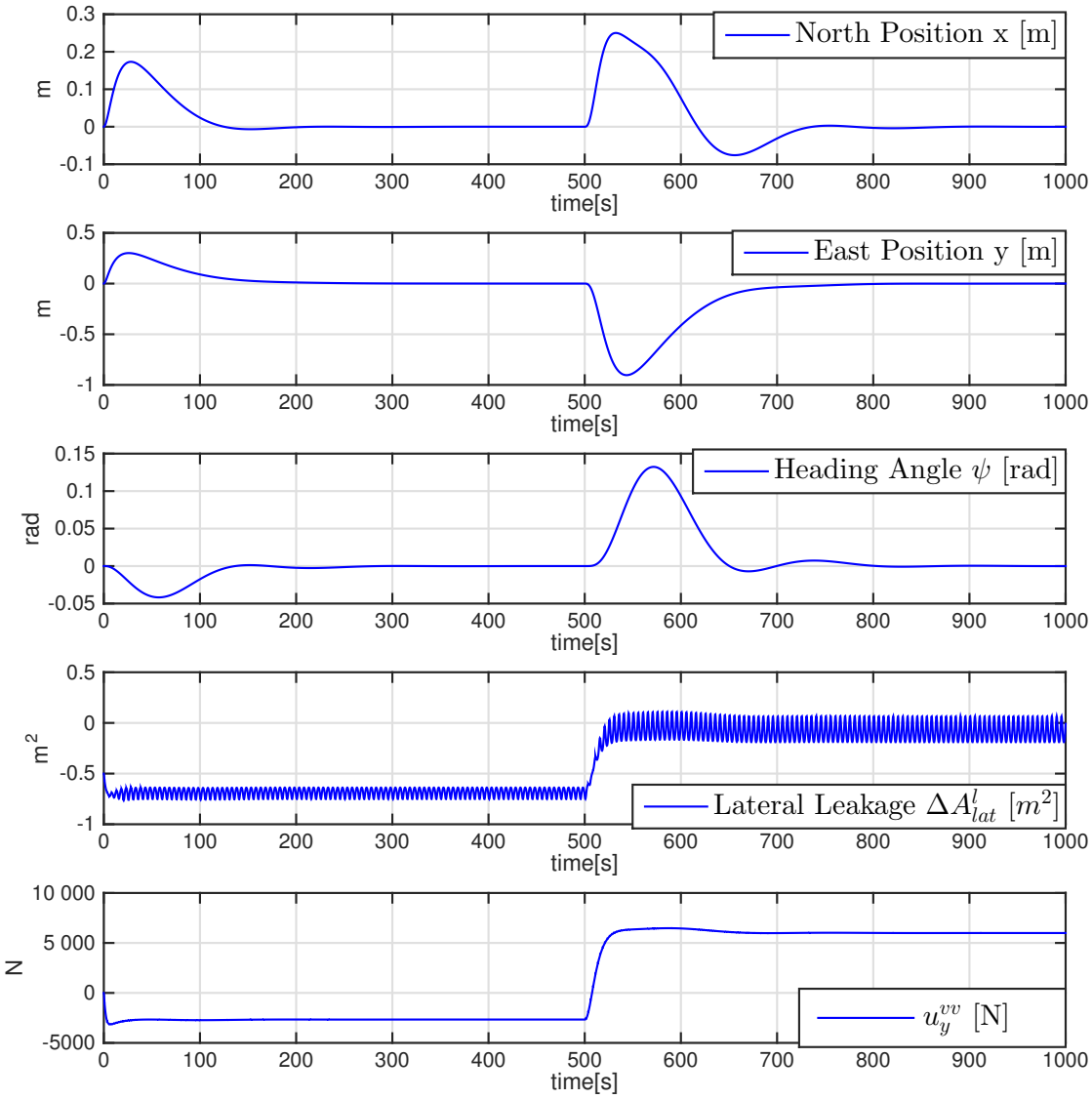

Figure 4.12: Run 5 Station keeping

4.6.3 Station Keeping - Run 6 - Constant Set Point

The conditions in this run is given by run 6, and the initial conditions are the same as the constant DP-set points, given by $\eta_d = [0 \quad 0 \quad 0]^T$. The loads and the simulation start at t=0, thus the initial transient as the integrator is loading. The feedback gains used are the same as for the previous simulation, and will be given in Appendix D.

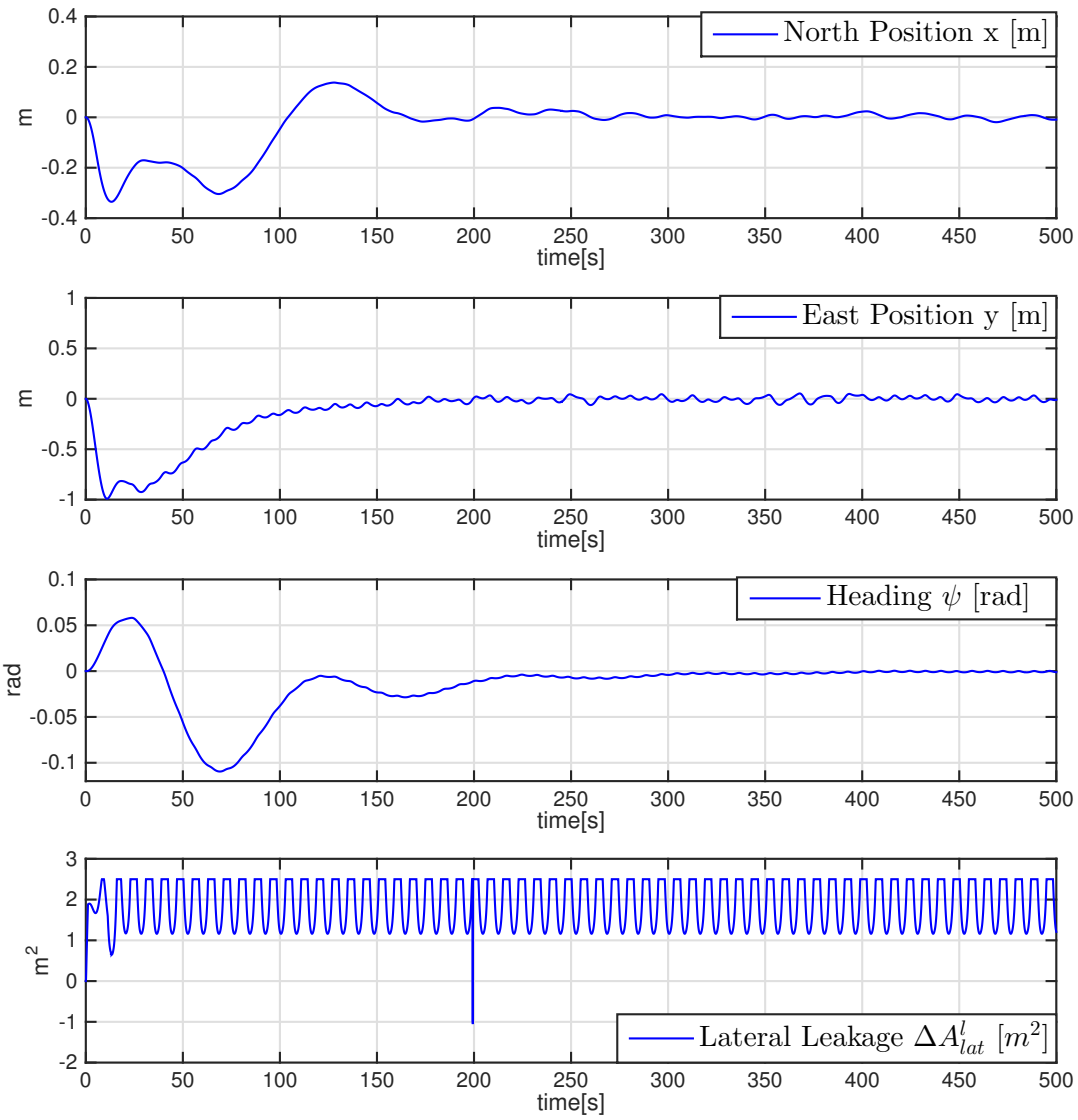

Figure 4.13: Run 6 Station keeping

We notice that these gains might not be optimal for the conditions in this run, which are quite severe, however they do work and we see that the system behaves nicely even when subject to relative strong, fluctuating, environmental loads. It is also apparent that the allocated thrust to the vent valves is above their capacity, by looking at the saturations in the lateral leakage area, which implies that the vent valves have not delivered the commanded thrust. However this did not seem to have any large inflictions on the system behavior, and could probably have been easily solved by reducing the allocatable vent valve thrust in thrust allocation algorithm, thus transferring a larger portion of the forces to the water jets.

4.7 Combined Heave Compensation and Station Keeping

This single run is meant to illustrate the potential of performing station keeping and heave compensation simultaneously. The WF conditions are the same as for run 1. The load in {n} is not modeled as being induced by wind or current, but is simply a load of constant magnitude and direction, 11000N and $\pi/4$, respectively. The reason we chose to just *hardcode* this load is to illustrate the capacity of the system when subject to a known load/situation. The uncertainties in the modeling of wind- and wave loads, as used above, are larger, which is why we feel this provides a better illustration of the capacity. The simulation is done as follows; Initial conditions and set points are $\eta_{3d,0} = \eta_d = [0 \quad 0 \quad -\pi/4]^T$. At t=100s the heave compensation controller is turned on, at t=200s the heading set point is changed to $\psi_d = 0$, at t=400s the heading set point is changed to $\psi_d = \pi/4$. The reasons for changing the set points is that as the vessel is pointing more in the direction of the constant load, more thrust is transferred to the water jets and less to the vent valves. The result is that the heave compensation is enhanced. Figure4.14 shows that there is some sort of inverse proportionality between the heave damping ratio and the vent valve thrust, just as expected. We also notice that the delivered thrust behaves more consistently immediately after the heave compensation controller is applied. This is because of the corresponding rise in mean pressure, and should be noted for further work.

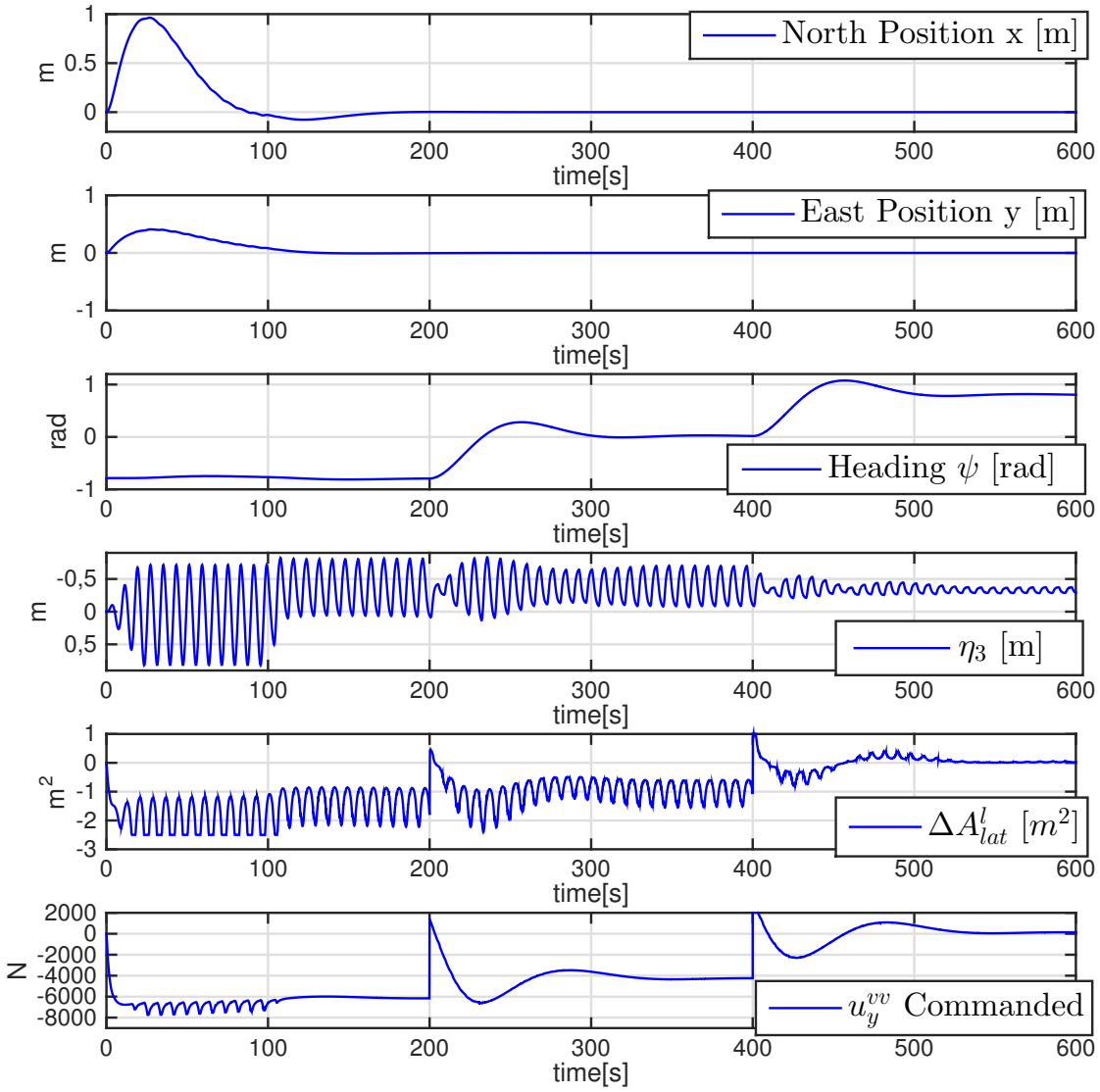

Figure 4.14: Combined Heave Compensation and Station Keeping

4.8 Discussions

All in all, the derived controllers seems to exhibit strong performance, and the plant behaves well in the simulated conditions. The potential for vertical motion damping has already been shown by previous work, but the derived controller performs very well here, by using the variations in the cushion pressure as an extra input. The damped motions are almost negligible for run 2, but even in the conditions represented by run 1 we see strong vertical motion damping which should provide a significant improvement on the onboard conditions. The potential for lateral motion damping is limited as the maximum thrust obtainable by the vent valve thrusters is, shown by the simulations, limited around 10,000N for the varying demands, the constant thrust delivering capacity is lower. Even though this is a significant thrust, the forces related to WF motions and 1st order wave loads are simply too large to be fully compensated for by the control system. Nonetheless, we experience a reduction in the lateral motions of between 18- and 50%, which is, after all, significant. The limitations lies in the conditions where significant damping is possible to obtain. For waves reaching 2m, which is a lot compared to normal operational conditions of comparable vessels, the achieved damping is only around 20%, however for smaller waves the relative damping increases significantly and the system could, hypothetically, become a highly valued aid in the process of docking the vessel to an offshore turbine. We must remember that this system does not require any additional hardware compared to already existing vessels, and could, theoretically, be implemented solely by the means of a software update. Neither will the usage of the system imply any significant additional fuel consumption, and in that perspective, a lateral motion damping of between 20 and 50% could be well worth the effort.

The DP system performs well, and position is maintained even in the rough conditions given by run 6. The vent valve thruster seems to deliver the demanded thrust accurately even in relatively large waves, and even if saturation is reached at some times the integrator in the controller increases the demanded thrust so that the difference in demanded and delivered thrust is delivered by the water jets instead. The last simulation shows that strong vertical motion damping can be obtained even when performing station keeping, and subject to relatively large loads. The vertical motion damping, in DP, can be enhanced by reducing the maximum allocatable vent valve thrust in the thrust allocation algorithm, or by changing the heading angle so that the thrust can be provided by longitudinal water jet thrust components instead.

Chapter 5

Concluding Remarks

5.1 Conclusion

For offshore wind farms to be competitive compared to their land based counterparts, measures must be taken in order to reduce the maintenance related costs and increase the accessibility of such plants. SESs are fast and fuel efficient, and due to active motion damping, even smaller vessels can be designed to feature the same seakeeping properties as much larger conventional OSVs. By this thesis we have shown that automatic control of vent valves on a SES can control the motion of the vessel in the horizontal domain. This is beneficial for a SES, since traditional bow thrusters has negative effects such as increased transit resistance and installation difficulties arises due to narrow side-hulls.

By the process plant model derived in chapter 2 and the control scheme derived in chapter 3, verified by the simulations in chapter 4, we show that we can utilize the linear momentum from the air flow driven by the potential energy in the air cushion in combination with the water jets to successfully perform station keeping when subject to relatively severe environmental loads of first and second order nature, and also damp the horizontal and vertical motions. Chapter 4 indicates that the vessel should be able to perform significant damping of WF motions, and reduce them to quite tolerable levels, even above the sea states defining the operational limit of comparable, similar sized vessels. This also holds for the station keeping capacities indicated by the simulations in chapter 4.6.3 and 4.7, which shows that the vent valves could serve well as a substitute for conventional bow thrusters, and exhibit strong performance even in relatively large sea states.

All the above can be achieved by the exact same set of actuators and sensors that can be assumed available on these vessels today, and if we regard the findings in this thesis as possible to achieve by the sole mean of a software update, this can become a significant contribution in making operation of such vessels and offshore wind farms less expensive and a lot more convenient for the crew and operators.

There are, off course, challenges left to solve. The consistency of the thrust delivered by the vent valves must be regarded in context with the impact on the station keeping performance if there are large deviations between delivered and commanded thrust. More thorough investigations also needs to be performed in order utilize the full potential of the vent valve thrust, and truly exploit the nature of the cushion pressure which exhibits a sinusoidal state trajectory in non-zero sea states. However, despite this, we find it appropriate to conclude the work by stating that the operation investigated for the scope of this thesis should be, indeed, feasible.

5.2 Further Work

The work in this thesis does serve as an indication that the desired operation of the plant is feasible. However, in order to achieve optimal performance of the system and increase the capacity, some issues should be addressed in the design of the control system.

For the WF motion damping problem, much care was given in ensuring that optimal phase was obtained by the control signals. However, for the slowly varying thrust demands, implied by the station keeping operation, another approach might be more optimal. By investigating figure 4.13 from chapter 4.7, we note that at the border of the vent valve thrust capacity, saturation is reached quite often due to the pressure variations in the cushion. This means that the demanded thrust is not achieved at these instants. If we implemented an idea of an *averaged* thrust in the thrust control, we could compensate for this thrust loss by exceeding the commanded levels immediately after the thrust loss, during the pressure peaks, thus avoiding some of the consequences of the differences between the commanded- and achieved thrust. Theoretically we should also be able to use the information about the saturation levels in the vent valves to reduce the maximum allocatable vent valve thrust, T_{max}, in the thrust allocation algorithm from section3.5.2, to avoid the high saturation levels. Note that all this is only able to improve the performance of the system at the very edge of

its capacity, and would have zero effect during normal operation.

A subject that, on the other hand, could improve the operation during normal conditions is the work presented by (Megretski, 1996), who addresses the problem of motion damping of highly saturated systems. By utilizing state-dependent feedback gains, the degree of saturation is decreased by reducing the magnitude of the feedback gains when large motion amplitudes are experienced, e.g. during the transient phase after control appliance, but also during steady-state operation to automatic choose the optimal gain levels. Nguyen et al. (2007) proposes a hybrid, sea state dependent DP controller which features some ideas that also could be applicable for the SES plant in this thesis in order to reduce the saturation levels of the vent valve actuators.

The equilibrium cushion pressure is strongly related to the bias leakage area, A_0. An increased pressure means that a larger vent valve thrust could be achieved at a smaller lateral leakage area. More thourough studies of the optimal bias opening with respect to achieved thrust should be performed, to find the optimal levels, but this must regarded as a mere optimization of the already existing model. The pressure lift immediately after appliance of the vertical motion damping controller in figure 4.14, and the following increased consistency in the lateral thrust serves as the indication that this approach might increase the performance.

Bibliography

Abdelaziz, T. H. and Valášek, M. (2005). State derivative feedback by lqr for linear time-invariant systems. In *Proc. of 16th IFAC World Congress*.

Ang Jr, M. H. and Tourassis, V. D. (1987). Singularities of euler and roll-pitch-yaw representations. *Aerospace and Electronic Systems, IEEE Transactions on*, (3):317–324.

Auestad, Ø. F., Gravdahl, J. T., Sørensen, A. J., and Espeland, T. H. (2014). Motion compensation system for a free floating surface effect ship. In *Proceedings of the 19th World Congress of the International Federation of Automatic Control, IFAC*, Cape Town, South Africa, August 24-29.

Auestad, Ø. F., Perez, T., Gravdahl, J. T., Sørensen, A. J., and Espeland, T. H. (2015). Boarding control system - for improved accessibility to offshore wind turbines. In *Proceedings of the 10th IFAC Conference on Manoeuvring and Control of Marine Craft (MCMC), IFAC*, Copenhagen, Denmark, August 24-26.

Balchen, J., Andresen, T., and Foss, B. (1999). Reguleringsteknikk. 1. utgave-in norwegian. *Tapir, Trondheim, Norge*.

Balchen, J. G., Jenssen, N. A., Mathisen, E., and Sælid, S. (1980). A dynamic positioning system based on kalman filtering and optimal control.

Balchen, J. G., Jenssen, N. A., and Sælid, S. (1976). Dynamic positioning using kalman filtering and optimal control theory. In *IFAC/IFIP symposium on automation in offshore oil field operation*, volume 183.

Basturk, H. I. and Krstic, M. (2013). Adaptive wave cancelation by acceleration feedback for ramp-connected air cushion-actuated surface effect ships. *Automatica*, 49(9):2591–2602.

Bulten, N. W. H. (2006). Numerical analysis of a waterjet propulsion system.

Butler, E. A. (1985). The surface effect ship. *Naval engineers journal*, 97(2):200–253.

Commons, W. (2008). Hydrojet scheme 1- ahead 2- astern. Wikimedia Pictures.

Cummins, W. (1962). The impulse response function and ship motions. Technical report, DTIC Document.

De Wit, C. (2009). *Optimal thrust allocation methods for dynamic positioning of ships*. PhD thesis, TU Delft, Delft University of Technology.

(DNV), D. N. V. (2011). Rules and regulatoins of mobile offshore units, special equipment and systems. additional class, part 6, chapter 7: Dynamic positioning systems. Rules for classification, DNV.

EEA (2008). Offshore Wind Energy: Action needed to deliver on the energy policy objectives for 2020 and beyond. European and Environment and Agency, Nov.

Faltinsen, O. (1993). *Sea loads on ships and offshore structures*, volume 1. Cambridge university press.

Faltinsen, O. M. (2005). *Hydrodynamics of high-speed marine vehicles*. Cambridge university press.

Faÿ, H., Marshall, N., and Delacour, J. (1990). *Dynamic positioning systems: Principles, design and applications*. Ed. Technip.

Fossen, T. I. (1994). *Guidance and control of ocean vehicles*, volume 199. Wiley New York.

Fossen, T. I. (2011). *Handbook of marine craft hydrodynamics and motion control*. John Wiley & Sons.

Fossen, T. I. and Johansen, T. A. (2006). A survey of control allocation methods for ships and underwater vehicles. In *Control and Automation, 2006. MED'06. 14th Mediterranean Conference on*, pages 1–6. IEEE.

Hamilton, C. (2007). Use of main drive waterjets as azimuth thrusters.

Hasselmann, K., Barnett, T., Bouws, E., Carlson, H., Cartwright, D., Enke, K., Ewing, J., Gienapp, H., Hasselmann, D., Kruseman, P., et al. (1973). Measurements of wind-wave growth and swell decay during the joint north sea wave project (jonswap). Technical report, Deutches Hydrographisches Institut.

Hespanha, J. P. (2009). *Linear systems theory*. Princeton university press.

Johansen, T. A., Fossen, T. I., and Berge, S. P. (2004). Constrained nonlinear control allocation with singularity avoidance using sequential quadratic programming. *Control Systems Technology, IEEE Transactions on*, 12(1):211–216.

Kalman, R. E. (1960). A new approach to linear filtering and prediction problems. *Journal of Fluids Engineering*, 82(1):35–45.

Kalman, R. E. and Bucy, R. S. (1961). New results in linear filtering and prediction theory. *Journal of Fluids Engineering*, 83(1):95–108.

Kaplan, P., Bentson, J., and Davis, S. (1981). Dynamics and hydrodynamics of surface-effect ships. *SNAME Trans*, 89:211–247.

Kaplan, P. and Davis, S. (1974). A simplified representation of the vertical plane dynamics of ses craft. Technical report.

Kurita, C. (1988). Critical flow restricting orifices. Technical report, Fermi National Accelerator Laboratory (FNAL), Batavia, IL.

Liepmann, H. W. (1961). Gas kinetics and gas dynamics of orifice flow. *J. Fluid Mech*, 10(1).

Lindegaard, K.-P. (2003). Acceleration feedback in dynamic positioning.

Megretski, A. (1996). L2 bibo output feedback stabilization with saturated control. In *Proc. 13th IFAC world congress*, volume 500, pages 435–440. Citeseer.

Nguyen, D., Sørbø, A., and Sørensen, A. (2009). Modelling and control for dynamic positioned vessels in level ice, in proc. 8th conf. *Manoeuvring and Control of Marine Craft (MCMC'2009), Sept*, pages 16–18.

Nguyen, T. D., Sørensen, A. J., and Quek, S. T. (2007). Design of hybrid controller for dynamic positioning from calm to extreme sea conditions. *Automatica*, 43(5):768–785.

OWA (2010). Offshore wind accelerator (owa) access competition overview and technical specification. *Carbon Trust*.

Schrimpf, P. (2013). Systems of Linear Equations.

SNAME (1952). Nomenclature for treating the motion of a submerged body through a fluid jr. *New York: Technical and Research Bulletin*, pages 1–5.

Sørensen, A. J. (2013). *Marine Control Systems - Propulsion and Motion Control of Ships and Ocean Structures*. Department of Marine Technology, NTNU.

Sørensen, A. J. and Egeland, O. (1995). Design of ride control system for surface effect ships using dissipative control. *Automatica*, 31(2):183–199.

Sørensen, A. J. and Strand, J. P. (2000). Positioning of small-waterplane-area marine constructions with roll and pitch damping. *Control Engineering Practice*, 8(2):205–213.

Steen, S. (1993). *Cobblestone effect on SES*. PhD thesis, Norwegian Institute of Technology.

Strand, J. P. and Fossen, T. I. (1999). Nonlinear passive observer design for ships with adaptive wave filtering. In *New Directions in nonlinear observer design*, pages 113–134. Springer.

Ulstein, T. and Faltinsen, O. (1995). Nonlinear effects of a flexible stern seal bag on cobblestone oscillations of a ses.

Veksler, A., Johansen, T. A., and Skjetne, R. (2012). Thrust allocation with power management functionality on dynamically positioned vessels. In *American Control Conference (ACC), 2012*, pages 1468–1475. IEEE.

White, F. (1986). *Fluid mechanics*. McGraw-Hill international editions. Mechanical engineering series. McGraw-Hill Ryerson, Limited.

Yun, L. and Bliault, A. (2012). *High performance marine vessels*. Springer.

Appendix A

Run 1

A.0.1 Various Parameters

- Wave frequency: 0.5[rad/s]
- Wave amplitude: 1m
- Equilibrium cushion pressure $p_0 = 2400Pa$
- Vessel Draft: 1m
- ρ_{c0}: 1.23 kg/m^3
- ρ_a: 1.24 kg/m^3
- p_0: 2400Pa
- γ=1.4
- c_n=0.61
- A_c=160m^2
- L: 20m
- x_{cp}: 0.7m
- l_x^{vv}=0m
- $l_x^{wj,p}$=-12.5m

- $l_y^{wj,p}$=-5m
- $l_x^{wj,sb}$=-12.5m
- $l_y^{wj,sb}$=5m

A.0.2 Hydrodynamic Coefficients

Added Mass Matrix:

$$M_A = \begin{bmatrix} 0.745e5 & 0 & 0 & 0 & 0 & 0 \\ 0 & 0.832e5 & 0 & -0.274e5 & 0 & -0.123e6 \\ 0 & 0 & 0.194e5 & 0 & 0.106e4 & 0 \\ 0 & -0.274e5 & 0 & 0.336e6 & 0 & 0.107e6 \\ 0 & 0 & 0.106e4 & 0 & 0.554e6 & 0 \\ 0 & -0.123e6 & 0 & 0.107e6 & 0 & 0.323e7 \end{bmatrix} \tag{A.1}$$

Rigid Body Mass Matrix:

$$M_{RB} = \begin{bmatrix} 92000 & 0 & 0 & 0 & 0 & 0 \\ 0 & 92000 & 0 & 0 & 0 & 0 \\ 0 & 0 & 92000 & 0 & 0 & 0 \\ 0 & 0 & 0 & 920000 & 0 & 0 \\ 0 & 0 & 0 & 0 & 57600000 & 0 \\ 0 & 0 & 0 & 0 & 0 & 5760000 \end{bmatrix} \tag{A.2}$$

Linear Damping Matrix:

$$D_p(\omega) = \begin{bmatrix} 0.413e4 & 0 & 0 & 0 & 0 & 0 \\ 0 & 0.799e4 & 0 & 0.5e4 & 0 & -0.391e4 \\ 0 & 0 & 0.235e5 & 0 & 0.277e4 & 0 \\ 0 & 0.5e4 & 0 & 0.468e6 & 0 & -0.508e4 \\ 0 & 0 & 0.227e4 & 0 & 0.67e6 & 0 \\ 0 & -0.391e4 & 0 & -0.508 & 0 & 0.269e6 \end{bmatrix} \tag{A.3}$$

Restoring Coefficients:

$$G_{\eta_{Rw}} = \begin{bmatrix} 0 & 0 & 0 & 0 & 0 & 0 \\ 0 & 0 & 0 & 0 & 0 & 0 \\ 0 & 0 & 330000 & 0 & 251000 & 0 \\ 0 & 0 & 0 & 6440000 & 0 & 0 \\ 0 & 0 & 251000 & 0 & 10500000 & 0 \\ 0 & 0 & 0 & 0 & 0 & 0 \end{bmatrix} \tag{A.4}$$

A.0.3 Controller

Linear Quadratic State Derivative Regulator Weighting Matrices:

$$Q = \begin{bmatrix} 1/0.1 & 0 & 0 & 0 & 0 \\ 0 & 1/0.1 & 0 & 0 & 0 \\ 0 & 0 & 1/0.1 & 0 & 0 \\ 0 & 0 & 0 & 1/0.1 & 0 \\ 0 & 0 & 0 & 0 & 0 \end{bmatrix} \tag{A.5}$$

$$R = \begin{bmatrix} 0.01 & 0 \\ 0 & 0.0001 \end{bmatrix}$$

Appendix B

Run 2

B.0.4 Various Parameters

- Wave frequency: 0.5[rad/s]
- Wave amplitude: 1m
- Equilibrium cushion pressure $p_0 = 2400Pa$
- Vessel Draft: 1m
- ρ_{c0}: 1.23 kg/m^3
- ρ_a: 1.24 kg/m^3
- p_0: 2400Pa
- γ=1.4
- c_n=0.61
- A_c=160m^2
- L: 20m
- x_{cp}: 0.7m
- l_x^{vv}=0m
- $l_x^{wj,p}$=-12.5m

- $l_y^{wj,p}$=-5m
- $l_x^{wj,sb}$=-12.5m
- $l_y^{wj,sb}$=5m

B.0.5 Hydrodynamic Coefficients

Added Mass Matrix:

$$M_A = \begin{bmatrix} 0.735e5 & 0 & 0 & 0 & 0 & 0 \\ 0 & 0.735e5 & 0 & -0.2514e5 & 0 & -0.114e6 \\ 0 & 0 & 0.273e5 & 0 & -0.168e3e4 & 0 \\ 0 & -0.251e5 & 0 & 0.496e6 & 0 & 0.964e5 \\ 0 & 0 & -0.168e3 & 0 & 0.774e6 & 0 \\ 0 & -0.114e6 & 0 & 0.964e5 & 0 & 0.228e7 \end{bmatrix} \tag{B.1}$$

Rigid Body Mass Matrix:

$$M_{RB} = \begin{bmatrix} 92000 & 0 & 0 & 0 & 0 & 0 \\ 0 & 92000 & 0 & 0 & 0 & 0 \\ 0 & 0 & 92000 & 0 & 0 & 0 \\ 0 & 0 & 0 & 920000 & 0 & 0 \\ 0 & 0 & 0 & 0 & 57600000 & 0 \\ 0 & 0 & 0 & 0 & 0 & 5760000 \end{bmatrix} \tag{B.2}$$

Linear Damping Matrix:

$$D_p(\omega) = \begin{bmatrix} 0.413e4 & 0 & 0 & 0 & 0 & 0 \\ 0 & 0.686e3 & 0 & -0.251e5 & 0 & -0.114e6 \\ 0 & 0 & 0.273e5 & 0 & -0.168e3 & 0 \\ 0 & -0.251e5 & 0 & 0.496e6 & 0 & 0.964e5 \\ 0 & 0 & -0.168e3 & 0 & 0.774e6 & 0 \\ 0 & -0.114e6 & 0 & 0.964e5 & 0 & 0.288e7 \end{bmatrix} \tag{B.3}$$

Restoring Coefficients:

$$G_{\eta_{Rw}} = \begin{bmatrix} 0 & 0 & 0 & 0 & 0 & 0 \\ 0 & 0 & 0 & 0 & 0 & 0 \\ 0 & 0 & 330000 & 0 & 251000 & 0 \\ 0 & 0 & 0 & 6440000 & 0 & 0 \\ 0 & 0 & 251000 & 0 & 10500000 & 0 \\ 0 & 0 & 0 & 0 & 0 & 0 \end{bmatrix} \tag{B.4}$$

B.0.6 Controller

Linear Quadratic State Derivative Regulator Weighting Matrices:

$$Q = \begin{bmatrix} 1/0.00000033 & 0 & 0 & 0 & 0 \\ 0 & 1/0.1 & 0 & 0 & 0 \\ 0 & 0 & 1/0.00000001 & 0 & 0 \\ 0 & 0 & 0 & 1/0.01 & 0 \\ 0 & 0 & 0 & 0 & 0 \end{bmatrix} \tag{B.5}$$

$$R = \begin{bmatrix} 0.07 & 0 \\ 0 & 6.2 \end{bmatrix}$$

Appendix C

Run 3

C.0.7 Various Parameters

- Wave frequency: 0.5[rad/s]
- Wave amplitude: 1m
- Equilibrium cushion pressure $p_0 = 2400Pa$
- Vessel Draft: 1m
- ρ_{c0}: 1.23 kg/m^3
- ρ_a: 1.24 kg/m^3
- p_0: 2400Pa
- γ=1.4
- c_n=0.61
- A_c=160m^2
- L: 20m
- x_{cp}: 0.7m
- l_x^{vv}=0m
- $l_x^{wj,p}$=-12.5m

- $l_y^{wj,p}$=-5m
- $l_x^{wj,sb}$=-12.5m
- $l_y^{wj,sb}$=5m

C.0.8 Hydrodynamic Coefficients

Added Mass Matrix:

$$M_A = \begin{bmatrix} 0.735e5 & 0 & 0 & 0 & 0 & 0 \\ 0 & 0.735e5 & 0 & -0.2514e5 & 0 & -0.114e6 \\ 0 & 0 & 0.273e5 & 0 & -0.168e3e4 & 0 \\ 0 & -0.251e5 & 0 & 0.496e6 & 0 & 0.964e5 \\ 0 & 0 & -0.168e3 & 0 & 0.774e6 & 0 \\ 0 & -0.114e6 & 0 & 0.964e5 & 0 & 0.228e7 \end{bmatrix} \tag{C.1}$$

Rigid Body Mass Matrix:

$$M_{RB} = \begin{bmatrix} 92000 & 0 & 0 & 0 & 0 & 0 \\ 0 & 92000 & 0 & 0 & 0 & 0 \\ 0 & 0 & 92000 & 0 & 0 & 0 \\ 0 & 0 & 0 & 920000 & 0 & 0 \\ 0 & 0 & 0 & 0 & 57600000 & 0 \\ 0 & 0 & 0 & 0 & 0 & 5760000 \end{bmatrix} \tag{C.2}$$

Linear Damping Matrix:

$$D_p(\omega) = \begin{bmatrix} 0.413e4 & 0 & 0 & 0 & 0 & 0 \\ 0 & 0.686e3 & 0 & -0.251e5 & 0 & -0.114e6 \\ 0 & 0 & 0.273e5 & 0 & -0.168e3 & 0 \\ 0 & -0.251e5 & 0 & 0.496e6 & 0 & 0.964e5 \\ 0 & 0 & -0.168e3 & 0 & 0.774e6 & 0 \\ 0 & -0.114e6 & 0 & 0.964e5 & 0 & 0.288e7 \end{bmatrix} \tag{C.3}$$

Restoring Coefficients:

$$G_{\eta_{Rw}} = \begin{bmatrix} 0 & 0 & 0 & 0 & 0 & 0 \\ 0 & 0 & 0 & 0 & 0 & 0 \\ 0 & 0 & 330000 & 0 & 251000 & 0 \\ 0 & 0 & 0 & 6440000 & 0 & 0 \\ 0 & 0 & 251000 & 0 & 10500000 & 0 \\ 0 & 0 & 0 & 0 & 0 & 0 \end{bmatrix} \tag{C.4}$$

C.0.9 Controller

Linear Quadratic State Derivative Regulator Weighting Matrices:

$$Q = \begin{bmatrix} 1/0.00000033 & 0 & 0 & 0 & 0 \\ 0 & 1/0.1 & 0 & 0 & 0 \\ 0 & 0 & 1/0.00000001 & 0 & 0 \\ 0 & 0 & 0 & 1/0.01 & 0 \\ 0 & 0 & 0 & 0 & 0 \end{bmatrix} \tag{C.5}$$

$$R = \begin{bmatrix} 0.05 & 0 \\ 0 & 5 \end{bmatrix}$$

Appendix D

Run 4

D.0.10 Various Parameters

- Wave frequency: 0.5[rad/s]
- Wave amplitude: 1m
- Equilibrium cushion pressure $p_0 = 2400Pa$
- Vessel Draft: 1m
- ρ_{c0}: 1.23 kg/m^3
- ρ_a: 1.24 kg/m^3
- p_0: 2400Pa
- c_n=0.61
- A_c=160m^2
- L: 20m
- x_{cp}: 0.7m
- l_x^{vv}=12.5m
- $l_x^{wj,p}$=-12.5m
- $l_y^{wj,p}$=-5m

- $l_x^{wj,sb}$=-12.5m
- $l_y^{wj,sb}$=5m

D.0.11 Hydrodynamic Coefficients

Added Mass Matrix:

$$M_A = \begin{bmatrix} 0.745e5 & 0 & 0 & 0 & 0 & 0 \\ 0 & 0.832e5 & 0 & -0.274e5 & 0 & -0.123e6 \\ 0 & 0 & 0.194e5 & 0 & 0.106e4 & 0 \\ 0 & -0.274e5 & 0 & 0.336e6 & 0 & 0.107e6 \\ 0 & 0 & 0.106e4 & 0 & 0.554e6 & 0 \\ 0 & -0.123e6 & 0 & 0.107e6 & 0 & 0.323e7 \end{bmatrix} \tag{D.1}$$

Rigid Body Mass Matrix:

$$M_{RB} = \begin{bmatrix} 92000 & 0 & 0 & 0 & 0 & 0 \\ 0 & 92000 & 0 & 0 & 0 & 0 \\ 0 & 0 & 92000 & 0 & 0 & 0 \\ 0 & 0 & 0 & 920000 & 0 & 0 \\ 0 & 0 & 0 & 0 & 57600000 & 0 \\ 0 & 0 & 0 & 0 & 0 & 5760000 \end{bmatrix} \tag{D.2}$$

Linear Damping Matrix:

$$D_p(\omega) = \begin{bmatrix} 0.413e4 & 0 & 0 & 0 & 0 & 0 \\ 0 & 0.799e4 & 0 & 0.5e4 & 0 & -0.391e4 \\ 0 & 0 & 0.235e5 & 0 & 0.277e4 & 0 \\ 0 & 0.5e4 & 0 & 0.468e6 & 0 & -0.508e4 \\ 0 & 0 & 0.227e4 & 0 & 0.67e6 & 0 \\ 0 & -0.391e4 & 0 & -0.508 & 0 & 0.269e6 \end{bmatrix} \tag{D.3}$$

Restoring Coefficients:

$$G_{\eta_{Rw}} = \begin{bmatrix} 0 & 0 & 0 & 0 & 0 & 0 \\ 0 & 0 & 0 & 0 & 0 & 0 \\ 0 & 0 & 330000 & 0 & 251000 & 0 \\ 0 & 0 & 0 & 6440000 & 0 & 0 \\ 0 & 0 & 251000 & 0 & 10500000 & 0 \\ 0 & 0 & 0 & 0 & 0 & 0 \end{bmatrix} \tag{D.4}$$

Linearized nonlinear damping used in LF model

$$D_{ln} = \begin{bmatrix} 226 & 0 & 0 \\ 0 & 500 & 0 \\ 0 & 0 & 200 \end{bmatrix} \tag{D.5}$$

Zero frequency added mass

$$M_{A0} = \begin{bmatrix} 0.202e6 & 0 & 0 \\ 0 & 0.402e6 & -0.212e6 \\ 0 & -2.212e5 & 0.77e7 \end{bmatrix} \tag{D.6}$$

Zero frequency linear damping

$$D_p = \begin{bmatrix} 0.140e0 & 0 & 0 \\ 0 & 0.200e0 & -0.449e-1 \\ 0 & -0.449e-1 & 0.482e1 \end{bmatrix} \tag{D.7}$$

D.0.12 Controller

Linear Quadratic State Derivative Regulator Weighting Matrices

$$Q = \begin{bmatrix} 1/0.1 & 0 & 0 & 0 & 0 \\ 0 & 1/0.1 & 0 & 0 & 0 \\ 0 & 0 & 1/0.1 & 0 & 0 \\ 0 & 0 & 0 & 1/0.1 & 0 \\ 0 & 0 & 0 & 0 & 0 \end{bmatrix}$$
$$R = \begin{bmatrix} 0.01 & 0 \\ 0 & 0.0001 \end{bmatrix} \tag{D.8}$$

DP PID Feedback Gains

$$k_i = \begin{bmatrix} 230 & 0 & 0 \\ 0 & 350 & 0 \\ 0 & 0 & 2600 \end{bmatrix}$$
$$k_p = \begin{bmatrix} 7000 & 0 & 0 \\ 0 & 17000 & 0 \\ 0 & 0 & 260000 \end{bmatrix} \tag{D.9}$$
$$k_d = \begin{bmatrix} 100000 & 0 & 0 \\ 0 & 250000 & 0 \\ 0 & 0 & 4000000 \end{bmatrix}$$

Quadprog parameters

Thrust inequality matrices:

$$A_{tc} = \begin{bmatrix} 1 & 0 & 0 & 0 & 0 & 0 & 0 & 0 \\ -1 & 0 & 0 & 0 & 0 & 0 & 0 & 0 \\ 0 & a_{11} & a_{12} & 0 & 0 & 0 & 0 & 0 \\ 0 & a_{21} & a_{22} & 0 & 0 & 0 & 0 & 0 \\ 0 & a_{31} & a_{32} & 0 & 0 & 0 & 0 & 0 \\ 0 & a_{41} & a_{42} & 0 & 0 & 0 & 0 & 0 \\ 0 & a_{51} & a_{52} & 0 & 0 & 0 & 0 & 0 \\ 0 & 0 & 0 & a_{11} & a_{12} & 0 & 0 & 0 \\ 0 & 0 & 0 & a_{21} & a_{22} & 0 & 0 & 0 \\ 0 & 0 & 0 & a_{31} & a_{32} & 0 & 0 & 0 \\ 0 & 0 & 0 & a_{41} & a_{42} & 0 & 0 & 0 \\ 0 & 0 & 0 & a_{51} & a_{52} & 0 & 0 & 0 \end{bmatrix} \tag{D.10}$$

$$b_{tc} = \begin{bmatrix} T_m a x_v v \\ -T_m i n_v v \\ b_1 \\ b_2 \\ b_3 \\ b_4 \\ b_5 \\ b_1 \\ b_2 \\ b_3 \\ b_4 \\ b_5 \end{bmatrix} \tag{D.11}$$

Where the different parameters used are given by

- a_{11} =40000
- a_{12} =-10720
- b_1 =3200000000
- a_{21} =40000
- a_{22} =10720
- b_2 =3200000000
- a_{31} =-5360
- a_{32} =89280
- b_3 =3200000000
- a_{41} =-69280
- a_{42} =0
- b_4 =1385600000
- a_{51} =-5360
- a_{52} =-89280
- b_5 =3200000000

The quadratic weighting matrix from the objective function is given by

$$G = \begin{bmatrix} 1 & 0 & 0 & 0 & 0 & 0 & 0 & 0 \\ 0 & 1 & 0 & 0 & 0 & 0 & 0 & 0 \\ 0 & 0 & 1 & 0 & 0 & 0 & 0 & 0 \\ 0 & 0 & 0 & 1 & 0 & 0 & 0 & 0 \\ 0 & 0 & 0 & 0 & 1 & 0 & 0 & 0 \\ 0 & 0 & 0 & 0 & 0 & 10000000000 & 0 & 0 \\ 0 & 0 & 0 & 0 & 0 & 0 & 10000000000 & 0 \\ 0 & 0 & 0 & 0 & 0 & 0 & 0 & 100000000000 \end{bmatrix} \tag{D.12}$$

The linear term is given by

$$c = \begin{bmatrix} 1 \\ 1 \\ 1 \\ 1 \\ 1 \\ 100000000 \\ 100000000 \\ 100000000 \end{bmatrix} \tag{D.13}$$

We implemented slack variables to ensure that we did not reach infeasible problems. However, those were never used/necessary in simulations and the values of the slack variables were 0 all the time, thus we disregarded them for the scope of this thesis. These correspond to the last three inputs in A_{tc}, G and c.

Appendix E

One-pager Wave Craft Information

WAVE CRAFT

SPEED-ACCESS-COMFORT

Video: www.um.no/WEB/um200.nsf/pages/Gallery

umoe mandal

umoe

STRONG performance – **LIGHT** materials

Umoe Mandal Wave Craft

The SES – Offshore Service Vessel concept is the next generation offshore wind farm service vessel. The SES (Surface Effect Ship) is lifted by an air cushion enclosed by side hulls and flexible rubber sealing aft and in the bow. By utilizing this air-cushion to stabilize vessel motions the vessel is able to access offshore turbines in higher sea states than possible today. The vessel type also offer very high service speed with excellent seakeeping and passenger comfort. This allows for reaching the offshore installations even when the distance to harbour is far and weather window for safe operation is narrow.

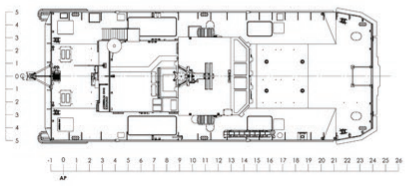

Main Characteristics - Wave Craft Express

- Class notation:	DNV + 1A1 HSLC R1 Wind Farm Service 1
- Length over all:	27.2m
- Width over all:	10.4m
- Draught:	0,7m on cushion
- Cargo capacity:	4 tons
- Transit speed:	40+ knots
- Propulsion:	Water jets powered by high-speed diesel engines
- Range:	700+ nautical miles
- Crew:	2-3
- Passengers:	12

The specifications can be customized based on specific client needs.

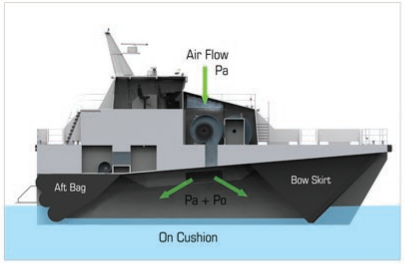

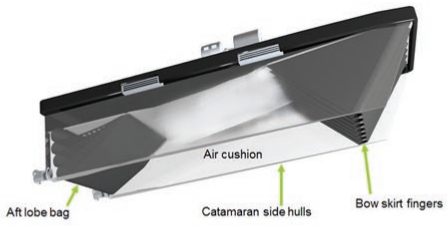

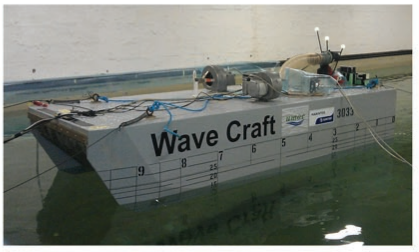

The active control of the air cushion has been confirmed in model testing.

With a 26m vessel, access for offshore wind turbines can be carried out in up to 2,5m significant wave height.
In swell the vessel can access in even larger wave heights.

The project is partly supported by The Research Council of Norway under the innovation programme MAROFF, Regionale Forskningsfond Agder (Regional research fond) and Innovation Norway.

The Umoe Mandal Wave Craft was among the 13 shortlisted concepts of initial 450 applications in the Carbon Trust Offshore Wind Accelerator Competition.

Forskningsrådet

CARBON TRUST

INNOVASJON NORGE

REGIONALE FORSKNINGSFOND AGDER

umoe mandal

umoe

Umoe Mandal AS
Phone: +47 3827 9200
www.um.no

Address:
Gismerøyveien 205
N-4515 Mandal, Norway

Contact:
Are Søreng: are.soreng@um.no
Trygve Halvorsen: Trygve.Halvorsen.Espeland@um.no

STRONG performance – **LIGHT** materials

Appendix F

Conference Poster From Poster Exhibition

Combined Dynamic Positioning and Optimal Wave Frequency Motion Damping on Surface Effect Ship

NTNU – Trondheim
Norwegian University of Science and Technology

Per Sondre Sodeland
persondr@stud.ntnu.no
Norwegian University of Science- and Technology
Supervisor: Prof. Asgeir J. Sørensen, co-supervisor: Øyvind F. Auestad, PhD
in co-operation with Umoe Mandal

umoe mandal

Introduction

The trend in the offshore wind industry is that the farms are located further and further from the shore. This necessitates larger platforms, with accommodation capacities, in order to perform service and crew transfers, since conventional offshore windmill service vessels are not able to travel the distance in one work day. Conventional Offshore Supply Vessels are slow, large and expensive vessels. A SES could be a strong alternative to such vessels. They are faster, cheaper, and due to active motion damping controllers they could be made significantly smaller than conventional OSVs, while still maintaining strong seakeeping properties. There are however some obstacles. Interaction with fixed offshore structure necessitates automatic control over the horizontal motion trajectories of the respective vessels. Conventional DP system are used in the oil industry in order to perform safe station keeping and low speed maneuvering. These feature bow thrusters, of the tunnel- or pod type, which are hard to fit on a SES due to the narrow bow design, which is to reduce water resistance and the hydrodynamic loads. Instead of such thrusters, we will investigate the possibilities of utilizing the potential energy in the air cushion of a SES as a source for lateral thrust, by controlling the air flow in the favoured direction. The quick dynamics of these systems makes them suitable for damping and control of both 1st and 2nd order motions. This thesis will propose a control system, which utilizes control of this air flow to damp first order motions and perform station keeping, simultaneously.

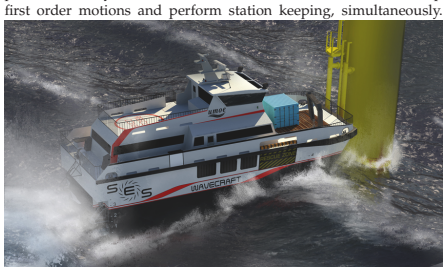

Figure 1: The Wave Craft from Umoe Mandal

Control System Design

The control design is dual, i.e. we want to perform station keeping and WF motion damping simultaneously. The DP- and WF controllers were designed individually, as linear state- and state derivative feedback controllers, respectively. The WF- controller is given according to

$$u_c^l = -k_{lqsdr}\eta_{WF} \tag{5}$$

where u_c^l contains the commanded leakage areas for the heave- and sway compensation respectively. The feedback gains are computed by a linear quadratic synthesis, by minimization of

$$J_{lqsd} = \int_0^\infty \dot{\eta}_{llqr}(t)'Q\dot{\eta}_{llqr}(t) + u(t)'Ru(t)dt. \tag{6}$$

The challenge with the WF motion damping was the highly limited actuator capacity. We derived a method to find the necessary relative trajectory weighting in the cost function above, in order to obtain a 90° phase difference between the two inputs in the control input vector. This is to reduce the level of mutual infliction of the respective control objectives. The DP controller is a simple PID-type, given by

$$\tau_{pid}(t) = -k_p e(t) - k_d\dot{e}(t) - k_i\int_0^T e(t)dt. \tag{7}$$

The thrust allocation, i.e. the mapping from commanded body fixed forces to actual thruster outputs/displacements, is done by presenting the problem as a quadratic optimization problem, on the form:

$$\min_{u_c\in\mathbb{R}^{r_h}} f(u_c) \quad \text{subject to the constraints} \quad \begin{matrix} A_{tc}u_c \le b_{tc} \in \mathbb{R}^q \\ Tu_c = \tau_c^h \in \mathbb{R}^{m_{LF}} \end{matrix}, \tag{8}$$

where $f(u_c)$ is the objective function, subject to minimization. We described the thrust envelope of the respective thrusters as set of linear, implicit inequalities, which are represented in the problem by the matrices A_{tc} and b_{tc}. The thrust control problem, which concerns the process of going from control output signals to actual forces and displacements of the various actuators was done by the relation

$$\Delta A_c^l = \frac{\rho_a u_c^{vv}}{2c_n\rho_c p_u(t)}, \tag{9}$$

for the vent valves, and

$$n_{wj} = v_{out}^{-1}\left(\sqrt{\frac{|u_{3d}^{wj}|}{\rho_w A_{nozzle}}}\right) \tag{10}$$

to find the required speed of the water jet impellers. The latter also need control of the azimuth (angle of net thrust), which was controlled by the state of the deflector shield and the discharge nozzle.

Concluding Remarks and Further Work

The results of the simulations indicates that the potential of performing station keeping by the current, available actuators on a SES is indeed large. There are some issues that need attention before this can be done, but they are minor and should be solvable. The next step would be to perform model tests, as there will always be uncertainties in a model like this, and it is not unlikely that there exists unmodeled dynamics able to affect the results. Model- or full scale tests of the vent valve thrust behaviour has never been performed, thus the qualitative assumptions are based solely on the results from these simulations.

What is a SES?

A SES is a vessel with a twin hull configuration in combination with an air cushion which is enclosed laterally by rigid side hulls and longitudinally by the flexible rubber $bow-$ and $stern$ seals. This allows for water jet propulsion, strong directional stability and high transit speeds (the $SES\ 100b$ reached 100 knots in 1963). The vertical dynamics are greatly influenced by the excess cushion pressure, $p_u(t)$, which in turn can be controlled by the outflow Q_{out}, through the $variable\ leakage\ area$, ΔA_{vert}^l and the speed of the $lift\ fans$, which provide the airflow into the cushion, Q_{in}. By proper control of these inputs, the cushion pressure can be influenced in a matter so that the vertical motions are greatly reduced.

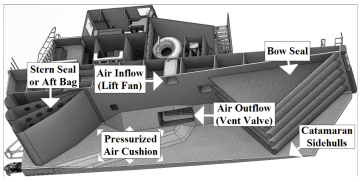

Figure 2: Key SES structure

Mathematical Model

The system dynamics is comprised of the regular linear seakeeping equations, both wave- and low frequency, and the uniform pressure equation which describes the behaviour of the cushion pressure when subject to external disturbances and controlled inputs. We will derive the dynamics based on Reynolds Transport Theorem.

$$\frac{\partial}{\partial t}(B_{sys}) = \frac{\partial}{\partial t}\left(\int_{CV}\beta_{re}\rho d\mathcal{V}\right) + \int_{CS}\beta_{re}\rho(\mathbf{V}\cdot\mathbf{n})dA. \tag{1}$$

From this, by conservation of mass we derive a nonlinear representation of the pressure dynamics, which includes state dependent $passive$ leakage areas to account for pressure effects of large vessel displacements in the vertical DOFs, and the lateral thrust force by conservation of linear momentum. The pressure dynamics is given by

$$\sum_{i=1}^{r} Q_i(\mu) - (K_2 + C_{n,RCS}\sum_{i=1}^{r}\Delta A_i)\sqrt{\frac{2(p_0+\mu(t)p_0)}{\rho_a}} = \left[-A_c x_{cp}\dot{\eta}_5 + A_c\dot{\eta}_3 + b\int_{\frac{-b}{2}}^{\frac{b}{2}}\dot{\xi}(x,t)dx\right] + K_1(p_a+\mu(t)p_0+p_0)^{\frac{1}{\gamma}-1}\dot{\mu}(t).$$

Denoted by the normalization cushion pressure variable $\mu(t) = \frac{p_u(t)-p_0}{p_0}$. The lateral vent valve thrust is given by

$$\sum U^{vv} = \sum_i -n\cdot c_n\cdot\rho_c A_i^l\frac{2(p_0+\mu(t)p_0)}{\rho_a}. \tag{2}$$

The above equations provides the external loads and controlled inputs in the generic vessel dynamics, given by

$$M\dot{\nu} + C_{rb}(\nu)\nu + C_A(\nu_r)\nu_r + D(\kappa,\nu_r) + G(\eta) = \tau \tag{3}$$

Which contains the dynamics of the vessel, when subject to the external body-fixed force vector τ. This is comprised of the actuator outputs and the environmental loads. The latter are modeled by the use of force RAOs, for the wave frequency (WF) problem, i.e.

$$\left|F_{wave1}^{dof}(\omega_k,\beta_i)\right| = \sqrt{Im_{wave1}\{dof\}(k,i)^2 + Re_{wave1}\{dof\}(k,i)^2},$$
$$\angle F_{wave1}^{dof}(\omega_k,\beta_i) = atan2(Im_{wave1}\{dof\}(k,i), Re_{wave1}\{dof\}(k,i)), \tag{4}$$

where $\left|F_{wave1}^{dof}(\omega_k,\beta_i)\right|$ and $\angle F_{wave1}^{dof}(\omega_k,\beta_i)$ denotes the magnitude and phase of the excitation force, respectively. Im_{wave1} and Re_{wave1} denotes the imaginary and real part of the RAO, which is computed by a the numeric seakeeping program ShipX, together with the remaining hydrodynamic and hydrostatic coefficients used in the simulations. The model is simulated by implementing it in MATLAB and Simulink.

Results and Simulations

All simulations were done for a generic, 90 ton, SES design.The first plot presents the station keeping capabilities of the vessel, when subject to a wind load and constant reference position being the zero states. The wind starts out from north-east with a 10m/s velocity, and turns more easterly at t=500s with an increase in windspeed to 15m/s. Some y-axis' have been normalized due to confidentiality issues.

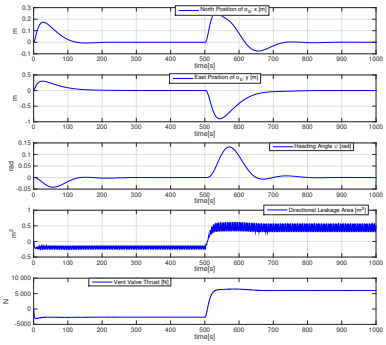

Figure 3: Station Keeping

The simulations of the derived model indicates that the vessel is able to perform station keeping and heave compensating simultaneously, as illustrated by the figure below where the vessel is subject to a constant wind load in the North-East direction, with a windspeed of 10m/s. The heave compensation controller is switched on at t=250s, the heading angle is changed to $\psi_{ref} = \pi/4$ at t=500s, and once more to $\psi_{ref} = \pi/6$ at t=750s.

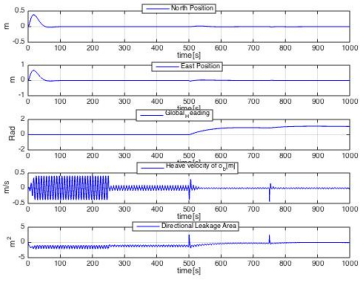

Figure 4: Combined heave compensation and station keeping

The heave motion damping is illustrated below for regular waves of angular frequency $\omega_o = 1.26[rad/s]$. The controller is turned on at t=150s.

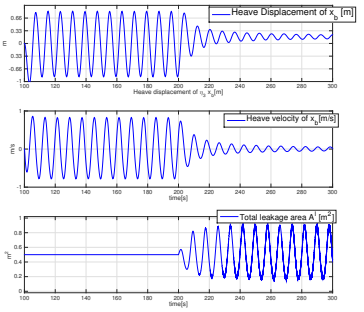

The sway motion damping capabilities of the vessel is illustrated in the next figure. The waves are relatively small to illustrate the effect of the controller when not subject to too large saturation levels. The controller is turned on at t=150s.

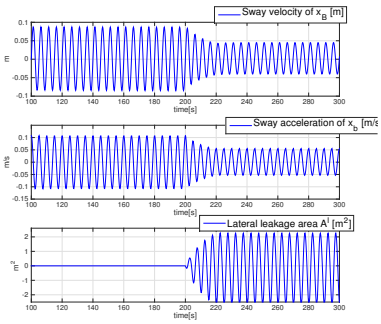

Figure 5: Wave frequency motion damping in sway

We have shown that station keeping of a SES is indeed possible with the actuators and thrusters already installed and available on such vessels. We obtain good performance, for a variety of conditions. The water jets, and their strong thrust capabilities, plays an important role here, but we were quite satisfied with the thrust delivering capacities of the vent valve, indicated by the simulations. We have also shown that it is possible to perform damping of the vertical motions and station keeping simultaneously, and that the motion damping performance is significantly enhanced by pointing the vessel towards the wind, to reduce lateral forces. The damping ratio of the sway-motion is smaller compared to the heave damping. This is due to the large inertial forces related to the WF motions and the relatively low thrust levels obtainable from the vent valves. However, we have shown that the motions can be reduced by between 20-30%, dependent on the conditions.